Accuracy Limitation of Road Profilers Based on a Single-Axis Accelerometer

Starodub, Inc.

Task Order ART-01
Contract DTFH61-06-D-00021

January 2007

FOREWORD

The main objectives of this project were to describe the accuracy limitations of road profilers based on a single-axis accelerometer, assess the sensitivity of single-accelerometer-based road profiling systems to errors in measured elevation profile caused by tilt and rotation of the profiling test vehicle, compare the realizable performance of single-accelerometer-based road profiling systems to the performance requirements for profile measurement to support construction acceptance testing and other applications defined in AASHTO and ASTM test provisions, and recommend guidelines regarding the use of road profiling equipment based on a single-axis accelerometer to measure pavement roughness for purposes of construction acceptance, asset management, and pavement research. The intended audience of this report are standards/guideline setting bodies, state highway agencies that use inertial profilers, equipment vendors, and researchers.

Insert Name of FHWA Director
Director, Office of Insert XXX
Research and Development

TECHNICAL REPORT DOCUMENTATION PAGE

1. Report No. FHWA-HRT-XX-XXX	2. Government Accession No.	3. Recipient's Catalog No.
4. Title and Subtitle Accuracy Limitation of Road Profilers Based on a Single-Axis Accelerometer (Phase I).		5. Report Date January 2007 6. Performing Organization Code:
7. Author(s) J. Mekemson and N. Gagarin		8. Performing Organization Report No.
9. Performing Organization Name and Address Starodub, Inc. 3504 Littledale Rd Kensington, MD 20895		10. Work Unit No. 11. Contract or Grant No. DTFH-06-D-00021 – Task Order ART-01
12. Sponsoring Agency Name and Address Insert Office Name Here Federal Highway Administration address city, state, zip		13. Type of Report and Period Covered Report January, 2007 14. Sponsoring Agency Code Insert FHWA sponsoring agency office code (i.e., HRTS-01)
15. Supplementary Notes FHWA Contracting Officer's Technical Representative (COTR): Dr. Kunik Lee / Robert Orthmeyer		

16. Abstract

The main objective of this project was to describe the accuracy limitations of road profilers based on a single-axis accelerometer. pitch, roll, and change in speed of an inertial profiler vehicle as a result of roadway alignment and driver operations were found to contribute to errors in inertial profile estimates and subsequent IRI calculations. Different features and their characteristics result in different accelerometer/laser inputs to inertial profile estimates and subsequent wavelengths input to the IRI filter. The geometry elements of a road and vehicle operations combine to produce both short-wave and long-wave effects on the profile and IRI measurements. Roadway elements and vehicle operations may cause a change in profile but do not necessarily mean a significant change in IRI. The factors are often occurring simultaneously and thus lead to a compounding of effects that can be difficult to isolate. The sequence of conditions for curvature, grade and cross slope that generate levels of pitch, roll, cross-trajectory and along trajectory accelerations capable of significant profile and IRI errors may be further quantified and classified using a road-vehicle simulation model. A simulation model may be the only reasonable method to fully explore in a controlled environment the impact of roll, pitch, and change in speed on inertial profile estimates as it relates to a road's alignment and cross section elements.

17. Key Words Inertial Profile, Accuracy, 1-D model, Pitch, Roll	18. Distribution Statement No restrictions. This document is available through the National Technical Information Service, Springfield, VA 22161.		
19. Security Classif. (of this report) Unclassified	20. Security Classif. (of this page) Unclassified	21. No. of Pages 151	22. Price N

Form DOT F 1700.7 (8-72) Reproduction of completed page authorized

SI* (MODERN METRIC) CONVERSION FACTORS

APPROXIMATE CONVERSIONS TO SI UNITS

Symbol	When You Know	Multiply By	To Find	Symbol
		LENGTH		
in	inches	25.4	millimeters	mm
ft	feet	0.305	meters	m
yd	yards	0.914	meters	m
mi	miles	1.61	kilometers	km
		AREA		
in^2	square inches	645.2	square millimeters	mm^2
ft^2	square feet	0.093	square meters	m^2
yd^2	square yard	0.836	square meters	m^2
ac	acres	0.405	hectares	ha
mi^2	square miles	2.59	square kilometers	km^2
		VOLUME		
fl oz	fluid ounces	29.57	milliliters	mL
gal	gallons	3.785	liters	L
ft^3	cubic feet	0.028	cubic meters	m^3
yd^3	cubic yards	0.765	cubic meters	m^3
	NOTE: volumes greater than 1000 L shall be shown in m^3			
		MASS		
oz	ounces	28.35	grams	g
lb	pounds	0.454	kilograms	kg
T	short tons (2000 lb)	0.907	megagrams (or "metric ton")	Mg (or "t")
		TEMPERATURE (exact degrees)		
^oF	Fahrenheit	5 (F-32)/9 or (F-32)/1.8	Celsius	^oC
		ILLUMINATION		
fc	foot-candles	10.76	lux	lx
fl	foot-Lamberts	3.426	$candela/m^2$	cd/m^2
		FORCE and PRESSURE or STRESS		
lbf	poundforce	4.45	newtons	N
lbf/in^2	poundforce per square inch	6.89	kilopascals	kPa

APPROXIMATE CONVERSIONS FROM SI UNITS

Symbol	When You Know	Multiply By	To Find	Symbol
		LENGTH		
mm	millimeters	0.039	inches	in
m	meters	3.28	feet	ft
m	meters	1.09	yards	yd
km	kilometers	0.621	miles	mi
		AREA		
mm^2	square millimeters	0.0016	square inches	in^2
m^2	square meters	10.764	square feet	ft^2
m^2	square meters	1.195	square yards	yd^2
ha	hectares	2.47	acres	ac
km^2	square kilometers	0.386	square miles	mi^2
		VOLUME		
mL	milliliters	0.034	fluid ounces	fl oz
L	liters	0.264	gallons	gal
m^3	cubic meters	35.314	cubic feet	ft^3
m^3	cubic meters	1.307	cubic yards	yd^3
		MASS		
g	grams	0.035	ounces	oz
kg	kilograms	2.202	pounds	lb
Mg (or "t")	megagrams (or "metric ton")	1.103	short tons (2000 lb)	T
		TEMPERATURE (exact degrees)		
^oC	Celsius	1.8C+32	Fahrenheit	^oF
		ILLUMINATION		
lx	lux	0.0929	foot-candles	fc
cd/m^2	$candela/m^2$	0.2919	foot-Lamberts	fl
		FORCE and PRESSURE or STRESS		
N	newtons	0.225	poundforce	lbf
kPa	kilopascals	0.145	poundforce per square inch	lbf/in^2

*SI is the symbol for the International System of Units. Appropriate rounding should be made to comply with Section 4 of ASTM E380.
(Revised March 2003)

TABLE OF CONTENTS

LIST OF FIGURES

LIST OF TABLES

LIST OF ACRONYMS AND ABBREVIATIONS

General Terms

AASHTO	American Association of State Highway and Transportation Officials
ASTM	American Society for Testing and Materials
FHWA	Federal Highway Administration
TFHRC	Turner-Fairbank Highway Research Center

Specific Terms

ART	Advanced Research Team
DHM	Digital Highway Measurement
DHMS	Digital Highway Measurement System
DMI	Distance Measurement Instrument

Measurements

CS	Cross Slope
DS	Delta Speed (Speed change)
Spd	Speed

Calculated Variables

AAD	Average Absolute Difference is the sum of the absolute differences of the paired terms of two equally sized vectors
AAD IRI80	AAD of the corrected and uncorrected acceleration IRI80
AAD IRI120	AAD of the corrected and uncorrected acceleration IRI80
AAD Profile	AAD of the corrected and uncorrected acceleration inertial profile
DOC	Degree-of-Curvature as the change in heading (bearing) in degrees over an arc distance of 100 ft (30.48 m)
IRI80	International Roughness Index (IRI) computed with internal speed parameter set at 80 km/h (50 mi/h)
IRI120	International Roughness Index (IRI) computed with internal speed parameter set at 120 km/h (75 mi/h)

1. INTRODUCTION

Sensitivity of single-accelerometer-based road profiling systems to errors in measured elevation profile caused by tilt and rotation of the profiling test vehicle has been suggested to be present in the common measurement procedures used for QC/QA and for long-term monitoring of pavement surfaces for ride quality. As these measurements are often used in determining pay factors for quality of pavement construction, sources of error need to be understood and accounted for in the measurement process and the application of the results to decision making.

Most current versions of road profiling equipment employ a common principle of operation. A single-axis accelerometer senses the vertical motion of the test vehicle to which it is mounted. Some combination of analog and digital signal processing and numerical integration converts the measured acceleration into an estimate of vertical position. At the same time, another sensor (typically a laser-based ranging device) measures the distance between the test vehicle and the pavement surface. The elevation profile of the pavement surface is then computed as the numerical difference between the estimated vehicle position and the vehicle-to-surface distance measurements. The quality of the elevation profile depends directly on the quality of its two constituent measurements.

The quality of the measurement of vehicle position is inherently limited by the use of a single-axis accelerometer:

- When an accelerometer is tilted from vertical (as is generally the case because of test vehicle roll and pitch), it generates an error proportional to one minus the cosine of the tilt angle, even though no vertical acceleration is present.
- Although most accelerometers are relatively insensitive to off-axis accelerations when they are perfectly vertical, they will detect a fraction—in proportion to the tangent of the tilt angle—of horizontal accelerations when they are tilted from vertical.
- In addition to linear accelerations, test vehicles also experience angular accelerations that may affect accelerometer response.
- The frequency and phase response of accelerometers, signal conditioning systems, and numerical integration algorithms may introduce frequency-dependent signal gain and delay, thereby limiting the quality of measurement at low frequencies, high frequencies, or both.

All of these limitations inherently affect the quality of the estimate of vertical position and, in turn, the quality of the profile measurement. Errors could be minimized through use of a six-degree-of-freedom inertial reference system employing three linear accelerometers and three rotation sensors (typically mechanical or optical gyroscopes), but such systems are significantly more complicated and expensive.

It is not known whether the accuracy limitations inherent in single-axis accelerometer road profilers are consistent with current requirements for profile measurement. For example, transportation agencies increasingly use road profilers—either high-speed systems mounted on motor vehicles or low-speed systems mounted on “golf cart” vehicles—to measure the ride

quality and determine pay factors for newly constructed pavements. Likewise, agencies attempt to detect relatively small changes in the roughness of in-service pavements for research or asset management purposes. In such applications small differences in ride quality indices (which are computed from measured elevation profiles) can be quite significant. The American Association of State Highway and Transportation Officials (AASHTO) and the American Society for Materials and Testing (ASTM) have defined standards to ensure that profiling equipment meets the requirements for these applications. However, it is unclear whether equipment based on a single-axis accelerometer can conform to these standards and meet the requirements under the range of conditions encountered in actual practice.

This project was undertaken to better understand the relationships between roadway features and resulting data collection vehicle operations effects on inertial profiling error and ride quality computations.

2. BACKGROUND

The objective and scope of the project were based on the needs assessment of a Pooled Funds Project expert task group on profile quality.

OBJECTIVES

- Describe the accuracy limitations of road profilers based on a single-axis accelerometer.
- Assess the sensitivity of single-accelerometer-based road profiling systems to errors in measured elevation profile caused by tilt and rotation of the profiling test vehicle and by frequency-dependent accelerometer response, assuming the range of highway grade, curvature, cross slope, and roughness reasonably encountered for rural and urban pavements in the United States, as well as the range of vehicle dynamics and test speeds typically encountered in testing.
- Compare the realizable performance of single-accelerometer-based road profiling systems to the performance requirements for profile measurement to support construction acceptance testing and other applications defined in AASHTO and ASTM test provisions.
- Recommend guidelines regarding the use of road profiling equipment based on a single-axis accelerometer to measure pavement roughness for purposes of construction acceptance, asset management, and pavement research.

SCOPE

- Describe the essential operating principles of equipment based on a single vertical accelerometer.
- Develop mathematical models relating the effect of test vehicle tilt and rotations and of limitations in the performance of accelerometers, analog signal conditioning, and numerical algorithms on measured elevation profile quality.
- Characterize the range of grade, curvature, cross slope, and roughness encountered for rural and urban pavements in the United States.
- Characterize the range of vehicle suspensions and test speeds typically employed in testing, including both high-speed and low-speed test vehicles.Describe and estimate the quantity of expected error in measured elevation profiles and derived ride quality indices. Assess the suitability and acceptable operating range for road profiling systems based on single vertical accelerometers.

3. TECHNICAL APPROACH

PROPOSED EXPERIMENTAL APPROACH

Experimental approach to generate the data needed to perform a comprehensive analysis is based on the nature of the problem, the type of data available for the study, and desired implementation guidelines. The general experimental approach is outlined as:

- Select a standard for inertial profiling model, filters, and output functions.
- Quantify the forces and changes in orientation subjected to the sensor base during data acquisition operations.
- Define ideal and apparent reference coordinate systems.
- Define acceleration measurement error model based on difference between the two coordinates systems.
- Define output metrics for parameters of interest derived from measurements.
- Estimate measurement errors, and propagated differences in output metrics using two distinct approaches: A) DHMS Database, B) Vehicle/Road Simulation.

The experimental approach is refined as the results of intermediate analysis may indicate.

THEORETICAL MODELS

Theoretical models related to the correction of the body normal acceleration to trajectory normal acceleration is present in this section. The theoretical models are 1) Speed-Curvature versus cross-trajectory accelerations, 2) design equation for cross slope (superelevation), and 3) relationship between vehicle roll and cross slope.

Speed—Curvature vs. Cross-Trajectory Accelerations

The following sections present the Speed—Curvature versus Cross-Trajectory relationship.

Differential Geometry

Let $\underline{X} = (O, \vec{i}_1, \vec{i}_2, \vec{i}_3)$ be a three-dimensional Cartesian coordinate system, then any point in the three-dimensional space can be expressed in terms of its coordinates as shown in equation 1:

$$\vec{x} = x_1\vec{i}_1 + x_2\vec{i}_2 + x_3\vec{i}_3 \tag{1}$$

Relating a series of points *x* using a scalar *u* in an affined system can be expressed as $\vec{x}_c = \underline{x}(u)$.

If the curve *c* described by $\underline{x}(u)$ lies in a plane, it is a plane curve. If not, it is a skew curve. Let $u = s$ where *s* is the length of curve arc measured from a fixed point on curve *c* described by $\underline{x}(u)$. Let $\vec{x} = x(s)$, then the derivatives of *x* are as shown in equation 2.

$$\vec{x}' = \frac{d\ x(s)}{ds}, \vec{x}'' = \frac{d^2x(s)}{ds^2}, \vec{x}''' = \frac{d^3x(s)}{ds^3} \tag{2}$$

Definitions

The following definitions are used in relating Speed–Curvature versus Cross–Trajectory Accelerations.

The principal triad is a set of orthogonal unit (orthonormal) vectors, $\vec{j}_1, \vec{j}_2, \vec{j}_3$ at point *x*.

Term $\vec{j}_1$ is tangent to the curve *c* described by *x(s)* and points in the direction of *s* increasing. It is the unit tangent vector.

Term $\vec{j}_2$ lies in the plane of vectors $\vec{j}_1$ and $\vec{j}_1' = \frac{d(\vec{j}_1)}{ds}$, and makes an acute angle with $\vec{j}_1'$. It is called the unit normal vector.

Term $\vec{j}_3$ is such that the vectors $\vec{j}_1, \vec{j}_2, \vec{j}_3$ form a right-handed triad (assuming that $\vec{j}_1' \neq 0$) . It is called the unit binormal vector.

The principal normal to the curve is the straight line that goes through point *x* and parallel to vector $\vec{j}_2$.

The binormal to the curve is the straight line that goes through point *x* and parallel to vector $\vec{j}_3$.

The normal plane is perpendicular to vector $\vec{j}_1$, including point *x*.

The osculating plane is perpendicular to vector $\vec{j}_3$.

Discretization of curve c: The Serret-Frenet Formulas

Let point *y* on curve *c* be near point *x*, then as defined in equations 3 and 4

$$\vec{x}y = \Delta\vec{x} \tag{3}$$

$$\lim_{\Delta s \to 0} \frac{\Delta\vec{x}}{\Delta s} = \vec{j}_1 = \vec{x}' \tag{4}$$

the Serret-Frenet Formulas are as follows in equation 5:

$$\begin{aligned} \vec{j}_1' &= \chi\, \vec{j}_2 \\ \vec{j}_2' &= \tau\, \vec{j}_3 - \chi\, \vec{j}_1 \\ \vec{j}_3' &= -\tau\, \vec{j}_2 \end{aligned} \tag{5}$$

where χ and τ are functions of the arc length *s* of curve *c*.

Note that $\chi = \lim_{\Delta s \to 0} \frac{\Delta\theta}{\Delta s}$ is the curvature of curve *c*, where θ is the angle between the tangents at points *x* and *y* on curve *c*. The curvature, χ, is the rate at which the tangent at point *x* rotates as *x* moves along curve *c*. The radius of curvature, ρ, is equal to the reciprocal of χ.

Note that $\tau = \lim_{\Delta s \to 0} \frac{\Delta\phi}{\Delta s}$ is the torsion of curve *c*, where ϕ is the angle between the binormials at points *x* and *y* on curve *c*. The torsion, τ, is the rate at which the binormial at point *x* rotates as *x* moves along curve *c*. The radius of torsion, σ, is equal to the reciprocal of τ.

Curvature, χ, and torsion, τ, are expressed in terms of the point definition of curve *c* in equations 6 and 7:

$$\chi = \sqrt{\vec{x}'' \cdot \vec{x}''} \tag{6}$$

$$\tau = \frac{1}{\chi^2} \vec{x}' \cdot (\vec{x}'' \times \vec{x}''') \tag{7}$$

The principal triad, $\vec{j}_1, \vec{j}_2, \vec{j}_3$, are also expressed in terms of the point definition of curve *c*: in equations 8, 9 and 10.

$$\vec{j}_1 = \vec{x}' \tag{8}$$

$$\vec{j}_2 = \frac{1}{\chi} \vec{x}'' \tag{9}$$

$$\vec{j}_3 = \frac{1}{\chi} \vec{x}' \times \vec{x}'' \tag{10}$$

Application of Differential Geometry to Mechanics

The position vector of the particle in the frame of reference defined by the Cartesian coordinate system $\underline{X} = (O, \vec{i}_1, \vec{i}_2, \vec{i}_3)$ is as defined in equation 11:

$$\vec{x} = \vec{O}x = x_1\vec{i}_1 + x_2\vec{i}_2 + x_3\vec{i}_3 \tag{11}$$

The velocity vector, $\vec{v}$, and the acceleration vector, $\vec{a}$, are defined in equations 12 and 13:

$$\begin{aligned}\vec{v} &= \frac{d\vec{x}}{dt} \\ &= \frac{d\ x_1}{dt}\vec{i}_1 + \frac{d\ x_2}{dt}\vec{i}_2 + \frac{d\ x_3}{dt}\vec{i}_3 \\ &= \dot{x}_1\vec{i}_1 + \dot{x}_2\vec{i}_2 + \dot{x}_3\vec{i}_3\end{aligned} \tag{12}$$

$$\begin{aligned}\vec{a} &= \frac{d\ \vec{v}}{dt} = \frac{d^2\vec{x}}{dt^2} \\ &= \frac{d^2\ x_1}{dt^2}\vec{i}_1 + \frac{d^2\ x_2}{dt^2}\vec{i}_2 + \frac{d^2\ x_3}{dt^2}\vec{i}_3 \\ &= \ddot{x}_1\vec{i}_1 + \ddot{x}_2\vec{i}_2 + \ddot{x}_3\vec{i}_3\end{aligned} \tag{13}$$

Relating the velocity and acceleration vectors to length of curve, *s*, and the principal triad in equations 14 and 15.

$$\vec{v} = \dot{s}\ \vec{j}_1 \tag{14}$$

$$\vec{a} = \ddot{s}\ \vec{j}_1 + \chi\ \dot{s}^2\ \vec{j}_2 \tag{15}$$

The case of a planar horizontal curve with radius *R* and constant speed is described in equation set 16:

$$\begin{aligned}&\dot{s} = v_t = cst \\ &x(t=0) = \begin{pmatrix} R \\ 0 \\ 0 \end{pmatrix} \\ &s(t) = \theta(t)\ R = v_t\ t \\ &\vec{x}(t) = \cos(\theta(t))\ \vec{i}_1 + \sin(\theta(t))\ \vec{i}_2\end{aligned} \tag{16}$$

The unit tangent and normal vectors of the principal triad are shown in equations 17 and 18:

$$\begin{aligned}\vec{j}_1 &= \vec{x}' \\ &= -\frac{\sin(\frac{s}{R})}{R}\vec{i}_1 + \frac{\cos(\frac{s}{R})}{R}\vec{i}_2\end{aligned} \tag{17}$$

$$\begin{aligned}\vec{j}_2 &= \frac{1}{\chi}\vec{x}'' \\ &= -\frac{\cos(\frac{s}{R})}{R^2}\vec{i}_1 - \frac{\sin(\frac{s}{R})}{R^2}\vec{i}_2\end{aligned} \tag{18}$$

The velocity and acceleration vectors are given by equations 19 and 20:

$$\vec{v} = \dot{s}\ \vec{j}_1 \Rightarrow \vec{v} = v_t\ \vec{j}_1 \tag{19}$$

$$\vec{a} = \ddot{s}\ \vec{j}_1 + \chi\ \dot{s}^2\ \vec{j}_2 \Rightarrow \vec{a} = \frac{v_t^{\,2}}{R}\ \vec{j}_2 \tag{20}$$

The previous equations were used to generate a graph of Radial Acceleration versus Radius of Curvature given a set of six velocities as shown in figure 1.

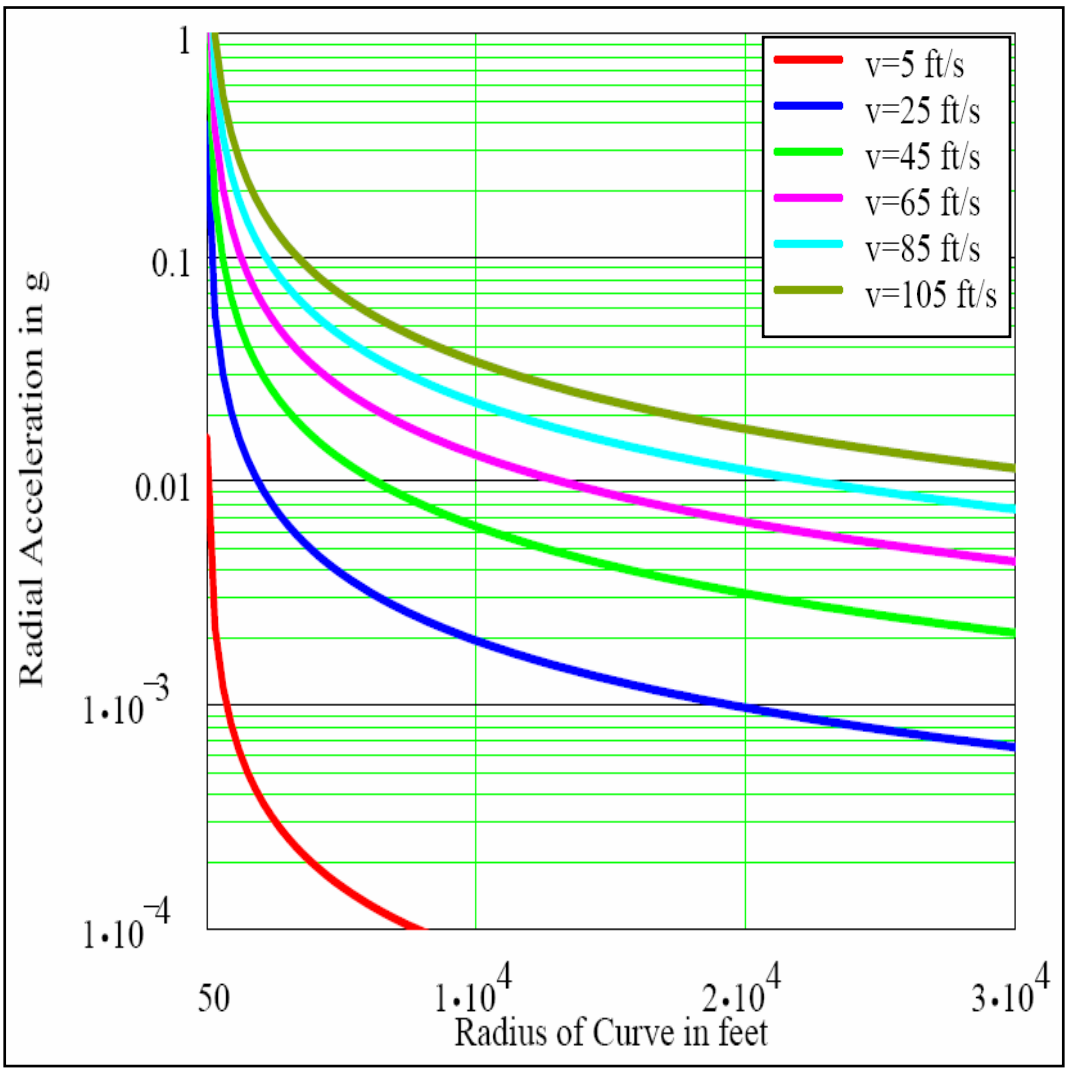

Figure 1. Graph. Radial Acceleration versus Radius of Curvature given a set of six velocities. (1 ft/s = 0.3048 m/s, 1 ft = 0.3048 m)

Design Equation for Cross Slope (Super Elevation)

Equation 21 shows the basic curve formula in both metric and US customary unit. It is arrived from the laws of mechanics governing vehicle motion on a curve where the moving vehicle is treated as a point mass.

Metric	US Customary
$\frac{0.01e+f}{1-0.01ef} = \frac{v^2}{gR} = \frac{0.0079V^2}{R} = \frac{V^2}{127R}$	$\frac{0.01e+f}{1-0.01ef} = \frac{v^2}{gR} = \frac{0.067V^2}{R} = \frac{V^2}{15R}$

where:
e = rate of roadway superelevation, percent;
f = side friction (demand) factor;
v = vehicle speed, m/s;
g = gravitational constant, 9.81 m/s^2;
V = vehicle speed, km/h;
R = radius of curve, m
	where:
	e = rate of roadway superelevation, percent;
	f = side friction (demand) factor;
	v = vehicle speed, ft/s;
	g = gravitational constant, 32.2 ft/s^2;
	V = vehicle speed, mph;
	R = radius of curve, ft

(21)

Relationship between Vehicle Roll and Cross Slope

Figure 2 shows an idealized vehicle model with corresponding vehicle mass and weight, left and right side springs, left and right wheel (spring) displacement, mass of vehicle radial force as a result of radial acceleration, spring forces as a function of left and right spring displacement and spring rates, radial friction forces at tires due to radial acceleration of vehicle, resulting vehicle roll, and pavement cross slope.

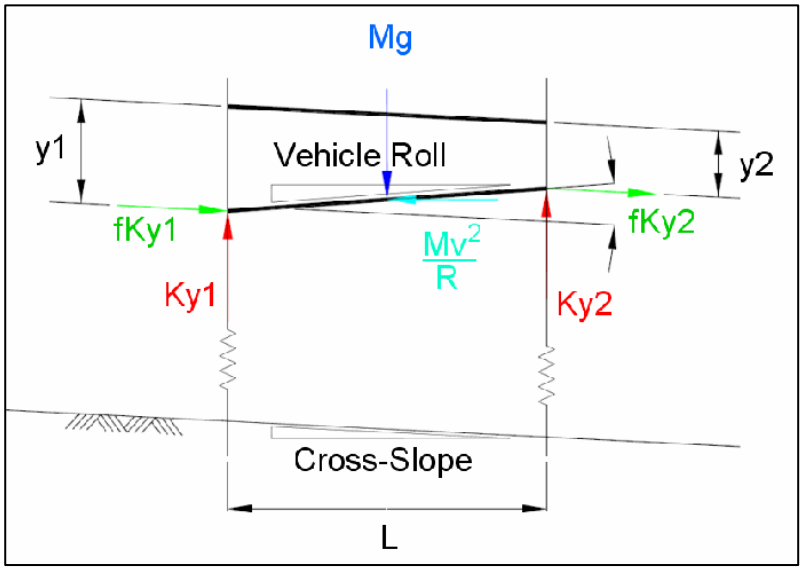

Figure 2. Illustration. Relationship between vehicle roll and pavement cross slope.

DATABASE APPROACH

The DHMS database contains 3-D body accelerations, 3-D normal accelerations, vehicle pitch and roll and heading, and pavement cross slope and grade data. The database was generated using FHWA's DHM system.

Three types of roadway sites with varying alignment characteristics were selected to include differing levels of cross slope, grade, horizontal, and vertical alignments. For each site, multiple runs were made at varying speed profiles providing varying levels of body and normal accelerations. For each site, the estimations of cross slope, horizontal and vertical alignments were consistent among runs.

The DHM database thus provides a wealth of accurate data as to the attitude of the vehicle and of the vehicle to the roadway. This data provides the resources to define a database approach to determining what parameters are affected by the roll and pitch of a vehicle. Given 3-D body accelerations, 3-D normal accelerations, vehicle pitch and roll and heading inertial Navigation unit (INU) data, and pavement cross slope and grade from the DHMS database, the basic approach is:

- Compute error estimates in acceleration due to changes in orientation of accelerometer based on 3-D body accelerations, 3-D normal accelerations, vehicle pitch and roll.
- Relate errors to cross slope, grade, and heading, and the rates of change in cross slope, grade, and heading.
- Compute corrected and estimated inertial profiles based on vertical accelerations normal to the trajectory of the vehicle and vertical accelerations with respect to body of the vehicle in a tilted orientation, respectively.
- Compute propagated differences in output metrics between corrected and uncorrected estimated inertial profiles.

Acceleration Correction Model

Vertical accelerations recorded by the DHM system are to be corrected for DHM vehicle pitch and roll. This section presents the derivation of the accelerometer correction model.

Figure 3 shows the coordinate system relating the Normal and Body Cartesian coordinates.

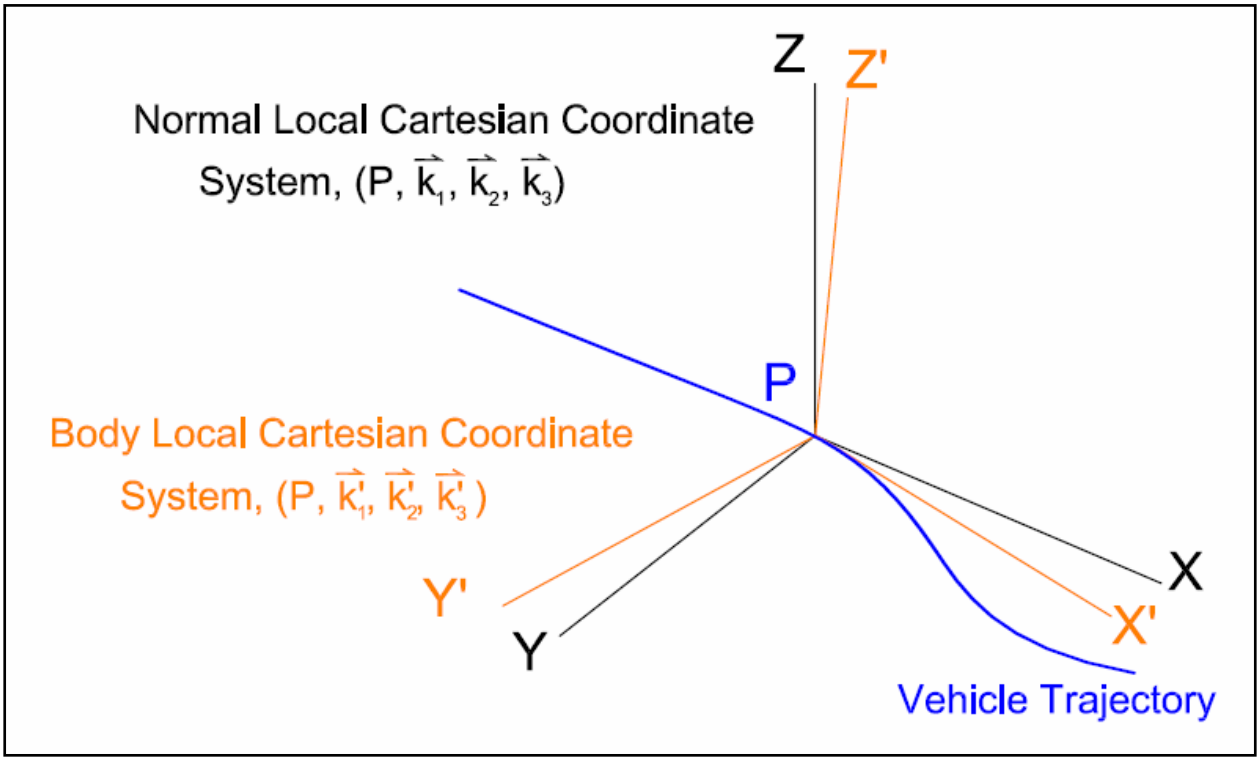

Figure 3. Illustration. Normal and Body local Cartesian coordinate system relationship.

Where the parameters are defined as:

- X = normal horizontal along trajectory track.
- Y = normal horizontal cross trajectory track axis.
- Z = normal vertical axis.
- X' = body horizontal along trajectory axis.
- Y' = body horizontal cross trajectory axis.
- Z' = body vertical axis.

Given X', Y', and Z' accelerations, the correction model is required to provide Z acceleration along the normal vertical axis. Derivation of the acceleration correction model is presented in this section.

The normal triad at point P is defined in a local Cartesian coordinate system $X = (P, \vec{k}_1, \vec{k}_2, \vec{k}_3)$, where P is a point on the vehicle trajectory.

If $\vec{v} = \begin{pmatrix} x \\ y \\ z \end{pmatrix}$ is a unit vector in a normal triad along a vehicle trajectory, where the x direction is horizontal along-trajectory parallel to vector $\vec{k}_1$, the y direction is horizontal cross-trajectory parallel to vector $\vec{k}_2$, and the z direction is vertical parallel to vector $\vec{k}_3$, then $\|\vec{v}\| = 1$.

The direction cosines of vector $\vec{v}$ are defined as follows in equation set 22:

$$\begin{cases} \cos\alpha = \dfrac{\vec{v}\cdot\vec{k}_1}{\|\vec{v}\|} = \begin{pmatrix} x \\ y \\ z \end{pmatrix} \cdot \begin{pmatrix} 1 \\ 0 \\ 0 \end{pmatrix} = x = l_{\vec{v}} \\ \cos\beta = \dfrac{\vec{v}\cdot\vec{k}_2}{\|\vec{v}\|} = \begin{pmatrix} x \\ y \\ z \end{pmatrix} \cdot \begin{pmatrix} 0 \\ 1 \\ 0 \end{pmatrix} = y = m_{\vec{v}} \\ \cos\gamma = \dfrac{\vec{v}\cdot\vec{k}_3}{\|\vec{v}\|} = \begin{pmatrix} x \\ y \\ z \end{pmatrix} \cdot \begin{pmatrix} 0 \\ 0 \\ 1 \end{pmatrix} = z = n_{\vec{v}} \end{cases} \tag{22}$$

Note that $\|\vec{v}\| = \sqrt{x^2 + y^2 + z^2} = 1$, or $\cos\alpha^2 + \cos\beta^2 + \cos\gamma^2 = 1$.

Changing coordinate systems from normal to body triads, where body triad, $\underline{X' = (P, \vec{k}_1', \vec{k}_2', \vec{k}_3')}$, is defined with respect to the body orientations caused by the pitch and roll angles, the coordinates of the unit vector $\vec{v}$ are defined as shown in equation 25:

$$\begin{bmatrix} x' \\ y' \\ z' \end{bmatrix} = \begin{bmatrix} l_{\vec{k}_1'} & m_{\vec{k}_1'} & n_{\vec{k}_1'} \\ l_{\vec{k}_2'} & m_{\vec{k}_2'} & n_{\vec{k}_2'} \\ l_{\vec{k}_3'} & m_{\vec{k}_3'} & n_{\vec{k}_3'} \end{bmatrix} \begin{bmatrix} x \\ y \\ z \end{bmatrix} \tag{23}$$

From body to normal triads translation, equation 24 is:

$$\begin{bmatrix} x \\ y \\ z \end{bmatrix} = \begin{bmatrix} l_{\vec{k}_1'} & l_{\vec{k}_2'} & l_{\vec{k}_3'} \\ m_{\vec{k}_1'} & m_{\vec{k}_2'} & m_{\vec{k}_3'} \\ n_{\vec{k}_1'} & n_{\vec{k}_2'} & n_{\vec{k}_3'} \end{bmatrix} \begin{bmatrix} x' \\ y' \\ z' \end{bmatrix} \tag{24}$$

Figure 4 shows the vehicle subject to pitch and roll and corresponding parameters defining this condition.

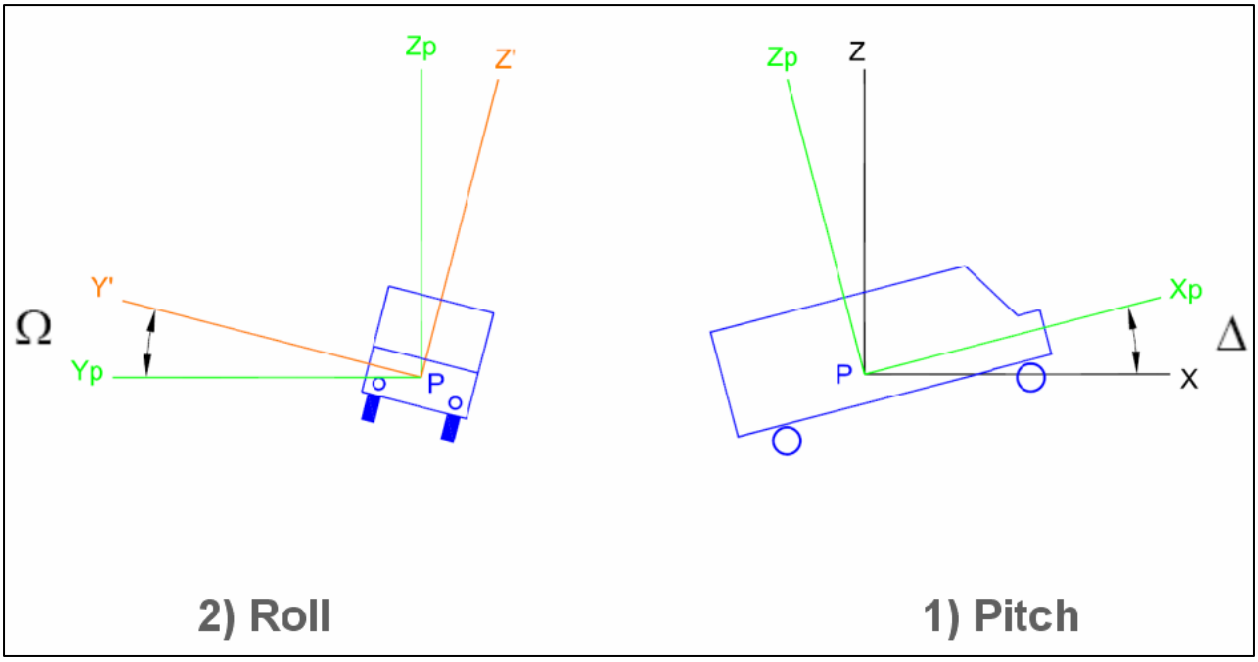

Figure 4. Vehicle subjected to pitch and roll parameter definition.

When the pitch, Δ, and roll, Ω, angular rotations are applied, two changes in coordinate systems are performed. The first coordinate change corresponds to the rotation with respect to the *y* axis, by a pitch angle between *x* and x^p as shown in matrix equation 25:

$$\begin{bmatrix} x^p \\ y^p \\ z^p \end{bmatrix} = \begin{bmatrix} \cos\Delta & 0 & \sin\Delta \\ 0 & 1 & 0 \\ -\sin\Delta & 0 & \cos\Delta \end{bmatrix} \begin{bmatrix} x \\ y \\ z \end{bmatrix} \tag{25}$$

The second coordinate change, equation 26, corresponds to the rotation with respect to the x^p axis, by a roll angle between y^p and y':

$$\begin{bmatrix} x' \\ y' \\ z' \end{bmatrix} = \begin{bmatrix} 1 & 0 & 0 \\ 0 & \cos\Omega & \sin\Omega \\ 0 & -\sin\Omega & \cos\Omega \end{bmatrix} \begin{bmatrix} x^p \\ y^p \\ z^p \end{bmatrix} \tag{26}$$

Expressing x', y', z' in terms of x, y, z: in matrix equation 27:

$$\begin{bmatrix} x' \\ y' \\ z' \end{bmatrix} = \begin{bmatrix} 1 & 0 & 0 \\ 0 & \cos\Omega & \sin\Omega \\ 0 & -\sin\Omega & \cos\Omega \end{bmatrix} \begin{bmatrix} \cos\Delta & 0 & \sin\Delta \\ 0 & 1 & 0 \\ -\sin\Delta & 0 & \cos\Delta \end{bmatrix} \begin{bmatrix} x \\ y \\ z \end{bmatrix} \tag{27}$$

Performing the matrix multiplication results in matrix equation 28:

$$\begin{bmatrix} x' \\ y' \\ z' \end{bmatrix} = \begin{bmatrix} \cos\Delta & 0 & -\sin\Delta \\ -\sin\Delta\sin\Omega & \cos\Omega & -\cos\Delta\sin\Omega \\ \sin\Delta\cos\Omega & \sin\Omega & \cos\Delta\cos\Omega \end{bmatrix} \begin{bmatrix} x \\ y \\ z \end{bmatrix} \tag{28}$$

Inversely, equation 29 is:

$$\begin{bmatrix} x \\ y \\ z \end{bmatrix} = \begin{bmatrix} \cos\Delta & -\sin\Delta\sin\Omega & \sin\Delta\cos\Omega \\ 0 & \cos\Omega & \sin\Omega \\ -\sin\Delta & -\cos\Delta\sin\Omega & \cos\Delta\cos\Omega \end{bmatrix} \begin{bmatrix} x' \\ y' \\ z' \end{bmatrix} \tag{29}$$

The apparent direction cosines of x', y', z' with respect to x, y, z and corresponding to a pitch rotation first and a roll rotation second are shown in matrix equation 30:

$$\begin{bmatrix} l_{\vec{k}_1'} & m_{\vec{k}_1'} & n_{\vec{k}_1'} \\ l_{\vec{k}_2'} & m_{\vec{k}_2'} & n_{\vec{k}_2'} \\ l_{\vec{k}_3'} & m_{\vec{k}_3'} & n_{\vec{k}_3'} \end{bmatrix} = \begin{bmatrix} \cos\Delta & 0 & -\sin\Delta \\ -\sin\Delta\sin\Omega & \cos\Omega & -\cos\Delta\sin\Omega \\ \sin\Delta\cos\Omega & \sin\Omega & \cos\Delta\cos\Omega \end{bmatrix} \tag{30}$$

Intuitively, the direction cosine between x and x', $l_{\vec{k}_1'}$, is equal to the cosine of the pitch angle, Δ, and the direction cosine between y and y', $m_{\vec{k}_2'}$, is equal to the cosine of the roll angle, Ω. Based on the basic definition, they are equal to:

$$\begin{cases} l_{\vec{k}_1'} = \vec{k}_1' \cdot \vec{k}_1 = \cos\Delta \\ m_{\vec{k}_2'} = \vec{k}_2' \cdot \vec{k}_2 = \cos\Omega \end{cases} \tag{31}$$

Other direction cosines are not intuitively expressed.

The direction cosines of interest in this study are those related to the normal vertical axis, defined in the body triad system in equation 32:

$$\begin{bmatrix} n_{\bar{k}_1'} \\ n_{\bar{k}_2'} \\ n_{\bar{k}_3'} \end{bmatrix} = \begin{bmatrix} -\sin\Delta \\ -\cos\Delta\sin\Omega \\ \cos\Delta\cos\Omega \end{bmatrix} \tag{32}$$

The equivalent normal acceleration, expressed in terms of the body accelerations, is defined in equation 33:

$$a_z = -\sin\Delta\, a_{x'} - \cos\Delta\sin\Omega\, a_{y'} + \cos\Delta\cos\Omega\, a_{z'} \tag{33}$$

The paired figures 5 and 6 on the next page show the corrected acceleration given two sets of horizontal x and y direction accelerations, and a constant vertical acceleration of 1g at pitch angles ranging from 0 – 10 degrees and roll angles ranging from 0 – 10 degrees.

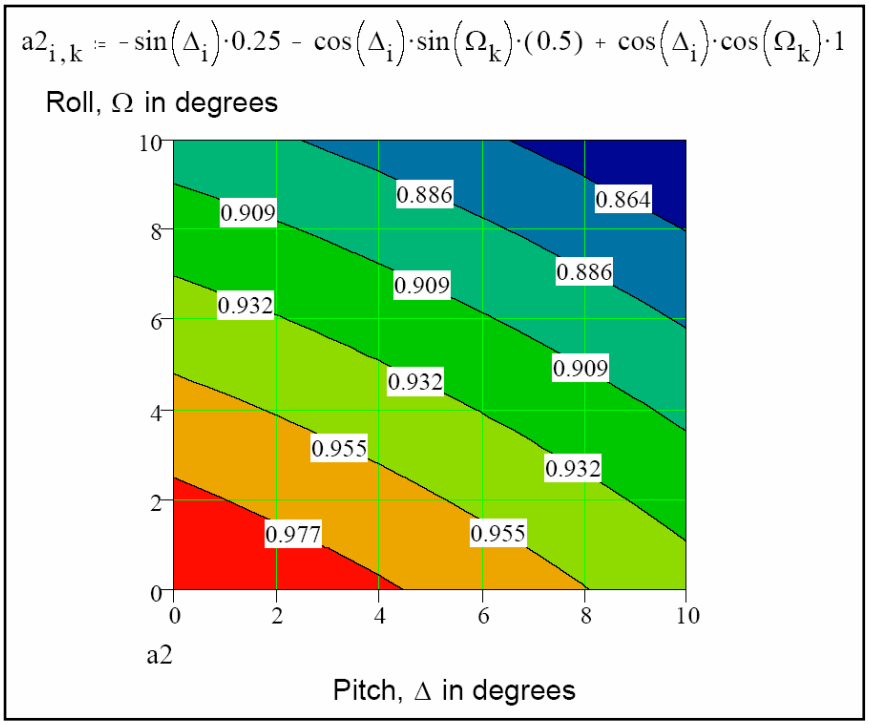

Figure 5. Isochart. Corrected normal acceleration given first set of measured body acceleration in three dimensions with pitch and roll.

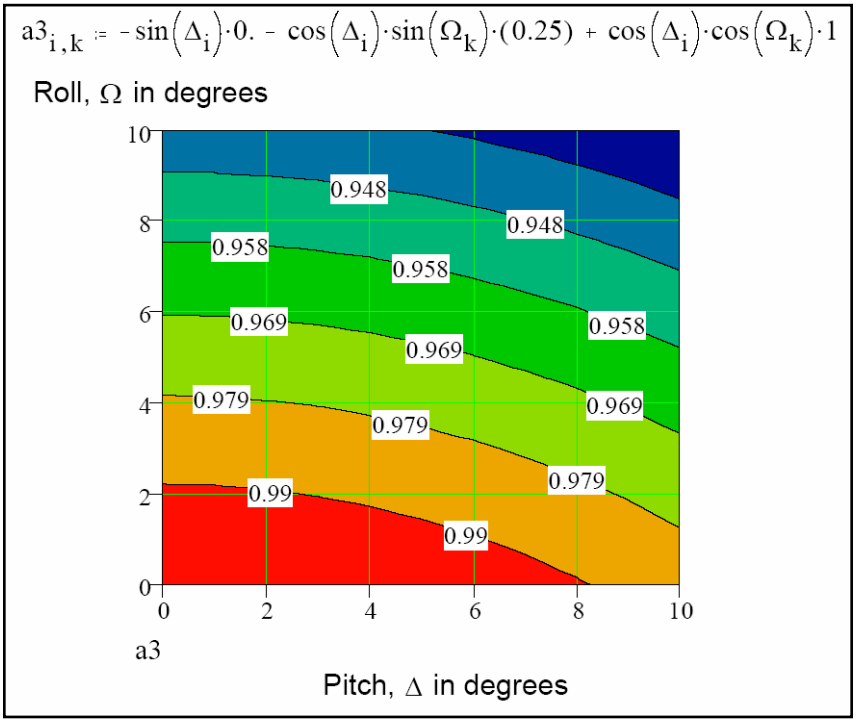

Figure 6. Isochart. Corrected normal acceleration given second set of measured body acceleration in three dimensions with pitch and roll.

Figures 7 and 8 show the histograms of the measured normal minus the corrected normal acceleration in g's for one of the two-lane rural roads and the one four-lane divided highway. Bin size is 0.002g for both histograms. The histogram for the two-lane road has a wider distribution than for the four-lane road as there are more roadway and vehicle operations features causing a greater frequency and level of accelerations and resulting pitch and roll changes.

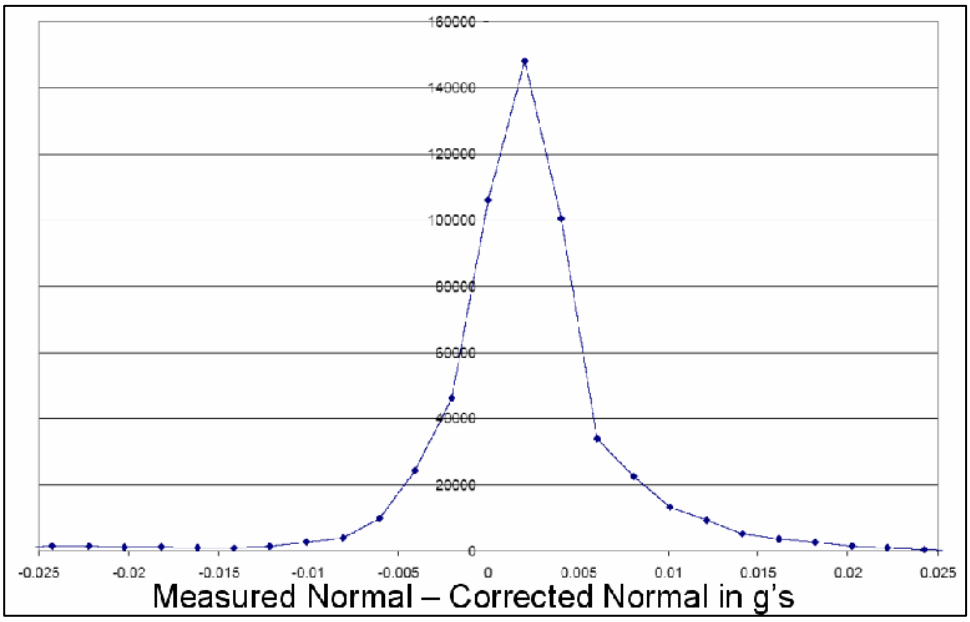

Figure 7. Histogram. Measured normal minus the corrected normal acceleration in g's for one of the two-lane rural roads .

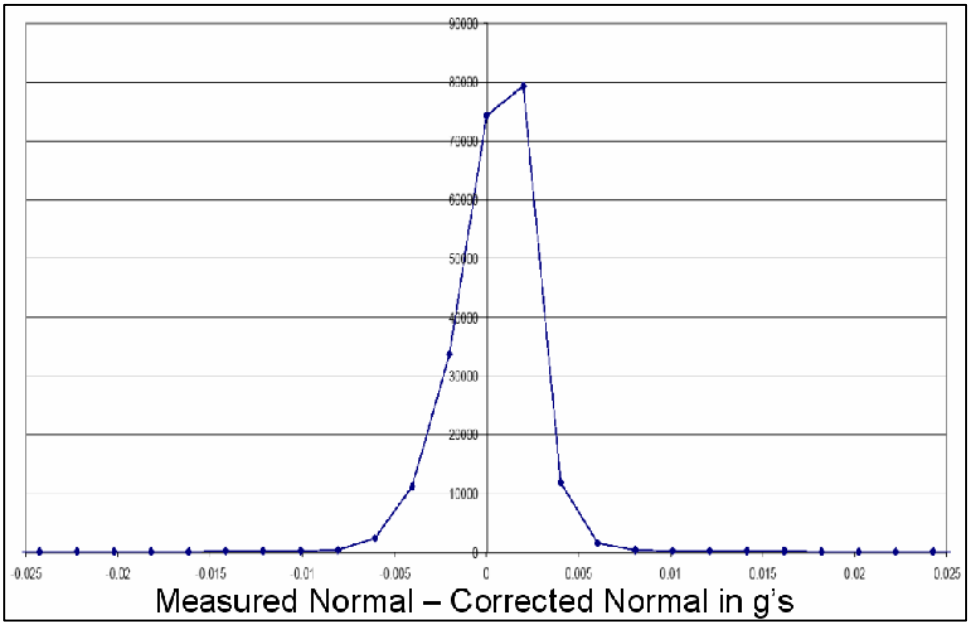

Figure 8, Histogram. Measured normal minus the corrected normal acceleration in g's for the four-lane divided highway.

Parameter Categorization/Typing

In order to help explore and compare geometry alignment and operational characteristics between sites and repeated runs, the absolute values of the alignment and operation characteristics were categorized into three categories – low (0), medium (1), and high (2),. The threshold values for this parameter categorization/typing are shown in table 1. This categorization representation of the data also permits an exploration of the distribution of the variables within the sampled space. This categorization can be conducted at different roadway section lengths as an aid in determining the appropriate section length to be used in the analysis.

Table 1. Threshold values for roadway/operation parameter categorization/typing.

Parameter	Low (0)	Medium (1)	High (2)
Speed (km/h (mi/h))	32.2 - 48.3 (20 - 30)	48.3 - 64.4 (30 - 40)	64.4+ (40+)
Roughness (m/km (im/mi))	0.47 - 1.34 (30 - 85)	1.34 - 2.13 (85 - 135)	2.13+ (135+)
Degree-of-curvature (DOC)	< 4 degrees	4 - 8 degrees	> 8 degrees
Grade (%)	< 2 %	2 - 4 %	> 4 %
Cross Slope (%)	< 3 %	3 - 5 %	>5 %
DOC / Cross Slope	< 1.5	1.5 - 3.0	> 3.0

VEHICLE/ROAD SIMULATION APPROACH

A data matrix composed of a sample of actual site data will not contain all possible situations encountered in the larger universe of the real world. Secondly, in the real world, it can be very difficult to isolate the compounding effects of more than one parameter on the attitude and motion of a vehicle as a result of both roadway alignment and roughness in combination with vehicle operator actions. Thus it can be difficult to identify a precise set of conditions under which an expected error of a known quantity can be determined for establishing criteria under which roughness accuracy and precision requirements can be relaxed. A vehicle/road simulation approach presents a scenario where the input parameters can be precisely controlled and the corresponding effects easily measured. Such an approach is outlined here.

Given vehicle characteristics, cross slope, vertical profile and horizontal alignments, and vehicle speed profile:

- Produce 3-D body accelerations, 3-D normal accelerations, vehicle pitch and roll using simulation software.
- Compute error estimates in acceleration due to changes in orientation of accelerometer based on 3-D body accelerations, 3-D normal accelerations, vehicle pitch and roll.
- Relate errors to cross slope, grade, and heading, and the rates of change in cross slope, grade, and heading.
- Compute corrected and estimated inertial profiles based on vertical accelerations normal to trajectory of vehicle and vertical accelerations with respect to body of vehicle in tilted orientation.

- Compute propagated differences in output metrics between corrected and uncorrected estimated inertial profiles.

Description of System

The system components used in a Vehicle/Road Simulation approach consists of a sensor base, coordinate system, an acceleration measurement error model, and an inertial profiling model.

Sensor Base

The sensor base consists of a 1-D accelerometer, laser height sensor, and a Distance Measurement Instrument (DMI). Figure 9 illustrates the sensor base. For the height measurement laser, dot size, range, resolution, and noise level are the properties of interest. For the accelerometer, g range, signal to noise ratio, and frequency response are important. For the DMI, resolution level determines sampling interval for spatial based data collection systems and interval accuracy for temporal based data collection systems.

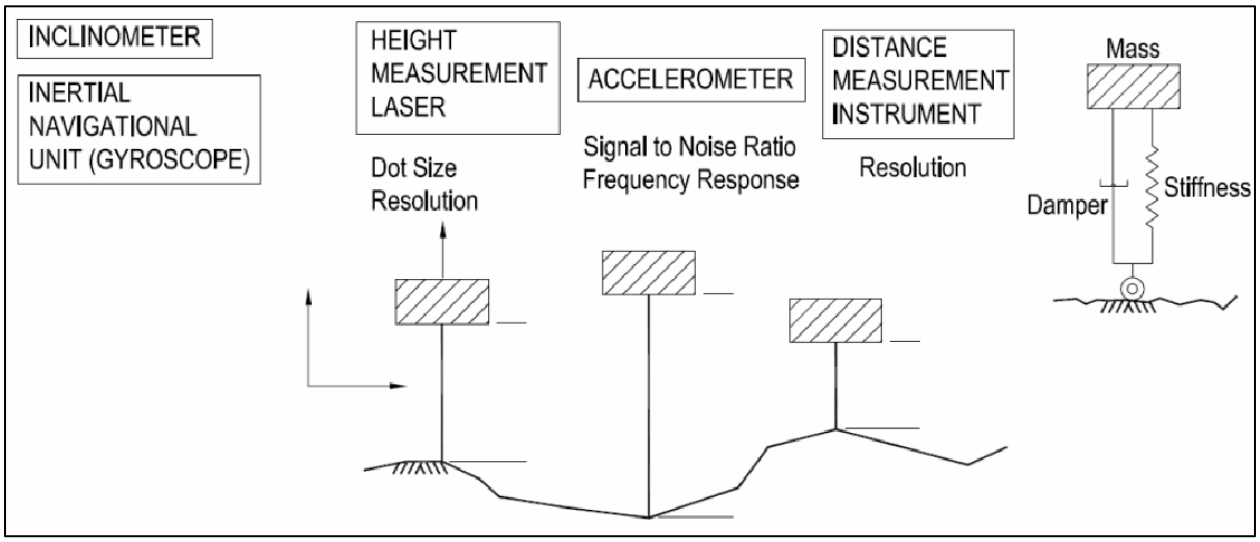

Figure 9. Illustration. Sensor base for inertial profiling vehicle/road simulation.

Coordinate System

The coordinate system for a vehicle/road simulation model is shown in figure 10. The figure shows the ideal local Cartesian coordinate system and the apparent local vehicle coordinate system. Ideal local Cartesian system squared up to the stationing system in which normal accelerations are measured with respect to vehicle trajectory (one vertical, one horizontal along trajectory, and one horizontal across trajectory) are used in the computation of corrected profile elevations. Vertical direction never changes in this coordinate system. Apparent local vehicle system squared up to the horizontal plane of the vehicle in which body accelerations measured are used in computation of *Estimated* profile elevations

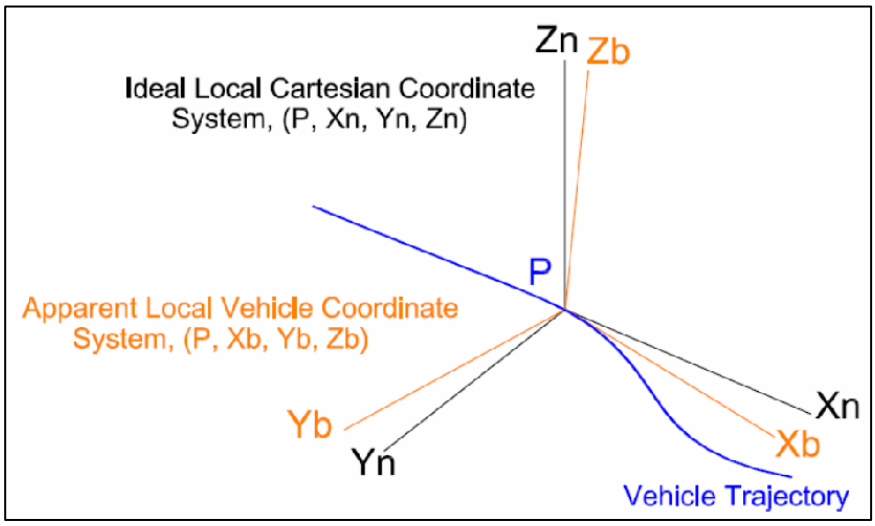

Figure 10. Illustration. Vehicle/road simulation model coordinate system.

The parameters in the figure are defined as:

- Xn = normal horizontal along trajectory track axis.
- Yn = normal horizontal cross trajectory track axis.
- Zn = normal vertical axis.
- Xb = body horizontal along trajectory axis.
- Yb = body horizontal cross trajectory axis.
- Zb = body vertical axis.

Acceleration Measurement Error Model

Acceleration measurement error model is derived in three-dimensions from violation of the one-dimension model assumptions. Equation 34 shows the acceleration error model:

$$\begin{aligned} \varepsilon &= -g && (1 - \cos\phi) \\ -a_{\text{Normal Vertical}} & && (1 - \cos\phi_z) \\ +a_{\text{Normal Horizontal Along Trajector}} & && \cos\phi_x \\ +a_{\text{Normal Horizontal Cross Trajectoy}} & && \cos\phi_y \end{aligned} \tag{34}$$

Where ϕ is the angle between the sensitive axis of the accelerometer and the true normal vertical direction. If ϕ does not change with time, there is no error. In this study, this term is neglected. Terms $\cos\phi_x$, $\cos\phi_y$, and $\cos\phi_z$ are the direction cosines between the ideal local Cartesian (Normal) and apparent local vehicle (Body) coordinate systems. Note that ϕ_x and ϕ_y are related to the pitch and roll angles, respectively. The direction angles are shown in figure 11.

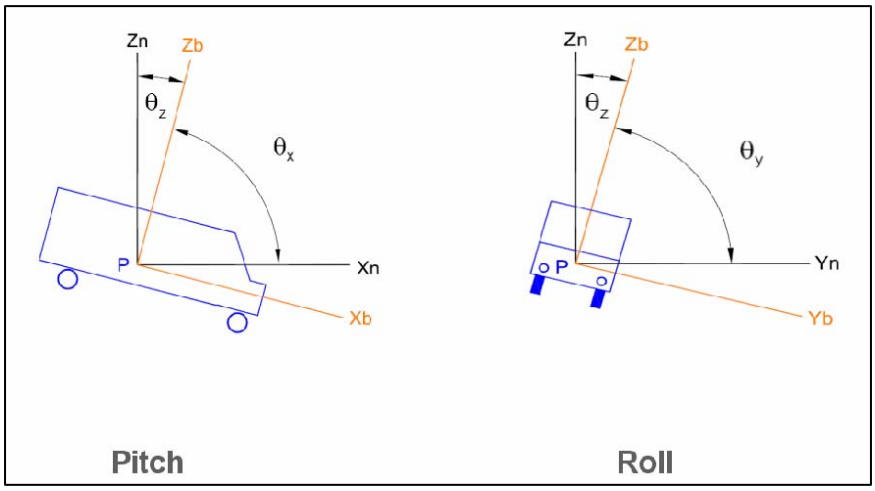

Figure 11. Illustration. Direction angles due to pitch and roll related to the two coordinate systems.

Inertial Profiling Model

The inertial profiling model is shown in figure 12. The profile computation algorithm computes the profile from one spatial profile point (i) to the next profile point (i+1). In the figure, this is a profile computation from graph point 1 to graph point 5, considering the computational components shown in the illustration. P is the profile measurement, H is the laser height measurements, a_i is the accelerometer measurement, v is vehicle speed, and dx is the spatial interval over which the profile is computed.

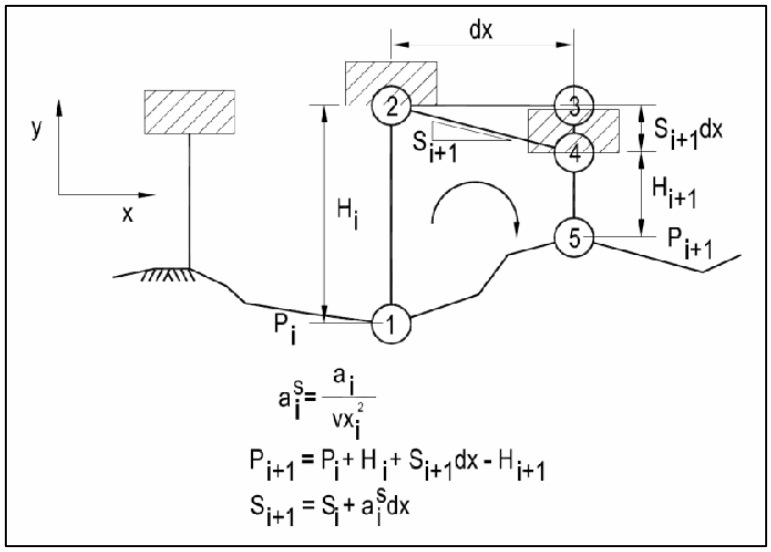

Figure 12. Illustration. Inertial profile model computational steps.

Output Metrics

Figure 13 presents the flow chart of the output from the inertial profile model through the standard filter processes followed by computation of metrics for subsequent analysis. Filter process is described in the following report sections.

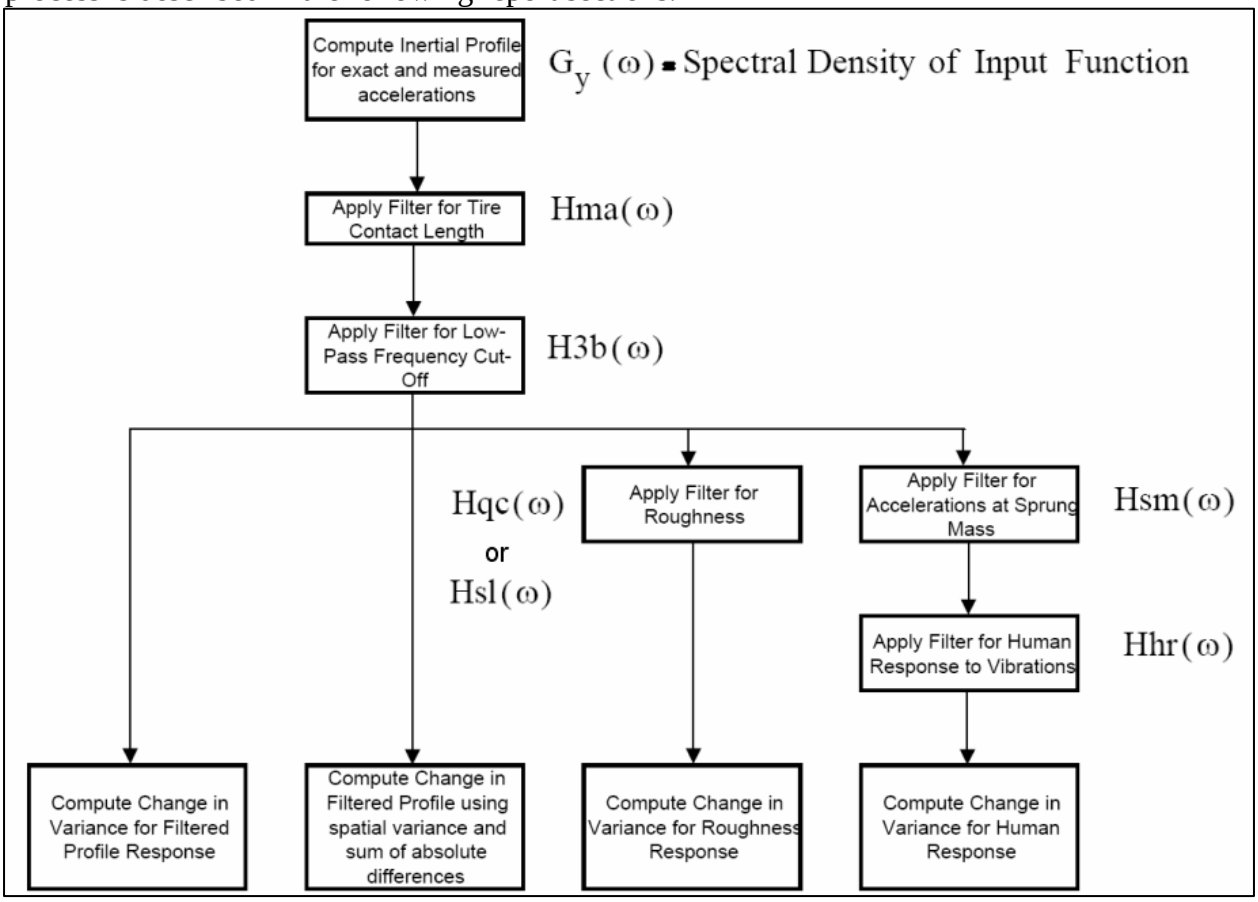

Figure 13. Flow chart. Flow chart of computational procedures and the resulting output metrics.

Differences in Frequency Response

Differences in frequency response is defined in equation 35:

$$\sigma^2 = \int_0^{\infty} (|H(\omega)|)^2 \cdot G_y(\omega)\, d\omega \qquad (35)$$

where $Gy(\omega)$ = spectral density of input function
$H(\omega) = \prod_i H_i(\omega)$ = combined response filter
σ^2 = mean square statistic or variance

Differences in Filtered Profiles

Equation 36 presents the computation of the metric for differences in filtered profiles.

$$SAD = \frac{\sum_{i=1}^{N} \left| (y_i)^{corrected} - (y_i)^{estimated} \right|}{N} \tag{36}$$

where $(y_i)^{corrected}$ = profile elevations estimated with corrected accelerations and heights
$(y_i)^{estimated}$ = profile elevations estimated with measured accelerations and heights
SAD = Sum of Absolute Differences

Frequency Response Functions

Frequency response functions include the 1) tire contact length filter, 2) the low-pass profile filter, 3) the Quarter-Car filter (IRI), and 4) the human response filter. Each of these is described in the following sections.

Moving Average Filter:

The frequency response of a moving average filter is defined in equation 37.

$$Hma(\omega, b) = \frac{\sin\left(\frac{\omega \cdot b}{2}\right)}{\frac{\omega \cdot b}{2}} \tag{37}$$

where b = base length of moving average
ω = circular frequency = 2pf

For a given sample rate S, and base length b of the moving average filter, a frequency response plot of the moving average filter for frequencies ranging from 0 to S/2 on the abscissa and the magnitude of Hma on the ordinate as shown in figure 14.

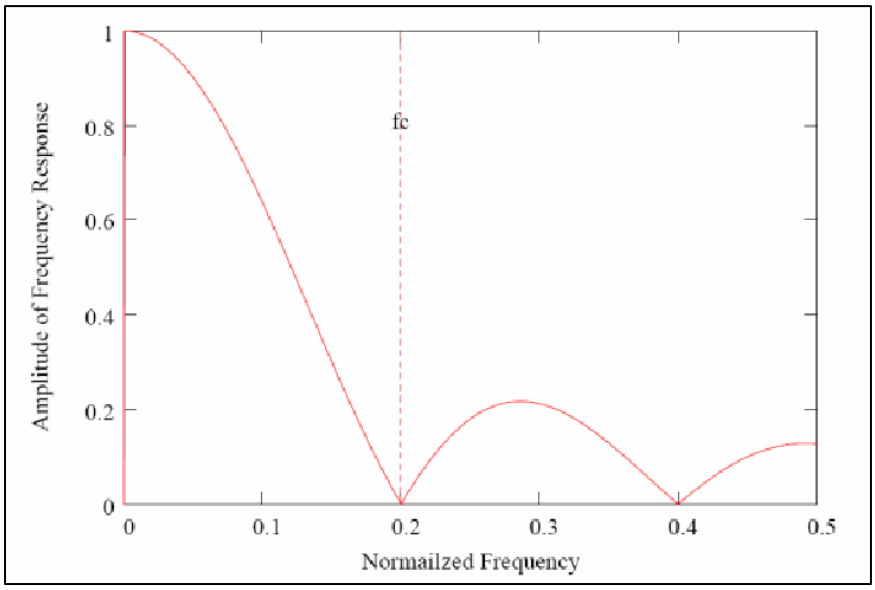

Figure 14. Graph. Frequency response of moving average filter.

Butterworth Filter:

The frequency response of a Butterworth filter is defined in equations 38 and 39.

$$\omega c := 2 \cdot \pi \cdot \frac{WC}{SR} \tag{38}$$

where SR = sampling rate in samples per distance interval
WC = filter breakpoint in cycles per distance interval

$$\Omega := \tan\left(\frac{\omega c}{2}\right) \tag{39}$$

The third order Butterworth filter in the s-plane is shown in equation 40.

$$Ha(s) := \left(\frac{1}{s + 1}\right) \cdot \left(\frac{1}{s^2 + s + 1}\right) \tag{40}$$

Using the bilinear transformation, the third order Butterworth filter in the complex z-plane is defined in equation 41.

$$H3b(z) := Ha\left[\frac{z - 1}{\Omega \cdot (z + 1)}\right] \tag{41}$$

The amplitude of and phase of frequency response of the Butterworth filter is shown in figure 15.

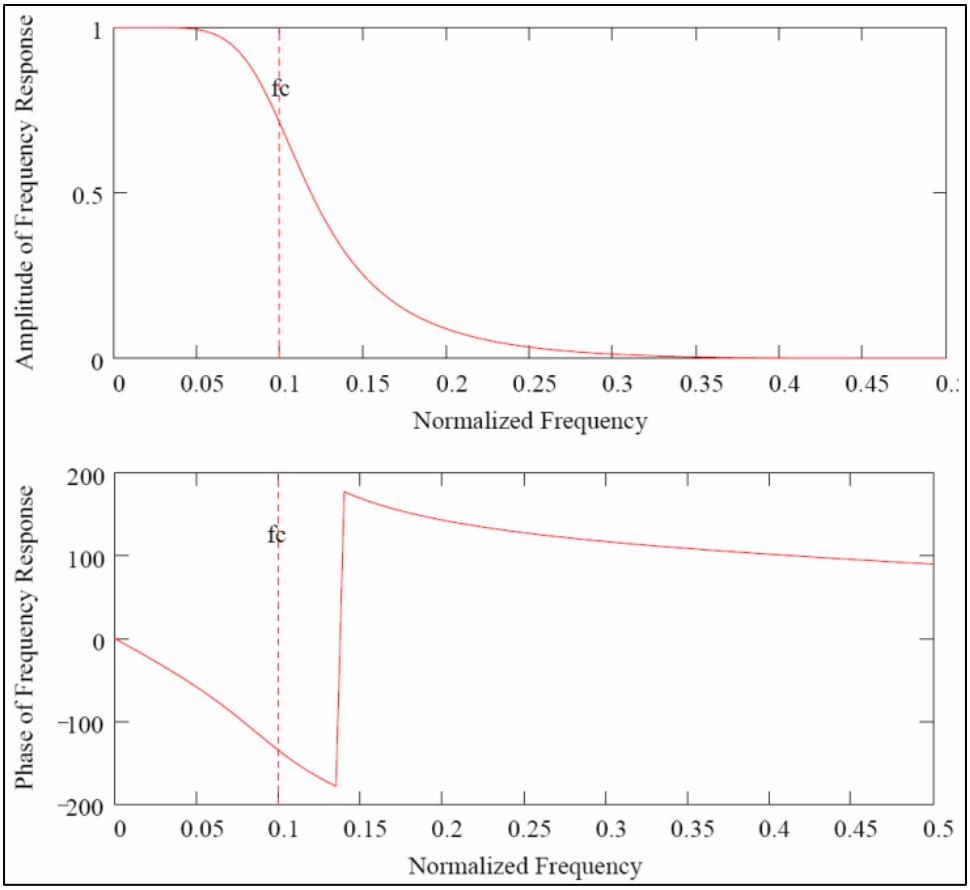

Figure 15. Graph. Frequency response of third order Butterworth filter.

The Butterworth filter as compared to the moving average filter ???

Quarter-Car Model:

The Quarter-Car model uses the computed inertial profile to calculate a vehicle response. The Quarter-Car model and corresponding response functions are presented in a series of figures 16 through 21. Three model components provided are the 1) relative motion between sprung and unsprung masses relative to the input road profile elevations shown in figures 16 and response function in figure 17, 2) relative slope of motion between sprung and unsprung masses relative to the input road profile slopes shown in figures 18 and response function in figure 19, and 3) acceleration of sprung mass relative to input road profile slope of elevations shown in figures 20 and response function in figure 21. The Quarter-Car Model parameters are well established by standards for usage in the Ride Quality Index named the International Ride Index (IRI).

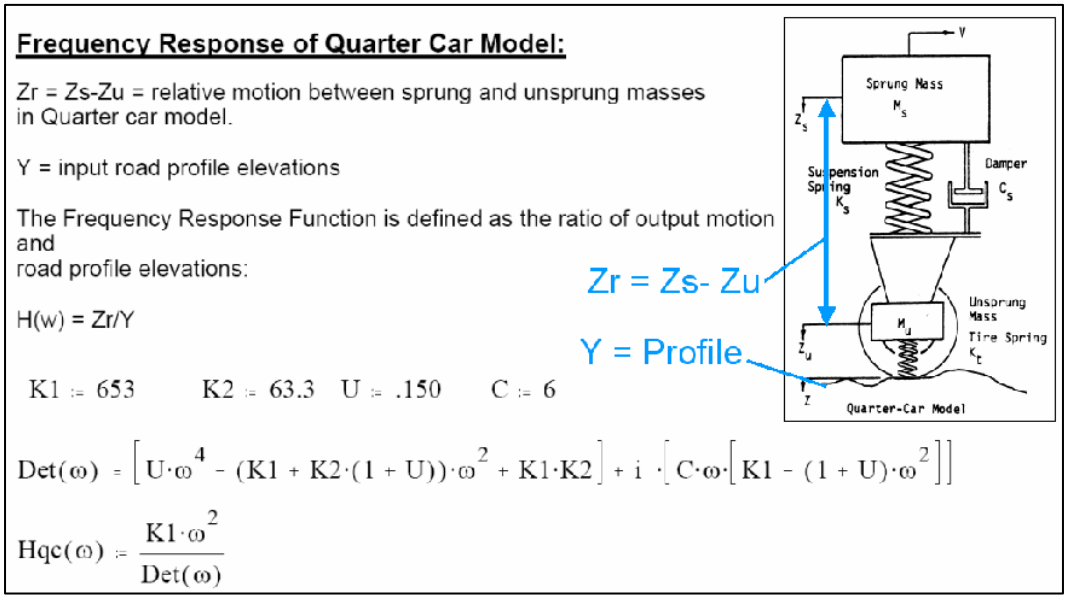

Figure 16. Illustration. Quarter-Car model response function showing displacement relative to road profile (Zr/Y).

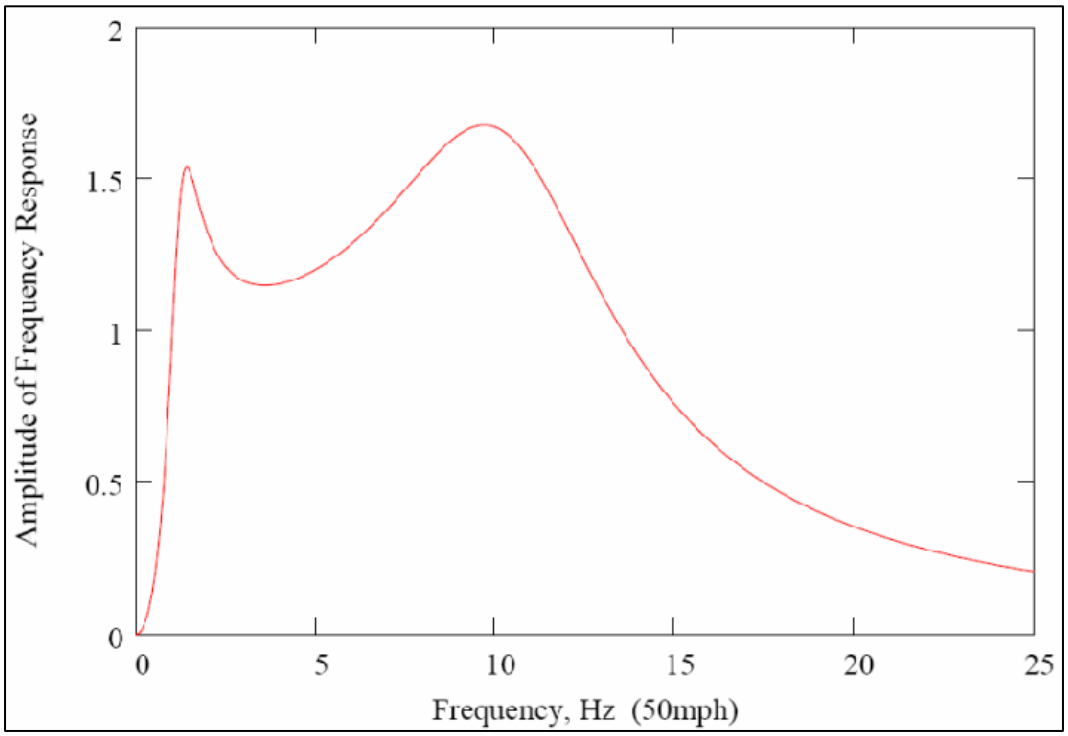

Figure 17. Graph. Response function showing displacement relative to road profile (Zr/Y).

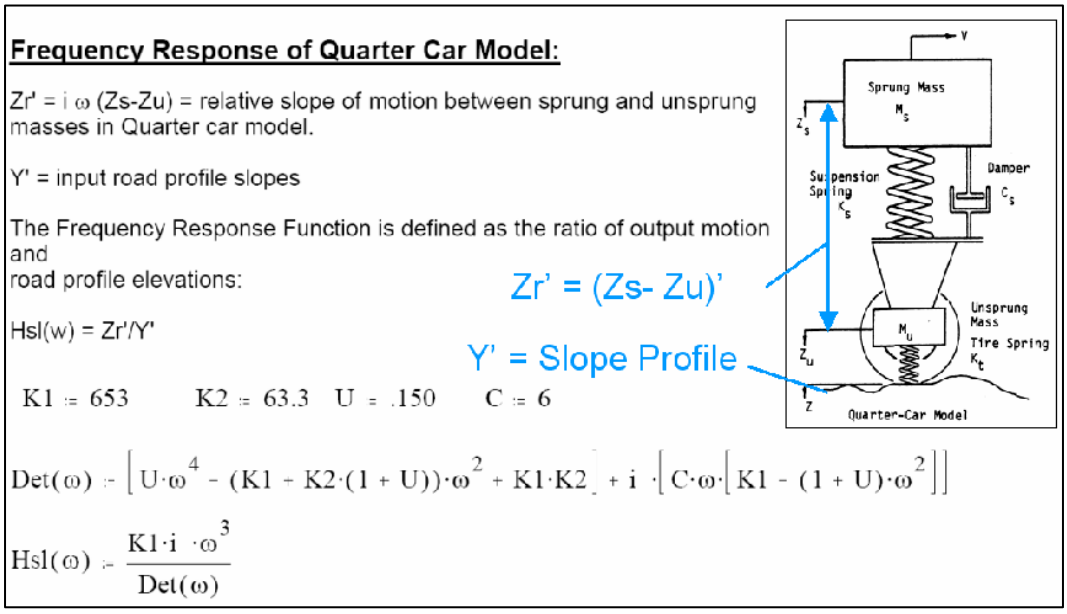

Figure 18. Illustration. Quarter-Car model response function showing displacement slope relative to road profile slope (Zr'/Y').

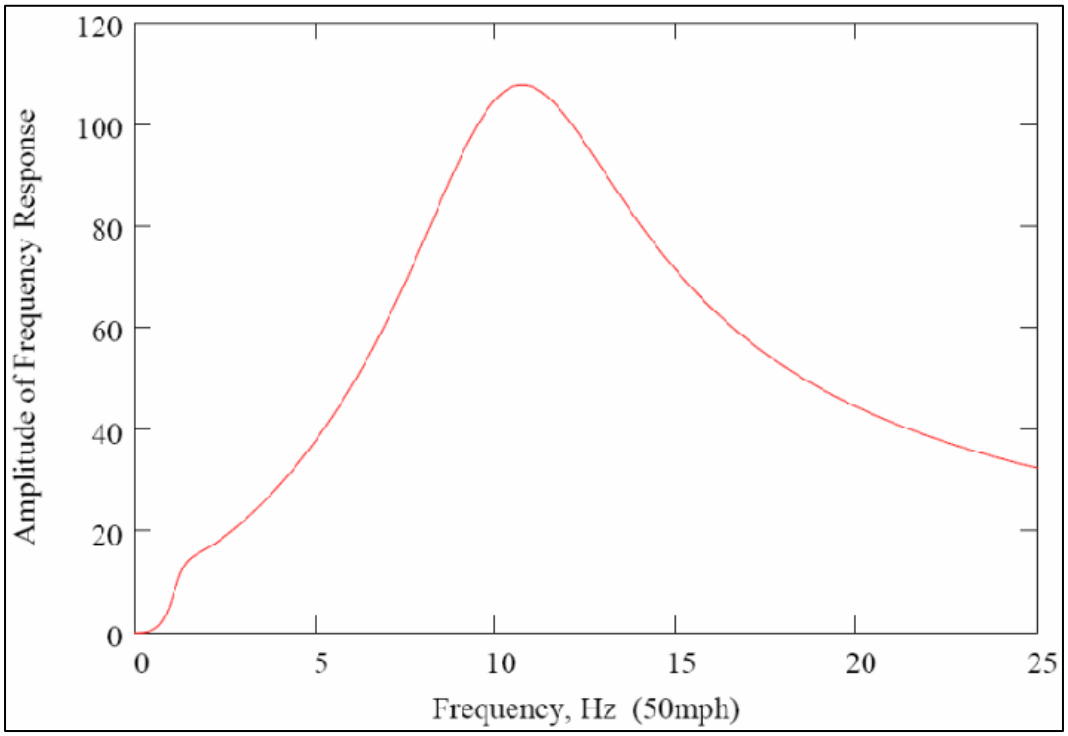

Figure 19. Graph. Response function showing displacement slope relative to road profile slope (Zr'/Y').

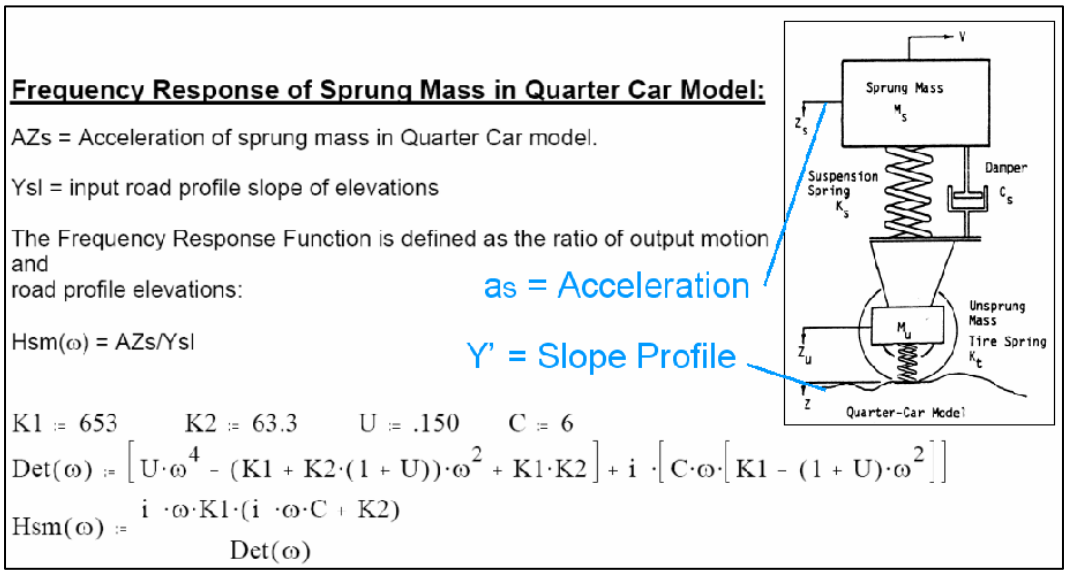

Figure 20. Illustration. Quarter-Car model response function showing acceleration of sprung mass relative to road profile slope (a_s/Y')

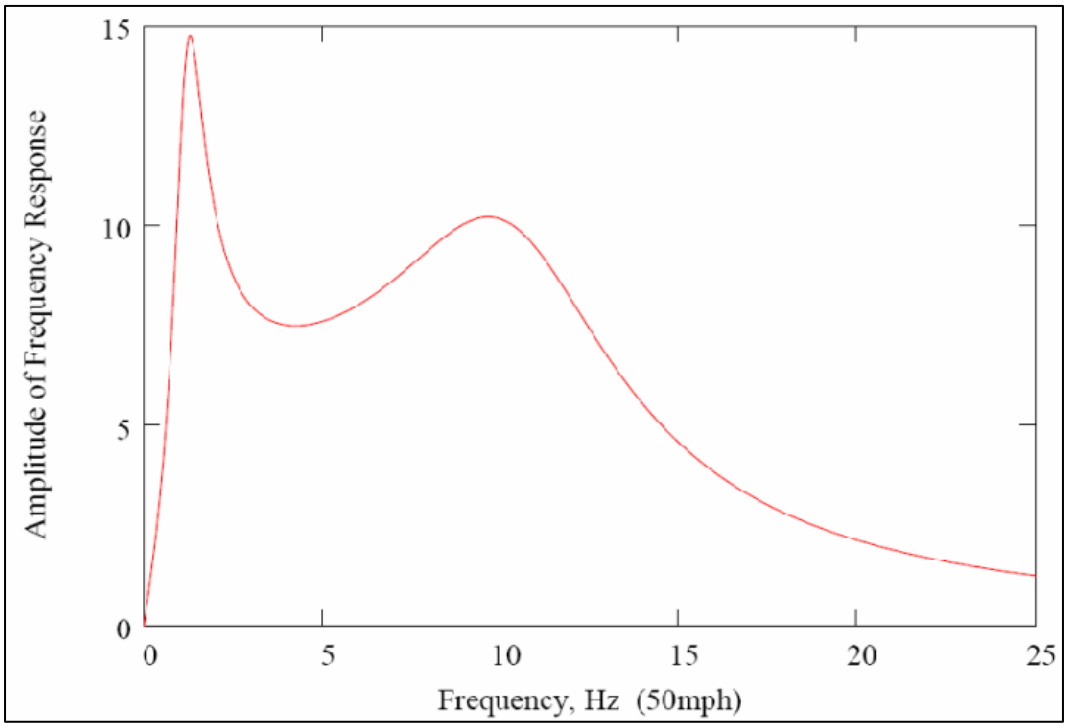

Figure 21. Graph. . Response function showing acceleration of sprung mass relative to road profile slope (a_s/Y').

Human Response:

Equation 42 and figure 22 presents the human response to vibration filter equation and plot as found in International Standard 2631 [1].

$$Hhr(\omega) := \frac{i \cdot \omega}{8 \cdot \pi + i \cdot \omega - \frac{\omega^2}{16 \cdot \pi}} \tag{42}$$

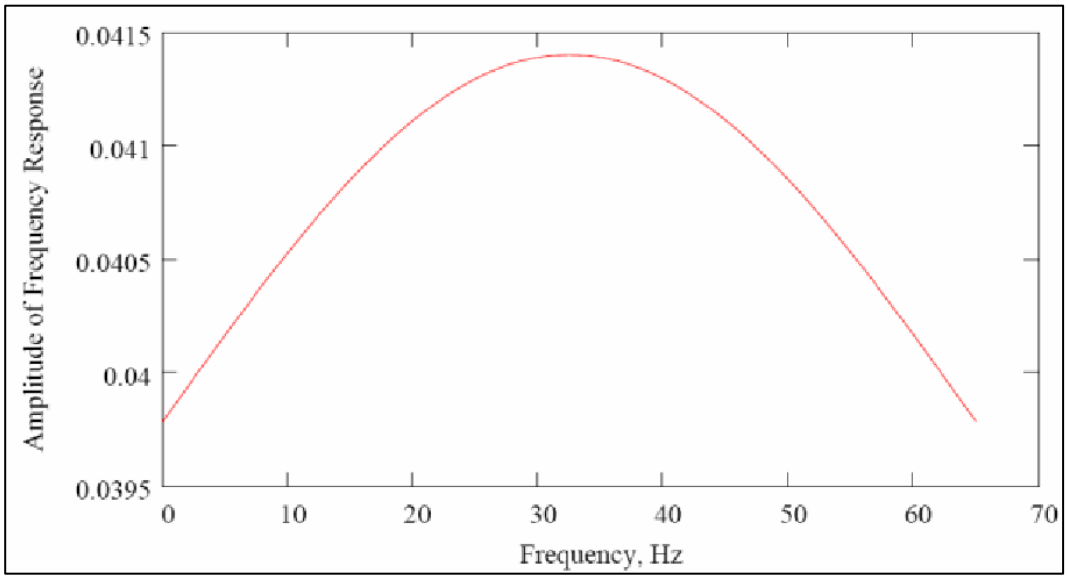

Figure 22. Graph. Plot of human response to vibration filter.

QUESTIONNAIRE

A questionnaire on inertial profilers was sent to the participants of the "TPF-5(063) Profile Quality" study. The purpose of Part 1 of the questionnaire was to ascertain what vehicle types (characteristics) and sensors were being used by the relevant agencies in their profiling vehicles. This information helps define the range of vehicle and sensor values for the inertial profiling simulations. Corresponding levels of error in single-axis accelerometer road profilers could then be determined. The summary results of Part 1 are presented in appendix A. The purpose of Part 2 of the questionnaire was to ascertain what are the participating state highway alignment design parameters to help define the range of values for the highway geometry parameters used in the inertial profiling simulations. The summary results of Part 2 are presented in appendix B.

4. DATA MATRIX

The bases of the data matrix are from the data collected during the prototype development of the DHM system. The sites include three two-lane roads and one four-lane divided highway. Selection criteria included roadway type, and severity of horizontal and vertical alignment. The roadway type and alignment severity for the four sites are summarized in table 2.

Route 851 is a two-lane rural road with poor horizontal and vertical alignment with respect to degree of curvature, cross slopes, and vertical grade change. The road has over a 122 meter (400 foot) elevation change, portions with a very rough ride quality, varying pavement coloring (white, black, mottled), good and poor pavement markings, some stops signs, and generally no shoulder. The road is approximately 9.47 km (5.88 mi) long. This road was considered a severe alignment test site. If the DHM system worked at this site in generating a repeatable 3-D profile, then it would probably work at any site.

Route 193 (Georgetown Pike) in Virginia is a two-lane rural/suburban road with many curves in a hilly terrain with no shoulders. This is a heavily traveled commuter route near Washington, D.C. The section of the road used as a test site is 6.76 km (4.2 mi) long. This road was considered a severe test site in terms of horizontal and vertical alignment.

Route 9 in Virginia is a two-lane rural road and was selected as the Virginia DOT is planning to make safety improvements to this road and the data collected by the DHM system would provide much needed information for developing the improvement plan. The 20.93 km (13.0 mi) test section of this road has a few traffic lights and passes through a small town. The road was considered moderate in terms of horizontal and vertical alignment.

The fourth site selected was the Route 460 bypass around Appomattox, VA. The 7.41 km (4.6 mi) long test section has very good roadway geometrics in terms of horizontal and vertical alignment and has well maintained pavement markings. The road was considered to have mild horizontal and vertical alignment with no curvature speed advisory signs required.

Table 2. Road type and severity of alignment of the four data matrix sites.

Level of Horizontal Curvature	Two-Lane Road	Four-Lane Divided Road
Severe	Route 851, 9.47 km (5.88 mi) Route 193, 6.76 km (4.2 mi)	
Moderate	Route 9, 20.93 km (13.0 mi)	
Mild		Route 460, 7.41 km (4.6 mi)

SITE ALIGNMENT SEVERITY ILLUSTRATIONS

The following figures in the next three sections illustrate the severe, moderate, and mild road alignment types and resulting vehicle operational characteristics for three of the sites.

Severe Alignment

Figure 23 shows a wide range in speed for six data collection runs for one of the two severe alignment sites. The operator attempted to collect data at specific speeds ranging from 40 km/h to 72 km/h (25 mi/h to 45 mi/h). Actual speed is constrained by road geometrics, specifically horizontal curves. Speed reductions occurred at common points along the road for the horizontal curves within the six runs. Other speed reductions are the result of interacting with other traffic.

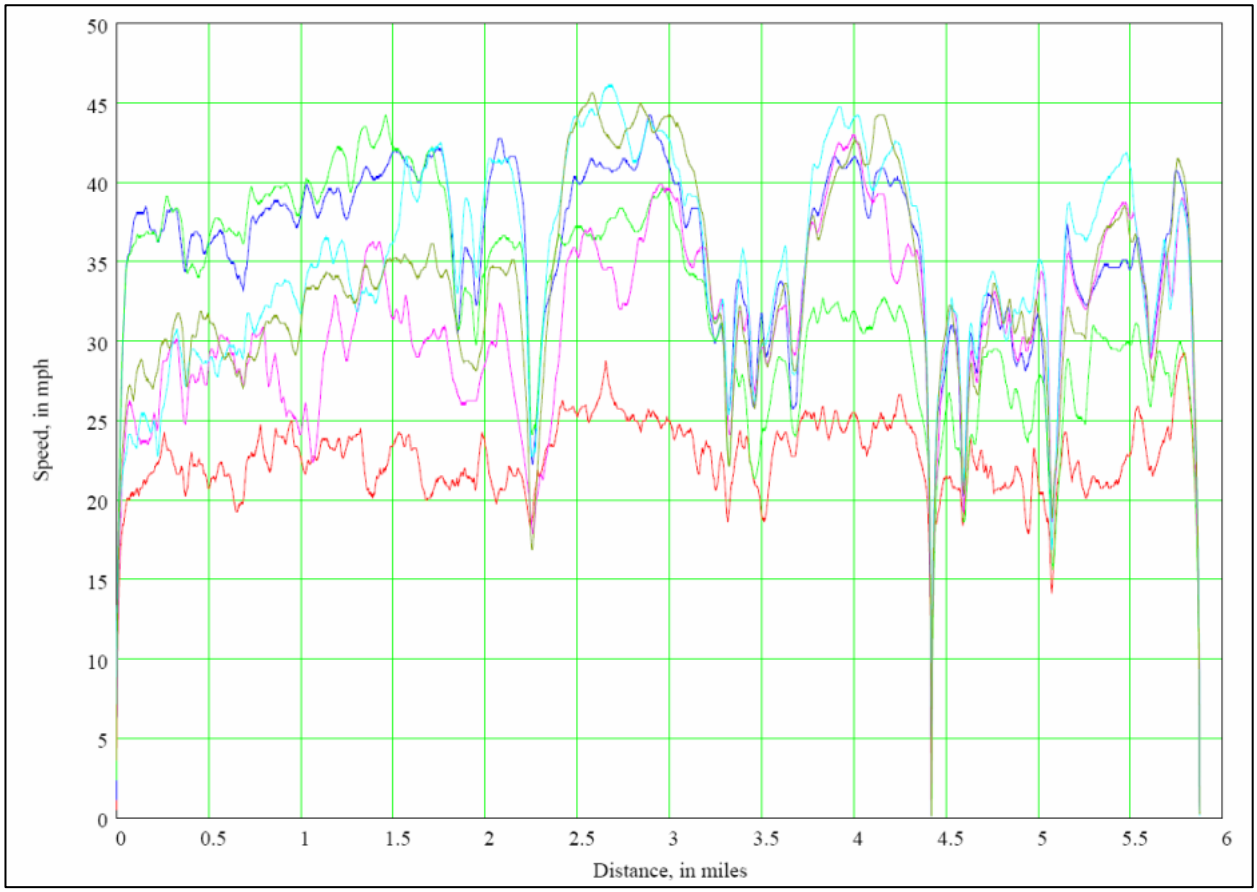

Figure 23. Graph. Severe alignment site with vehicle opeerator specific speed target constrained by horizontal curves.

Figure 24 is the heading information for six data collection runs on the same severe site as shown in figure 23. Frequent changes in heading are the result of the numerous horizontal curves on the two-lane rural road. The heading data for the six runs repeat except for one instance where a stopped US mail vehicle was passed by the DHM vehicle.

Figure 24. Graph. Severe alignment site with repeated heading data for six repeated runs showing frequent and severe changes in heading.

Figure 25 is the cross slope information for six data collection runs on the severe site. Frequent changes in cross slope are the result of the numerous horizontal curves on the two-lane rural road. The cross slope for the six runs repeat except for one major instance where a stopped US mail vehicle was passed by the DHM vehicle. Other diversions in cross slope are the result of the vehicle cutting too close to the inside of a horizontal curve where the lanes are narrow and edge drop-offs are present.

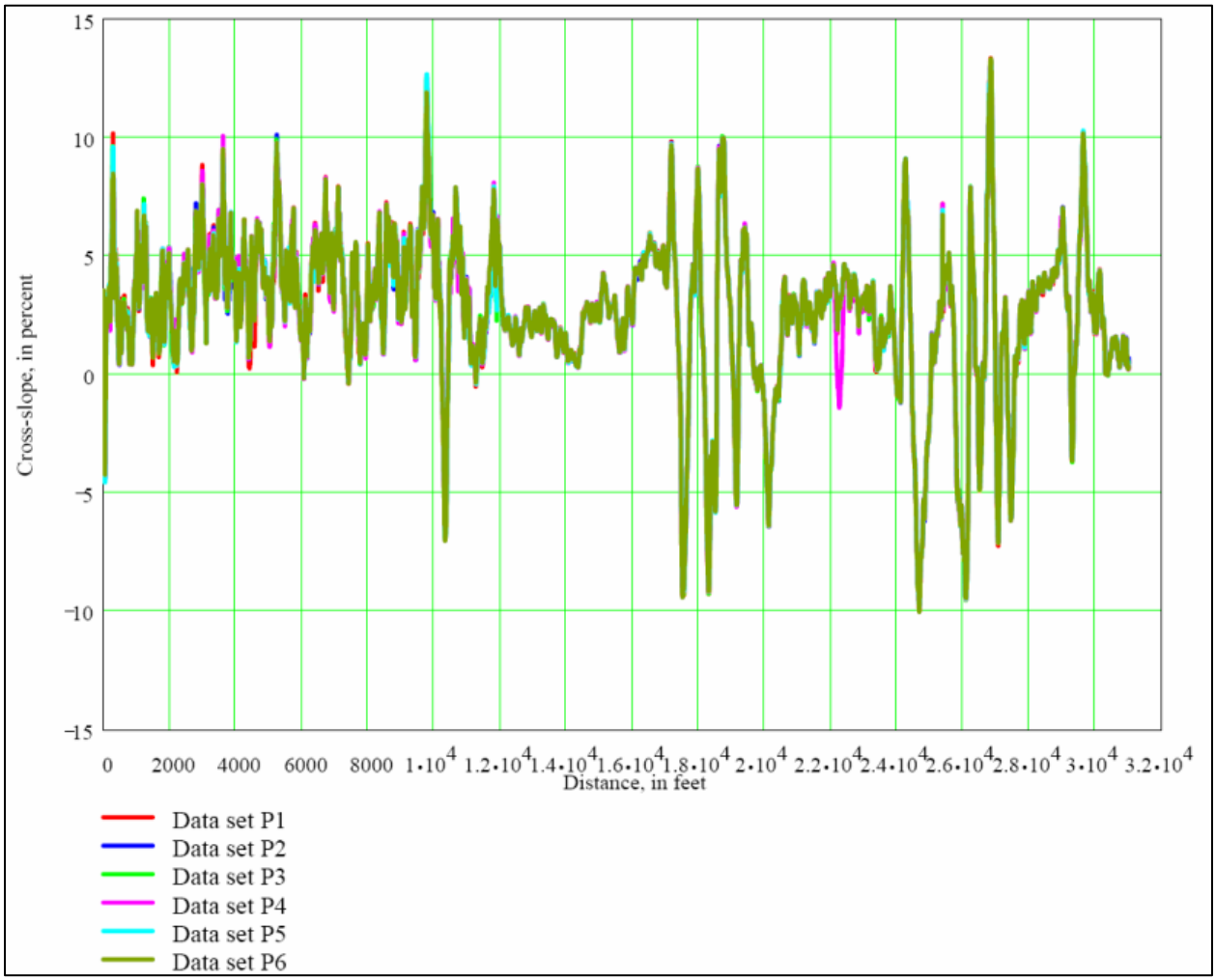

Figure 25. Graph. Severe alignment site with repeated cross slope data for six repeated runs showing frequent and severe changes in cross slope.

Figure 26 is a detailed view of cross slope information for a distance for 304.8 m (1000 ft) for the six data collection runs on the severe site. X-axis has a grid interval of 30.48 m (100 ft). Frequent changes in cross slope are visible. Again, the cross slope for the six runs repeat very well with small deviations due to wandering within the narrow lanes with little edge-of-pavement support structure allowing asphalt pavement edge deformations. Consistency in cross slope is not present as oscillations of about 1 percent are apparent.

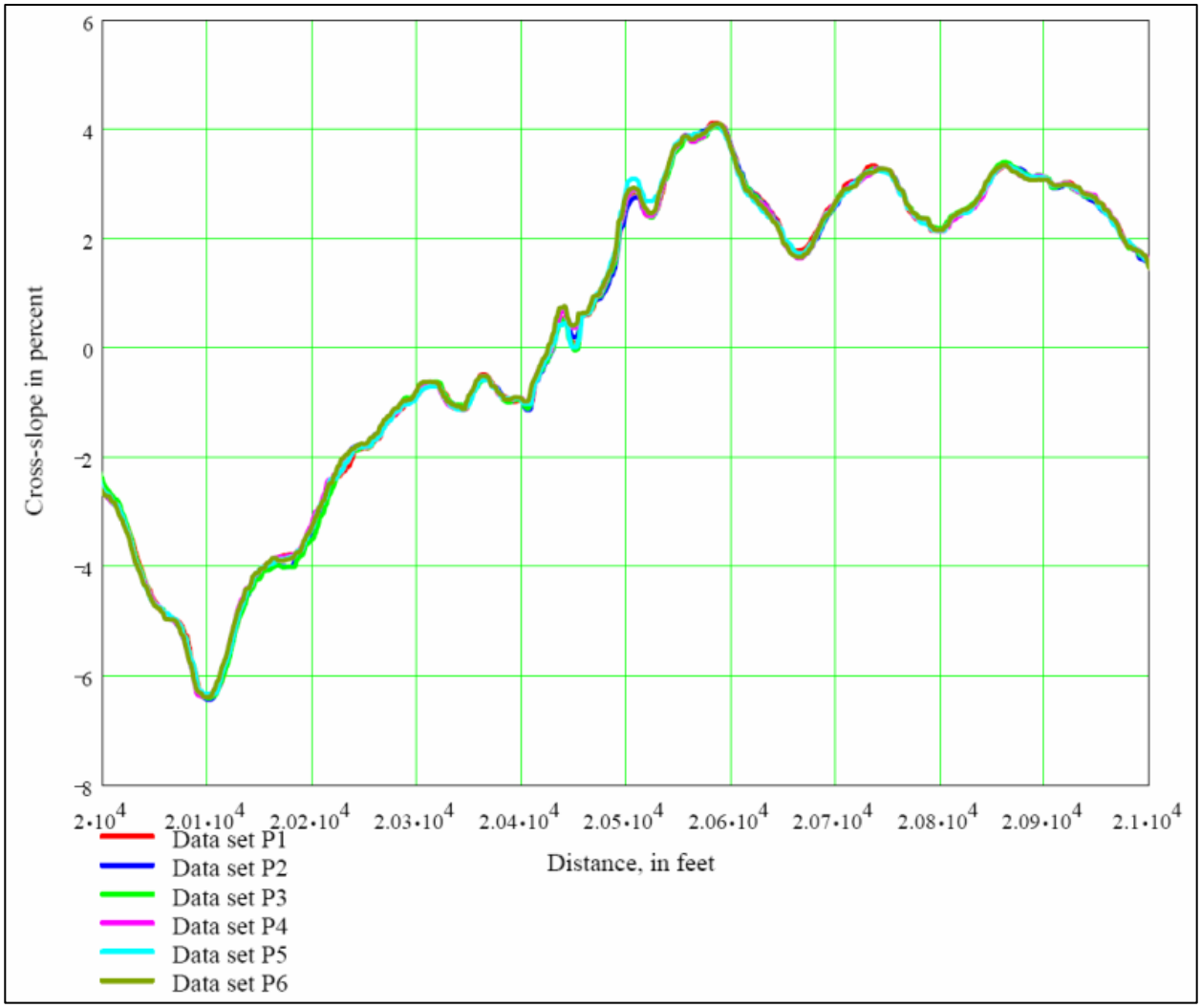

Figure 26. Graph. Detailed view of a portion of the severe alignment site with repeated cross slope data for six runs showing frequent and severe changes in cross slope.

Figure 27 shows the INU measured accelerations in g's (scale is +/- 0.5g) relative to body coordinates (left) and normal (right) coordinates for approximately 80 seconds of data. Differences between horizontal body and normal cross trajectory accelerations (top pair) are apparent with the normal acceleration having a greater range. For the body and normal along track accelerations (middle pair) the higher body values in the early part of the data are clearly visible. For the vertical accelerations (bottom pair), differences are not as readily apparent at this scale.

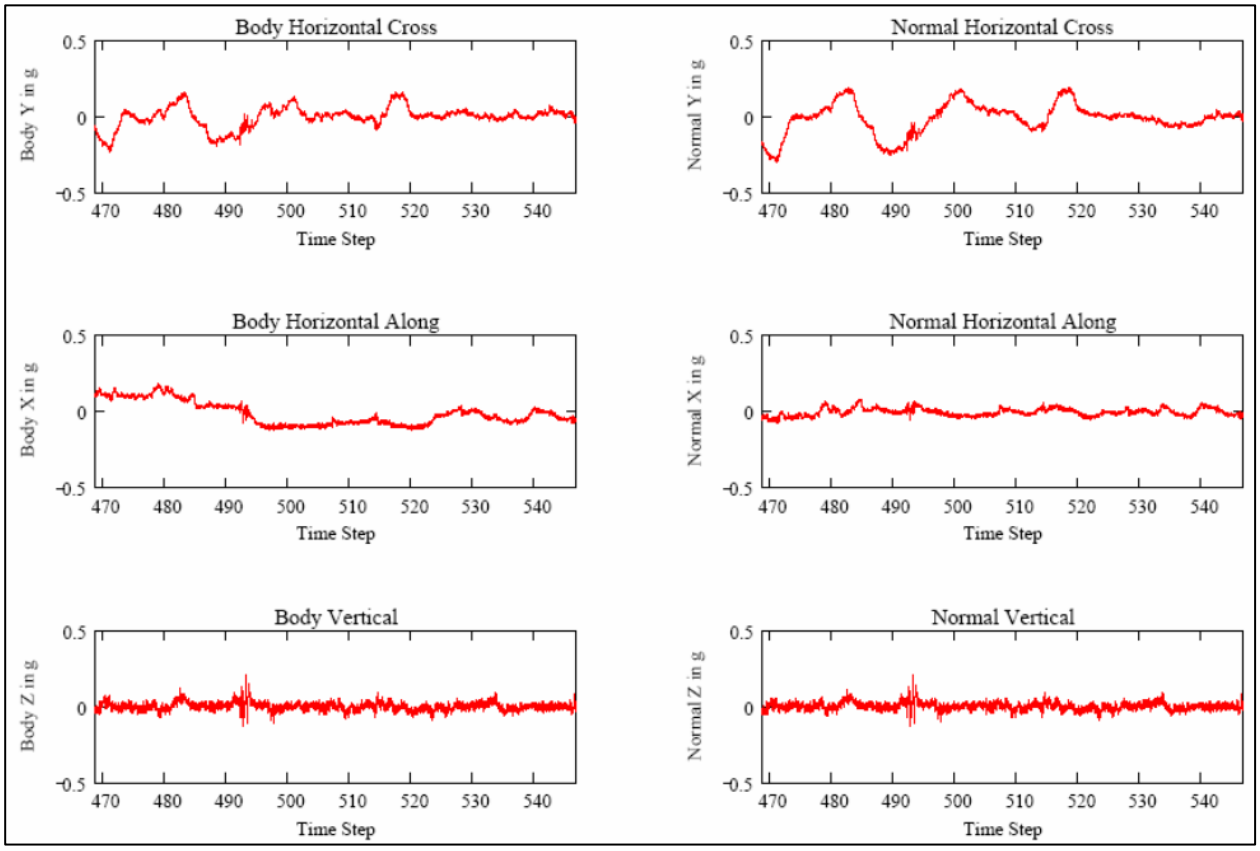

Figure 27. Graph. INU measured body (left) and normal (right) accelerations for the severe alignment site.

Figure 28 shows the difference between the INU output body vertical and normal vertical accelerations. Scale range is +/- 0.02 g's. About 900 seconds of data is shown. In computing position data, the INU continuously corrects for pitch and roll effects. Portions of the graph appear as if they may be correlated to roadway geometry features, most likely cross slope changes and bumps. A large portion of the data falls within a narrow band of 0 to –0.03 g's possibly showing a general trend of acceleration correction for a road with a normal crown for pavement drainage. Spikes in the data are also present showing presence of short-term but significant road features. The compounding of roadway features and vehicle operations makes identifying relationships difficult from a visual perspective in this figure for this site.

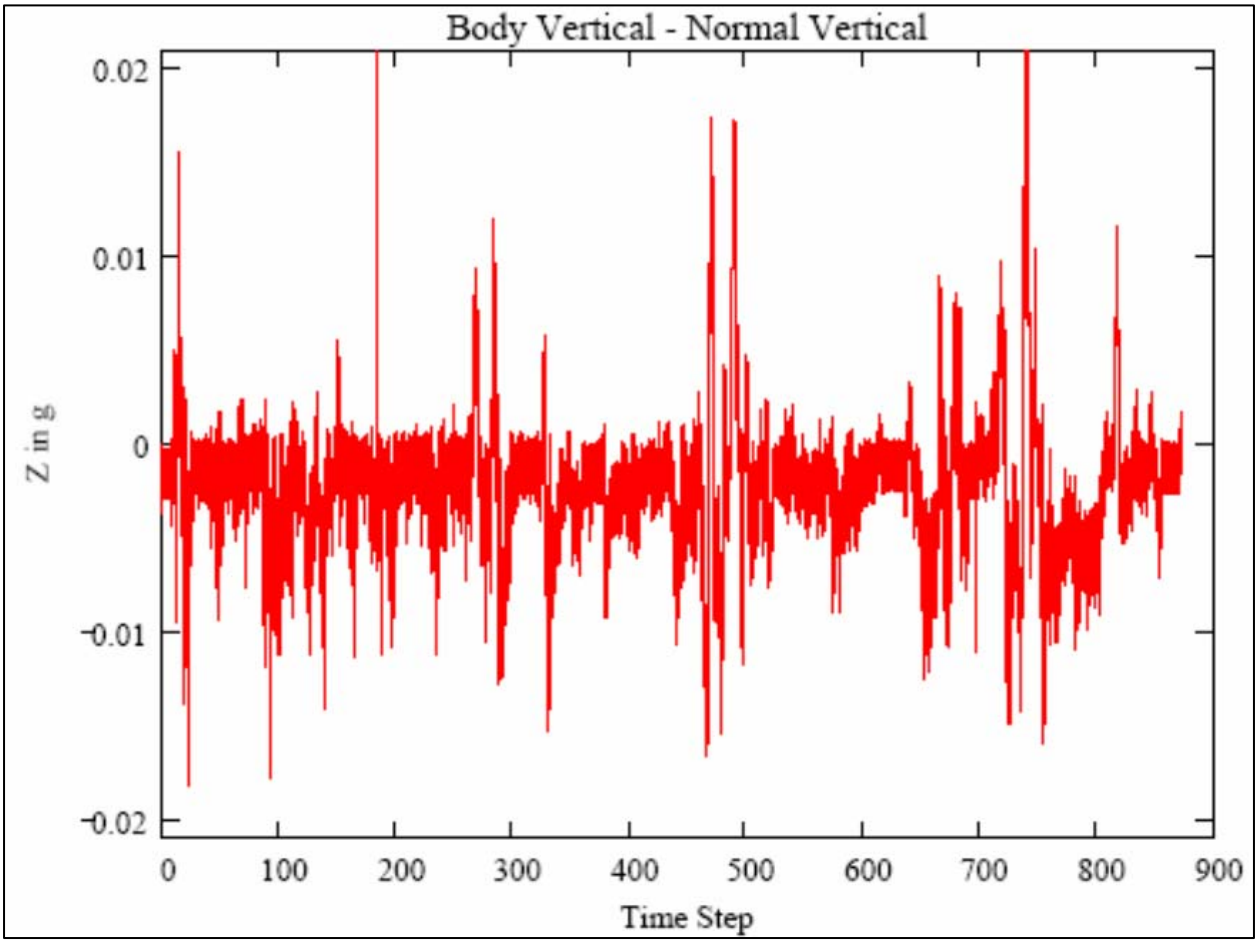

Figure 28. Graph. INU body vertical minus normal vertical acceleration for the severe alignment site.

Moderate Alignment

Figure 29 show the speed profiles for the six data collection runs for the moderate site. This site is roughly 22 km (13.5 mi) long. Vehicle operator attempted to maintain target speeds ranging from 72 km/h to 88 km/h (45 mi/h to 55 mi/h). Speed reductions for some horizontal curves are evident as well as occasional speed reductions for a traffic control signal, reduced speed limit of 40 km/h (25 mi/h) going through a small rural town, and occasionally, interference from other traffic.

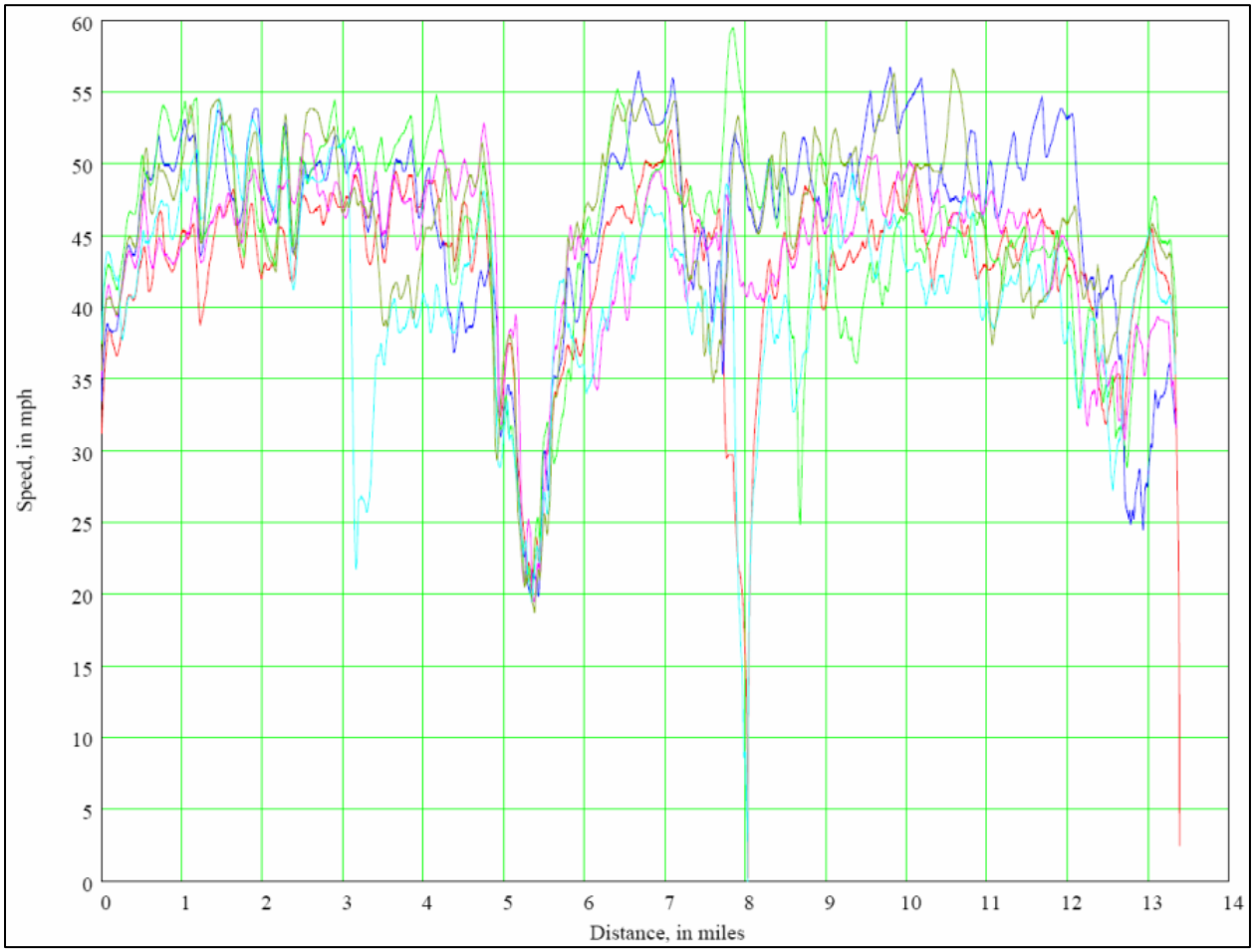

Figure 29. Graph. Moderate alignment site speed profiles.

Figure 30 shows the heading data for the six repeated runs for the moderate alignment two-lane rural road site. The six data collection heading data repeats very well. Vehicle heading ranges from 60 to about 202 degrees. It can be seen that the road has a significant number of horizontal curves. During one run, a stopped US mail vehicle was passed and is seen as a deviation from the heading data of the other five data collection runs near the middle of the graph.

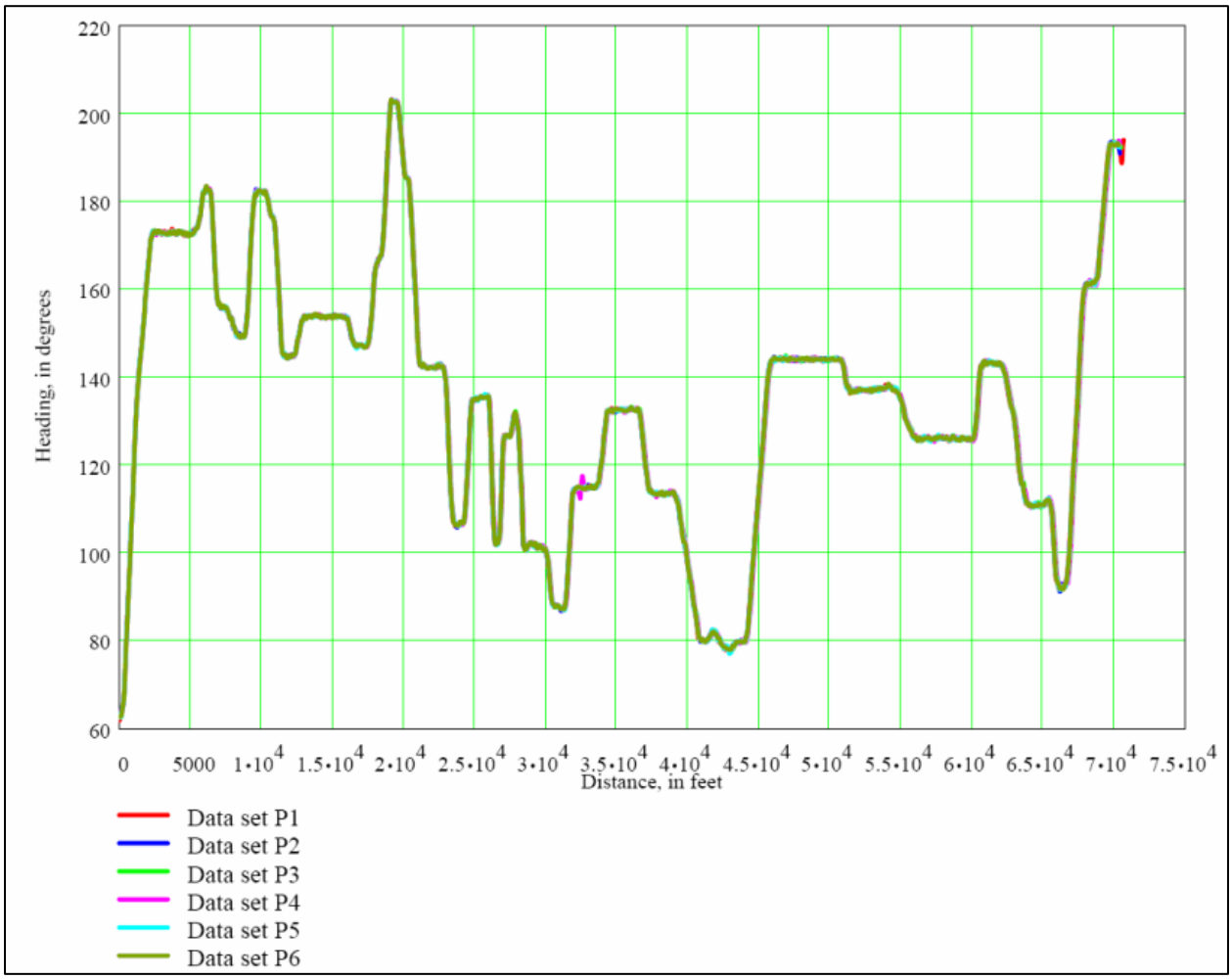

Figure 30. Graph. Moderate alignment severity site heading data.

Figure 31 is the cross slope data for the six repeated runs for the moderate alignment site. The data repeats very well for the six runs. Major changes in cross slope generally match the change in heading data in the previous figure. Cross slope ranges from –8% to +12 %. Some cross slope noise (inconsistent cross slope) is present for this site but is less than that for the severe site example. A two percent cross slope is the dominant cross slope value indicating the presence of a normal crown for cross-pavement drainage.

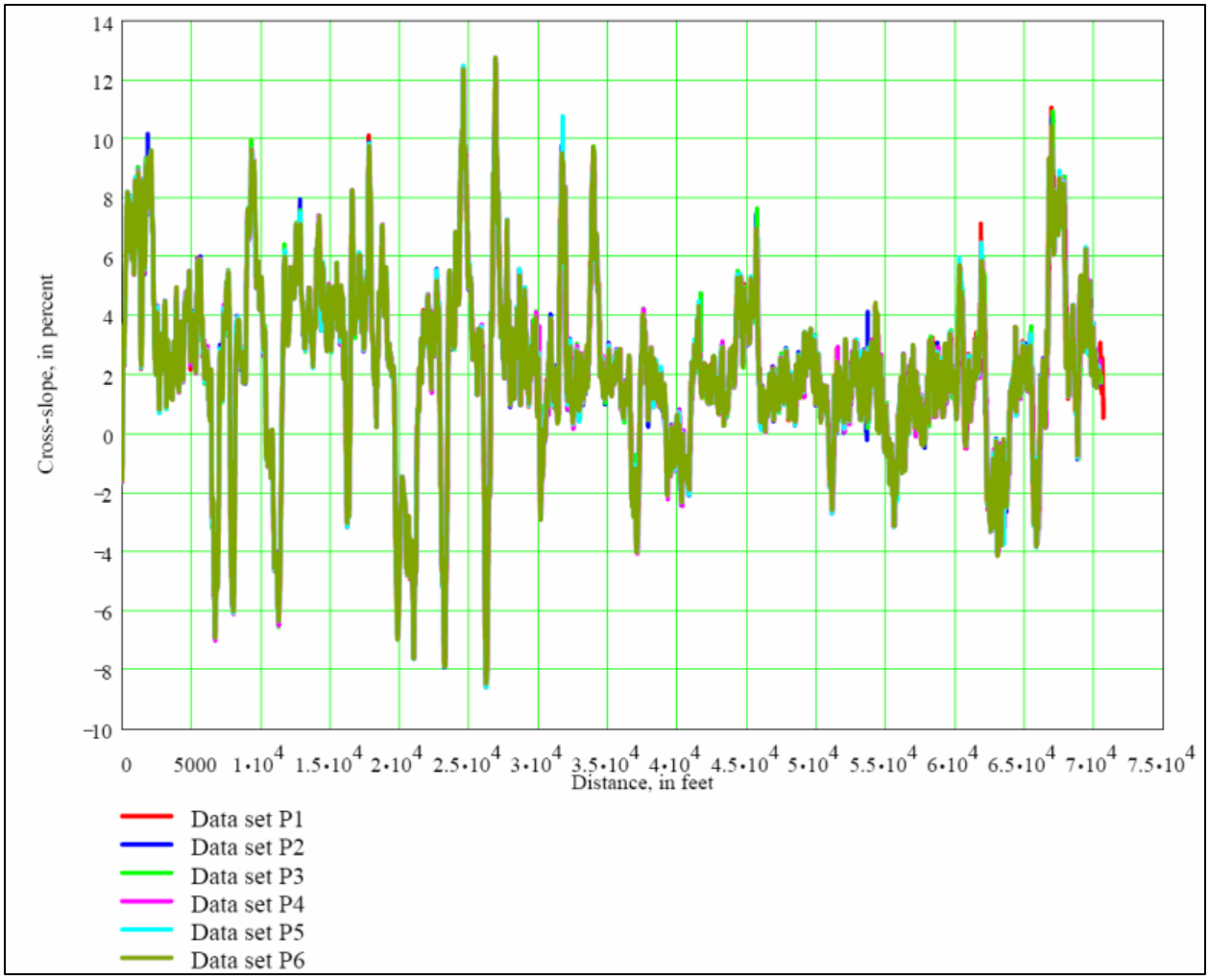

Figure 31. Graph. Moderate alignment site cross slope data.

Figure 32 is a detailed view of cross slope information for a distance of 274.3 m (900 ft) for the six data collection runs on the moderate site. The changes in cross slope are not as choppy as that for the severe site but some oscillation is present near transition points. These oscillations in cross slope may be by design as part of the transitioning to the next curve. Data is very repeatable.

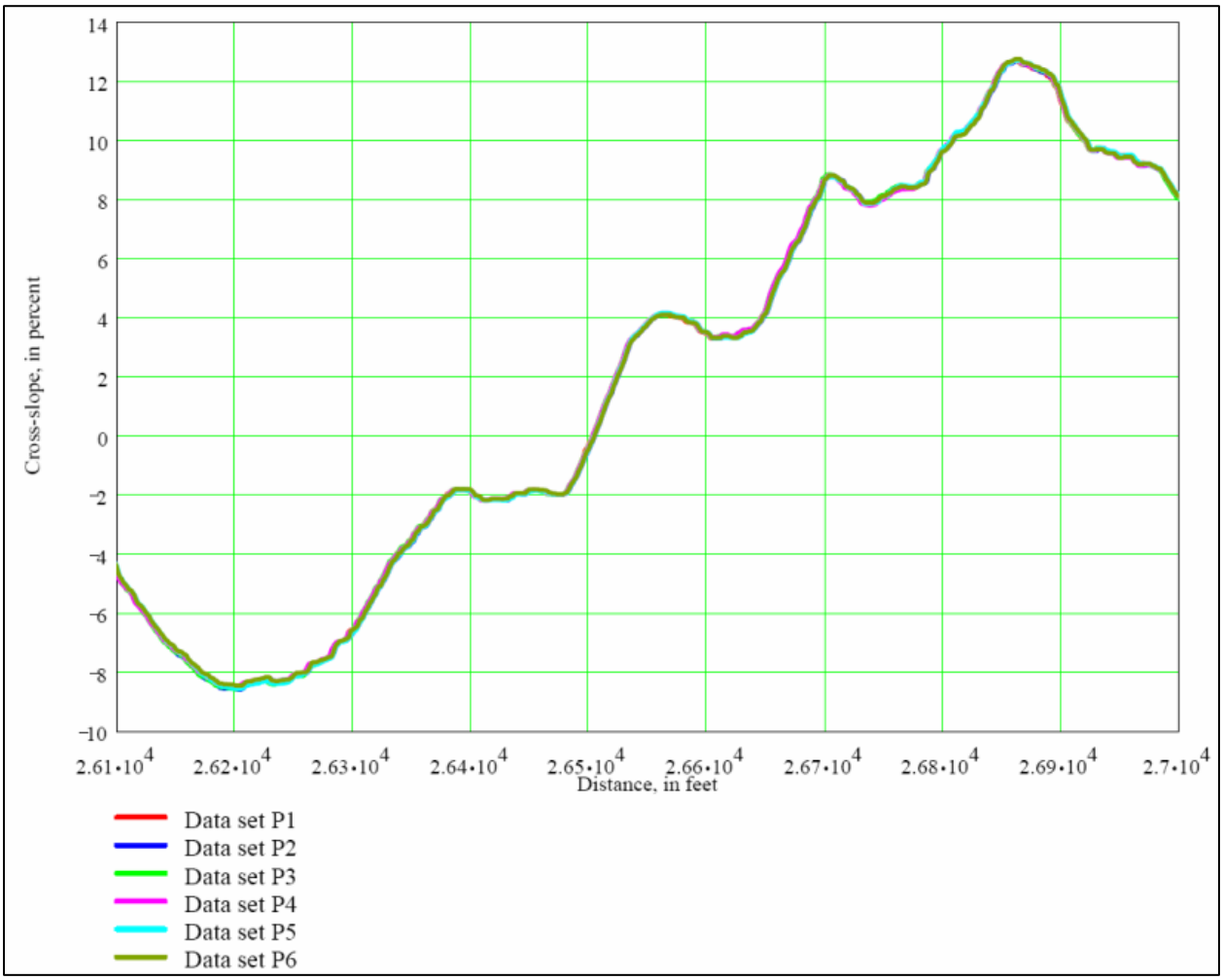

Figure 32. Graph. Moderate alignment site detailed view of a portion of the cross slope data.

Figure 33 shows the INU measured 3-D accelerations relative to body coordinates (left) and normal coordinates (right) for a portion of the moderate alignment site. Vertical scale is again +/- 0.5g. About 150 seconds of data are shown. The body cross trajectory accelerations and normal cross trajectory accelerations (top pair) are more similar than the case for the severe site. But differences still exist as expected. Differences are more apparent in the body and normal along trajectory plots (middle pair). Differences in the body and normal vertical accelerations are not easily seen (bottom pair).

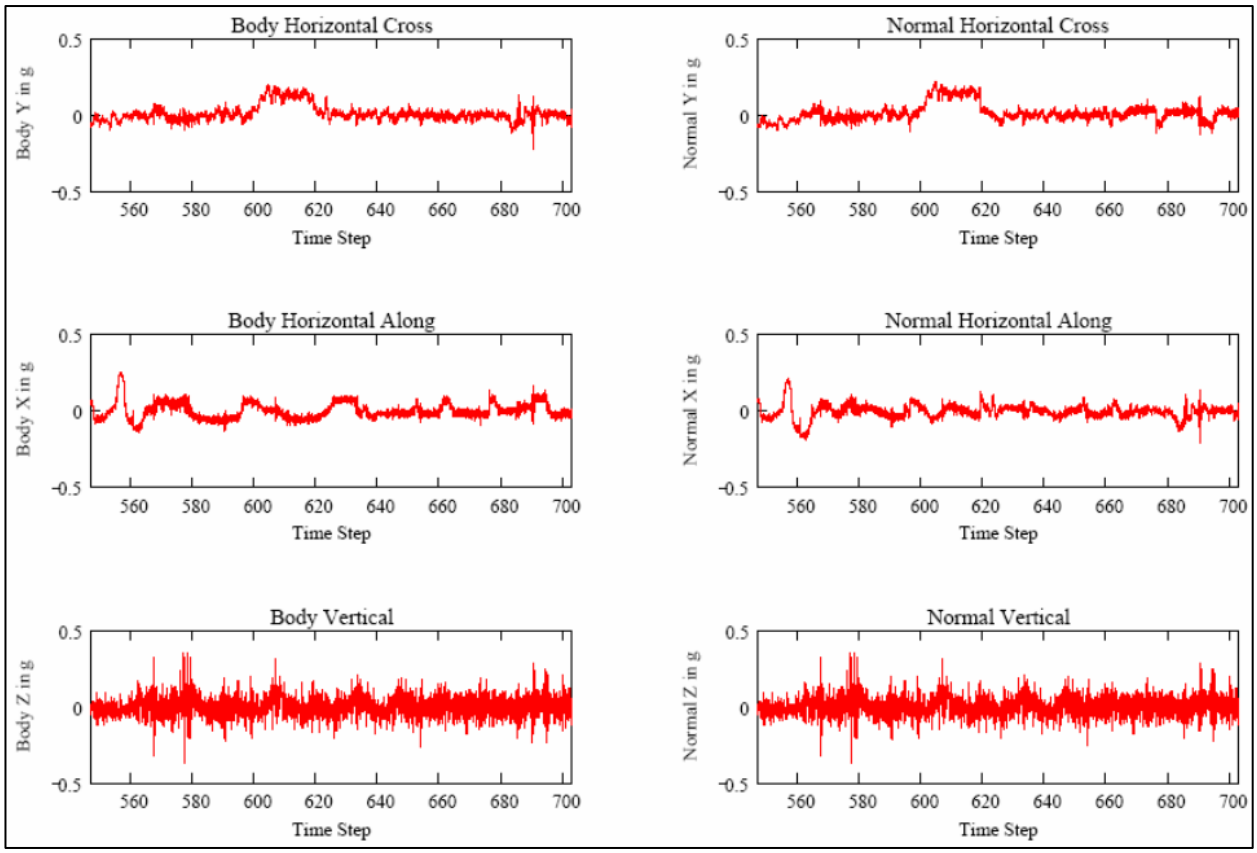

Figure 33. Graph. INU measured body (left) and normal (right) accelerations for the moderate alignment site.

Figure 34 shows the difference between the INU body vertical and normal vertical accelerations for the moderate site. In computing position data, the INU internally corrects for pitch, roll and change in heading. The differences in vertical accelerations are smaller than for the severe site as the moderate site has a better design in terms of its alignment with respect to grade, cross slope, and degree-of-curvature. The road is also smoother than the severe site. Vertical scale of +/- 0.01g is half of the scale used to show the severe site differences in vertical accelerations. Time span is about 15 seconds.

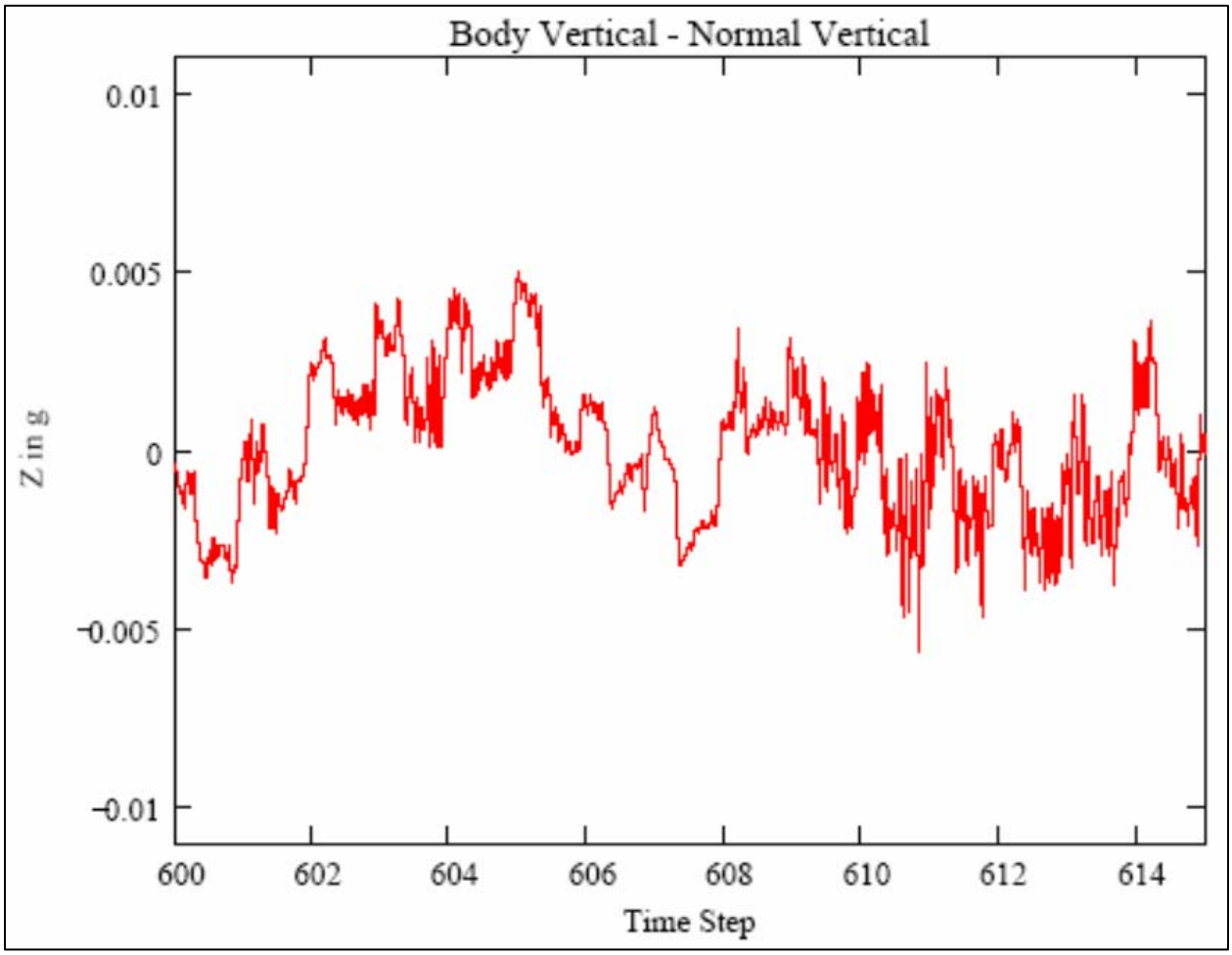

Figure 34. Graph. INU body vertical minus normal vertical acceleration for moderate site.

Mild Alignment

Figure 35 shows the speed profile for the six data collection runs for the mild alignment four-lane divided highway site. Vehicle operator attempted to maintain target speed of 72 km/h (45 mi/h) except for one run at a target speed between 56 km/h and 64 km/h (35 mi/h and 40 mi/h). Speed reductions for horizontal curves are not evident as was the case for the severe and moderate sites. Most variations in speed are due to operator input and some interference from other traffic. Speed profiles had a range of 6 to 10 km/h (4 to 6 mi/h). Begin and end data show accelerating to and from target speeds.

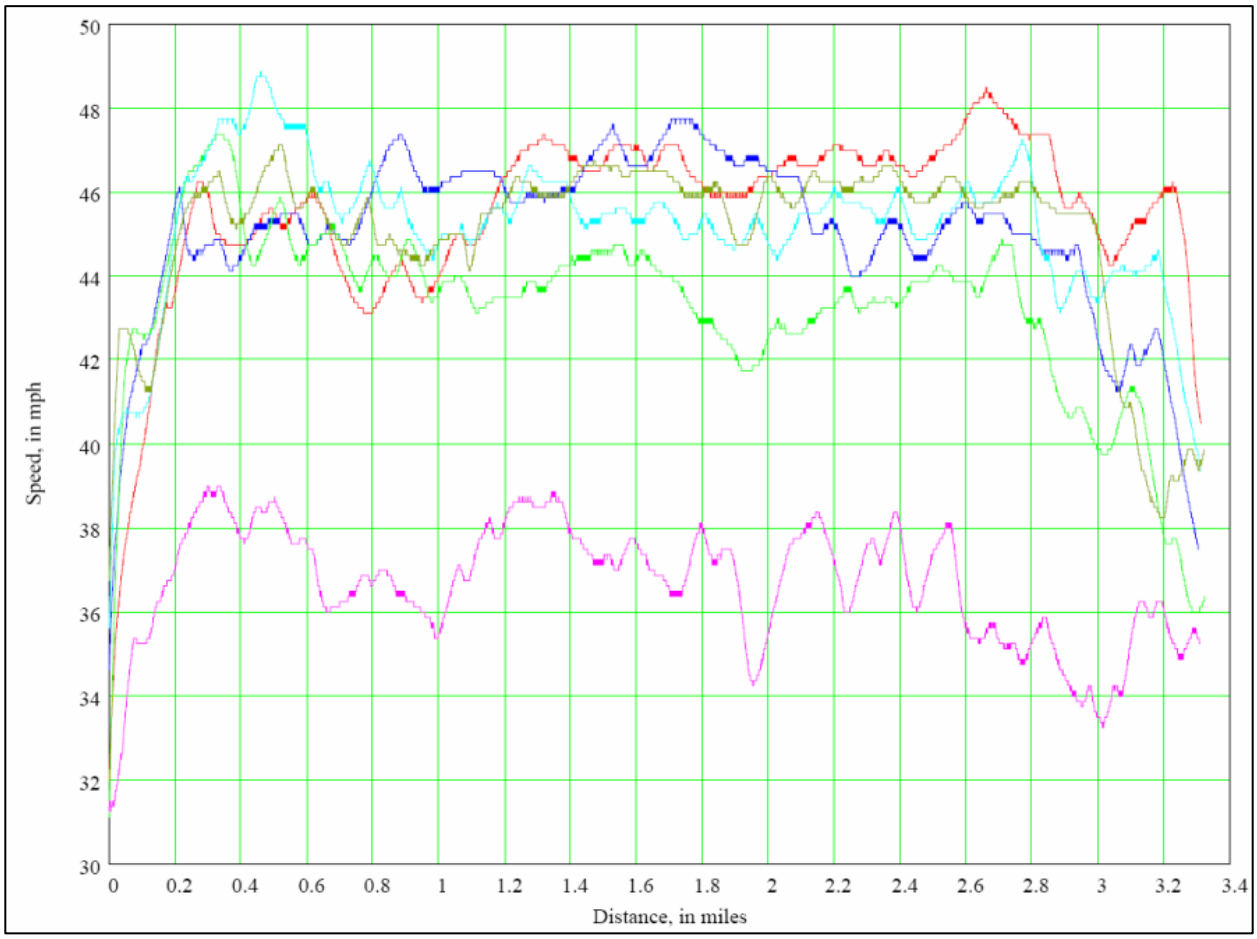

Figure 35. Graph. Mild alignment site speed profiles.

Figure 36 shows the heading data for six data collections runs for the mild alignment site. The slow change in heading denotes horizontal curves with low degrees-of-curvature and long length. Heading data is very repeatable.

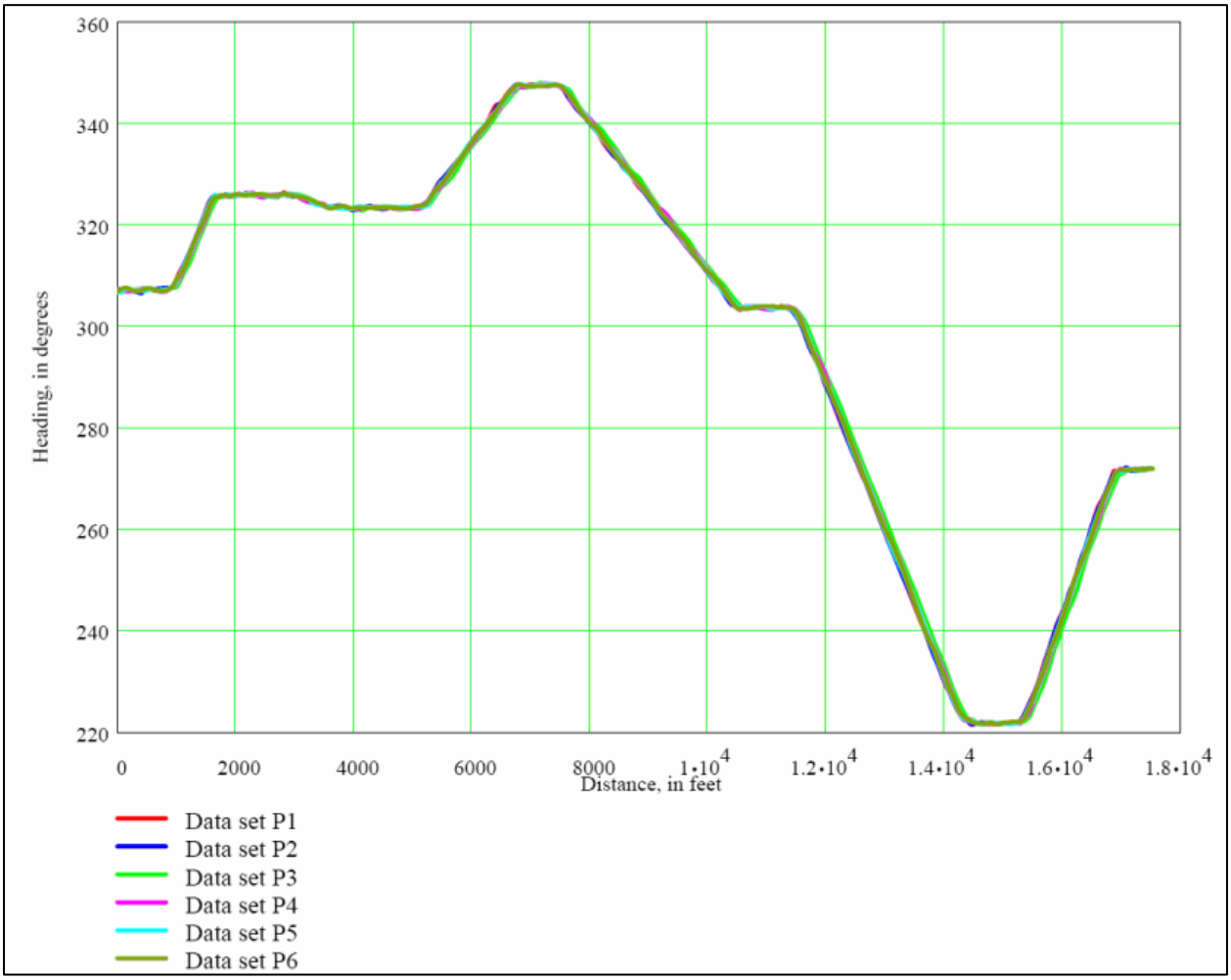

Figure 36. Graph. Mild alignment site heading data for six data collection runs.

Figure 37 shows the cross slope date for the six repeated runs for the mild alignment site. This four-lane divided highway has long, gentle horizontal curves with a properly designed cross slope. Note that cross slope is very consistent and is not “noisy” as compared to the severe and moderate alignment sites. The standard two percent cross slope represents the normal crown of the pavement for water drainage. This road consists primarily of long curves with short tangent sections between the curves.

Figure 37. Graph. Mild alignment site cross slope data.

Figure 38 shows the INU measured 3-D accelerations relative to body coordinates (left) and normal coordinates (right) for the mild alignment site. The ordinate scale is 0.2g for the mild alignment site compared to 0.5g for the severe and moderate alignment site. The differences between the body and normal horizontal cross accelerations (top pair) are very visible for this approximately150 seconds of data. Body and normal along trajectory acceleration differences (middle pair) are not as apparent as for the cross trajectory. This site has the most consistent speeds and the least changes in elevation profile. Visual differences in body and normal vertical accelerations are not apparent (bottom pair). There is a general lack of roadway features outside of the long curves with good cross slope design present in the data that would generate differences between body and normal vertical acceleration measurements.

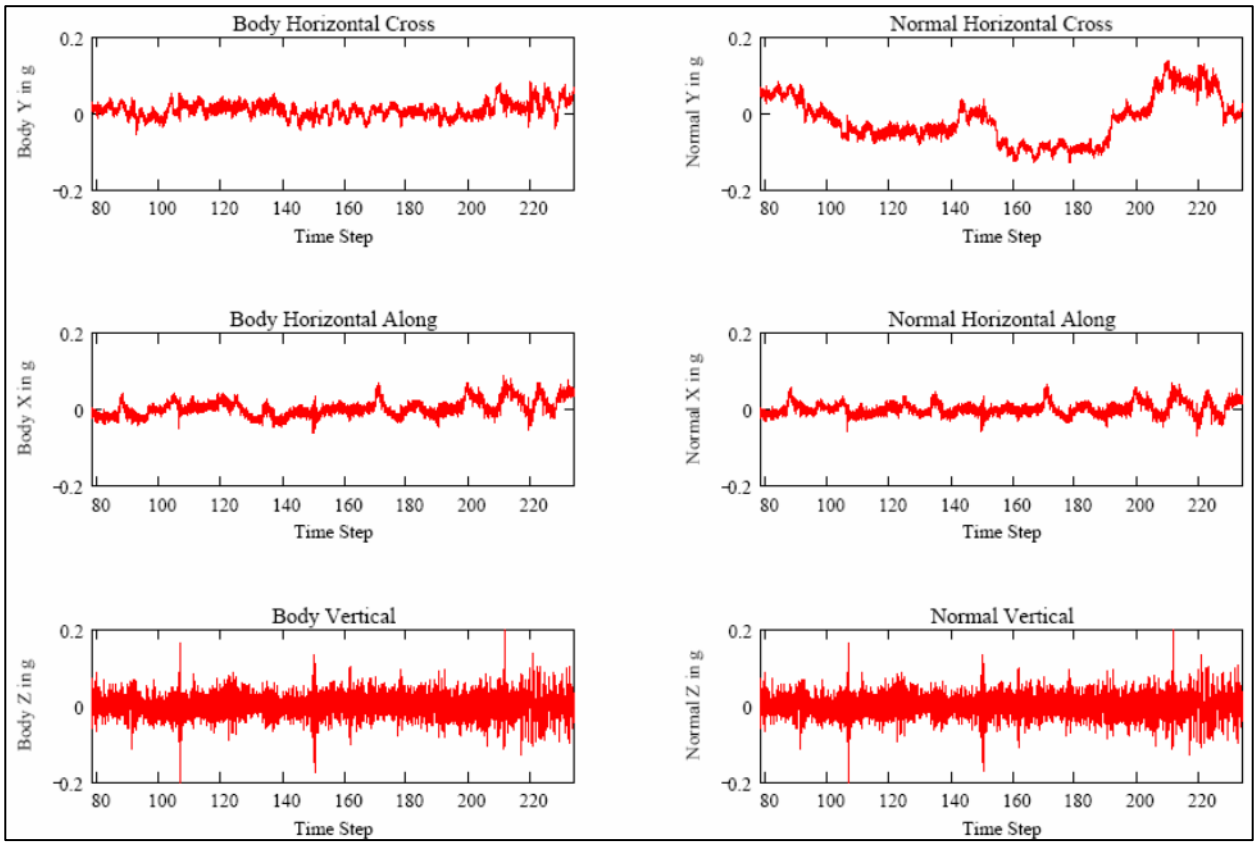

Figure 38. Graph. INU measured body (left) and normal (right) accelerations for the mild alignment site.

Figure 39 shows the difference between the INU body vertical and normal vertical accelerations for the full 250 seconds of data. Ordinate scale is +/- 0.01g. In computing position data, the INU internally corrects for pitch, roll, and change in heading. The differences in accelerations are smaller than for the severe or moderate site as the mild site has a better design in terms of its alignment with respect to grade and cross slope. Of significance in this figure, is that the differences in the two accelerations visually correlate very well with the roll data shown in figure 37. For this mild alignment site, roll is a dominating physical feature in that other roadway variables present in the severe and moderate case are not significantly present in the this case. The one-to-one correspondence of roll to vertical accelerometer error is clearly seen.

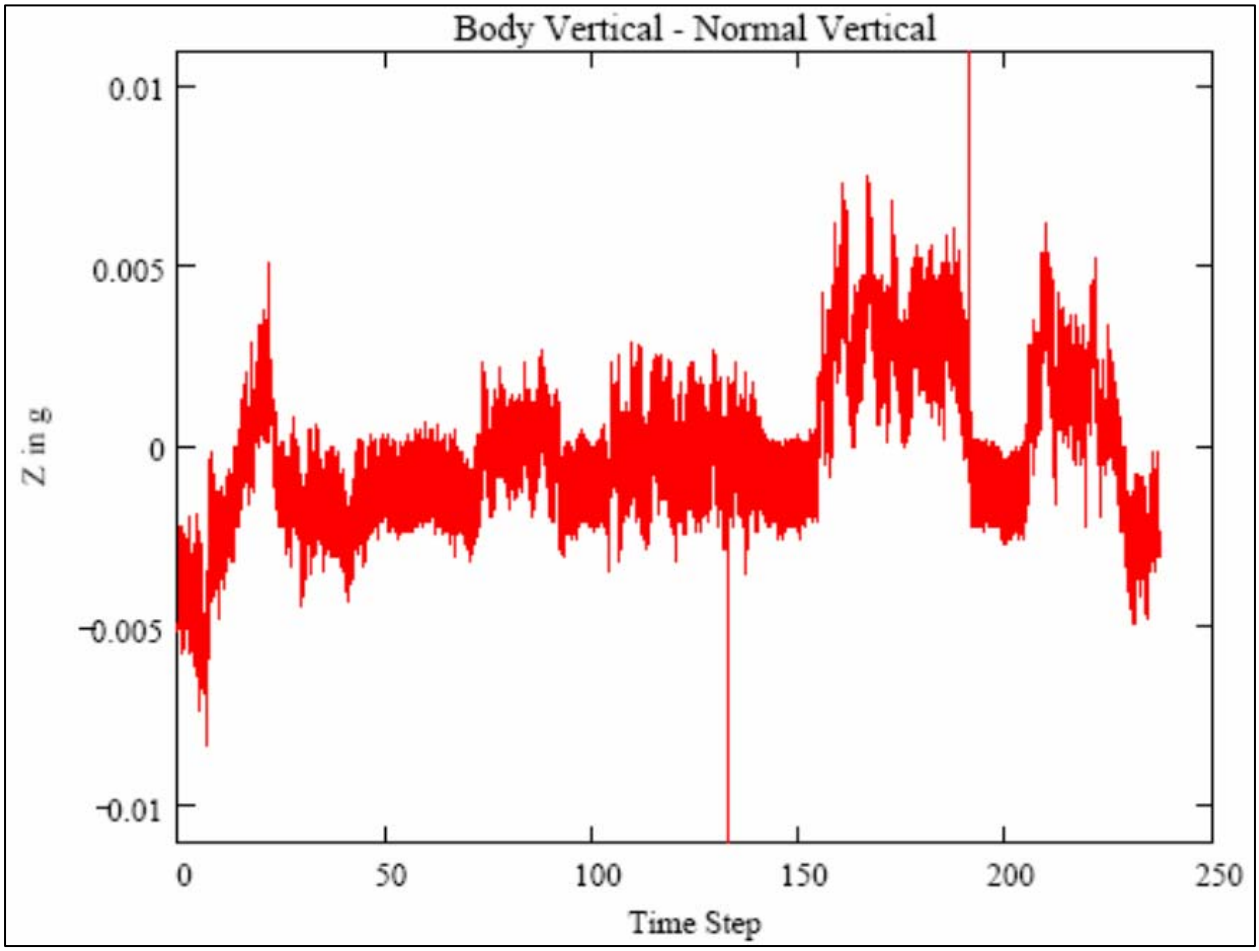

Figure 39. Graph. INU body vertical minus normal vertical acceleration for mild site.

5. DATA PROCESSING

This section presents the data processing of the DHMS data to generate a database upon which the attitude and operation of the vehicle resulting from traveling the road that impacts inertial profile computations and subsequent IRI computations can be analyzed. Data processing consists of synchronizing raw and previously preprocessed temporal and spatial data into a common analysis database, categorizing/typing roadway and operation characteristics and measurement parameters to define and compare basic characteristics between and within sites, compute the profile and IRI for both corrected and uncorrected accelerometer measurements, and to perform an initial data mining as a guide to how the analysis may proceed.

DATA SYNCHRONIZATION

Some of the DHMS sensors and acquisition boards sample at different rates as a function of their hardware design. The sensors on the DHMS system are all temporally based in the current prototype design. Some sensors, such as the GPR system to be added to the DHMS in the future, are spatial based. If a master computer cannot perform a hard-wired synchronization, then the master computer must keep temporal track of each system so that synchronization of the data can be performed in a post-acquisition processing step. Synchronization of the data and other preparation of the analysis database are performed within a series of processing steps.

PARAMETER AND ROAD SECTION CATEGORIZATION/TYPING

In order to help explore and compare geometry alignment and operational characteristics between sites and within repeated runs, alignment and operation characteristic were categorized into three categories – low (0), medium (1), and high (2),. The threshold values for this parameter categorization/typing are shown in table 3. This categorization representation of the data also permits an exploration of the level representation of the variables within the sampled space.

Table 3. Threshold values for roadway/operation parameter categorization/typing.

Parameter	Low (0)	Medium (1)	High (2)
Speed (km/h (mi/h))	32.2 - 48.3 (20 - 30)	48.3 - 64.4 (30 - 40)	64.4+ (40+)
Roughness (m/km (im/mi))	0.47 - 1.34 (30 - 85)	1.34 - 2.13 (85 - 135)	2.13+ (135+)
Degree-of-curvature (DOC)	< 4 degrees	4 - 8 degrees	> 8 degrees
Grade (%)	< 2 %	2 - 4 %	> 4 %
Cross Slope (%)	< 3 %	3 - 5 %	>5 %
DOC / Cross Slope	< 1.5	1.5 - 3.0	> 3.0

A three-parameter subset was used in establishing a “Section Type” definition. Table 4 shows these three parameters and the Section Type assignment.

Table 4. Roadway section type definition based on parameter categorization/typing.

DOC / CS Low (0)	IRI Low (0)	IRI Medium (1)	IRI High (2)
Grade Low (0)	1	2	3
Grade Medium (1)	4	5	6
Grade High (2)	7	8	9
DOC / CS Medium (1)	**IRI Low (0)**	**IRI Medium (1)**	**IRI High (2)**
Grade Low (0)	10	11	12
Grade Medium (1)	13	14	15
Grade High (2)	16	17	18
DOC / CS High (2)	**IRI Low (0)**	**IRI Medium (1)**	**IRI High (2)**
Grade Low (0)	19	20	21
Grade Medium (1)	22	23	24
Grade High (2)	25	26	27

This categorization can be conducted at different roadway section lengths as an aid to determine the appropriate section length to be used in the analysis representative of the sample space for statistical analysis.

Tables 5 and 6 present the section type counts for roadway section lengths of 160.93 and 16.093 m (0.10 mi and 0.01 mi).

Table 5. Roadway section type count for section length of 160.93 m (0.10 mi)

DOC / CS Low (0)	IRI Low (0)	IRI Medium (1)	IRI High (2)
Grade Low (0)	91	279	182
Grade Medium (1)	18	193	192
Grade High (2)	30	191	217
DOC / CS Medium (1)	**IRI Low (0)**	**IRI Medium (1)**	**IRI High (2)**
Grade Low (0)		11	15
Grade Medium (1)		20	23
Grade High (2)		18	44
DOC / CS High (2)	**IRI Low (0)**	**IRI Medium (1)**	**IRI High (2)**
Grade Low (0)		6	6
Grade Medium (1)			3
Grade High (2)		7	44

Table 6. Roadway section type count for section length of 16.093 m (0.01 mi)

DOC / CS Low (0)	IRI Low (0)	IRI Medium (1)	IRI High (2)
Grade Low (0)	954	2660	1989
Grade Medium (1)	191	1928	1992
Grade High (2)	253	1999	2012
DOC / CS Medium (1)	**IRI Low (0)**	**IRI Medium (1)**	**IRI High (2)**
Grade Low (0)		148	190
Grade Medium (1)	2	131	156
Grade High (2)	13	297	372
DOC / CS High (2)	**IRI Low (0)**	**IRI Medium (1)**	**IRI High (2)**
Grade Low (0)	2	70	54
Grade Medium (1)		8	30
Grade High (2)		82	454

The shorter section length results in more section types being represented and increases the number of samples for each cell of the table. A correlation analysis reported in a later section of the report was performed to determine how the two sections lengths compare in terms of representing the sample space.

COMPUTATIONAL FLOW

The computational flow for generating the analysis database is presented in appendix C.A series of figures for the five program steps required to prepare the data for analysis is provided in this appendix.

Given the above generated analysis database for sections of the roadway of a given length, correlations between independent and dependent variables can be performed and other statistical techniques used to identify relationships and their statistical significance. Plots of the various metrics help illustrate the various relationships that may exist.

INITIAL DATA MINING

Appendix D contains the results of some of the initial data mining.

6. ANALYSIS

SELECTION OF VARIABLES

Figure 40 shows the interrelationship of the variables used in the analysis.

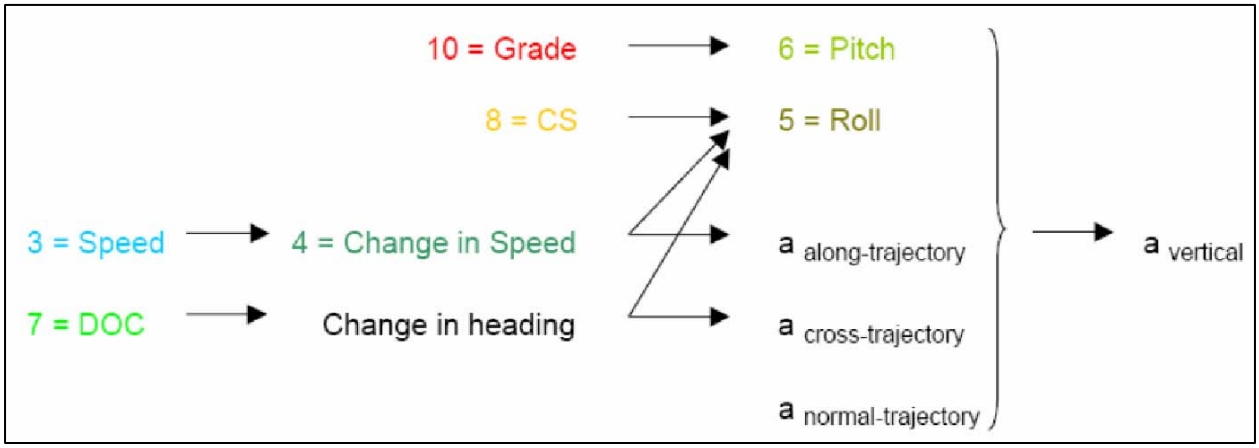

Figure 40. Illustration. Interrelationship of the variables used in analysis.

Grade of road and pitch of vehicle are closely related. Roll of the vehicle is affected by pavement cross slope, speed and change in speed of the vehicle in a horizontal curve, and the degree-of-curvature of the horizontal curve. Speed, change in speed, and degree-of-curvature affect along- and cross-trajectory accelerations. From these body horizontal trajectory accelerations and the body normal-trajectory acceleration (vertical),the real-world normal vertical acceleration is needed for the 1-D inertial profiling model.

In figure 41 the independent variables for the analysis are shown along with two options for dependent variables. Option 1 is the roadway section Average Absolute Difference (AAD) parameters or the roadway section Correlations for the inertial profiles and IRI values. The choice of dependent variable option is a function of which option provides the largest range of values within the sample space, thereby allowing easier detection of significant relationships.

Also of importance is the selection of roadway section length. A section length of too great a distance will result in the averaging or dampening of the variables, especially on a road with severe alignment where the change in heading, grade, and cross slope can occur in a short distance. Too short a section length may not permit the reliable estimate of parameters such as degree-of-curvature. Two section lengths were explored (16.09m and 160.93m (0.01 mi /52.8 ft and 0.10 mi/528.0 ft)).

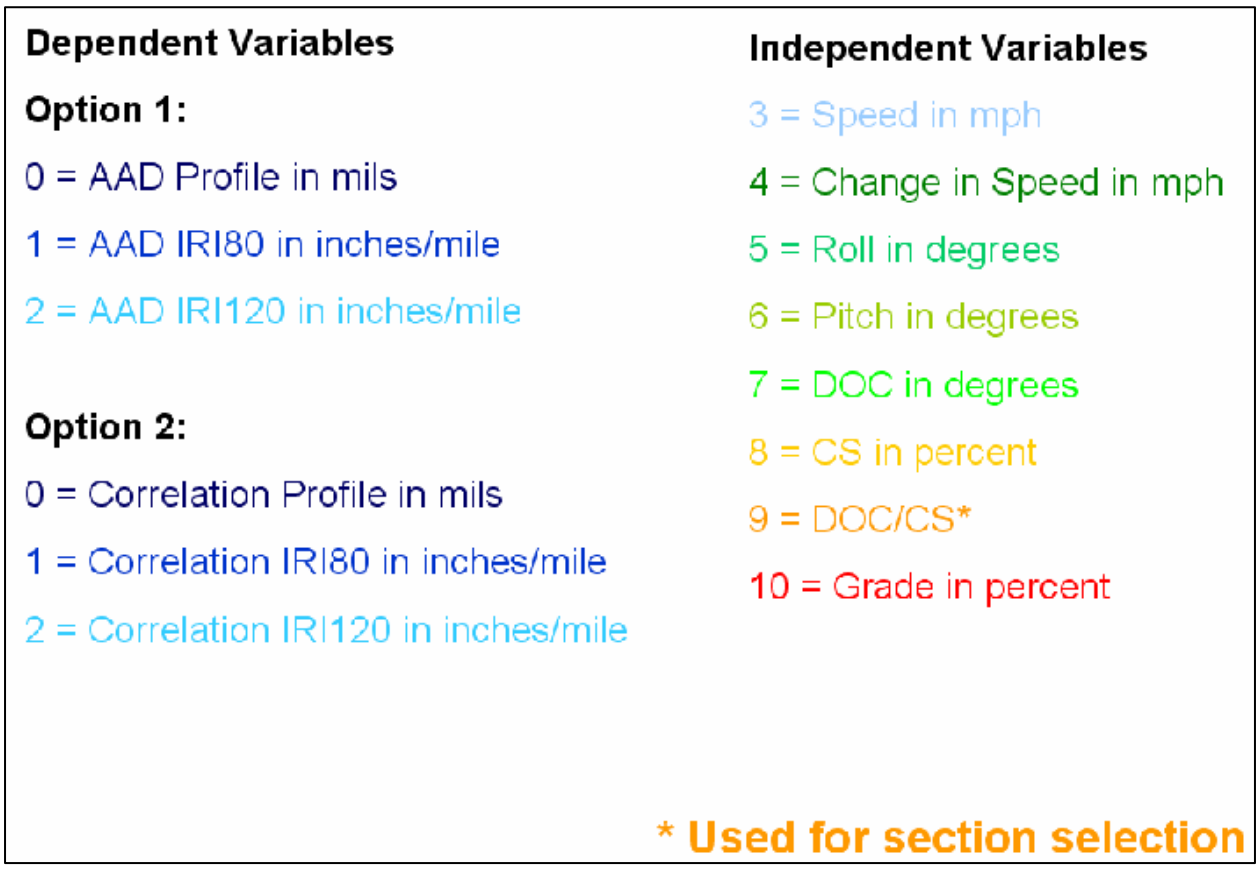

Figure 41. List. Independent variables (right) and two options for dependent variables (left) for analysis.

SAMPLE PLOTS SHOWING DATA VARIETY

Prior to performing an analysis of the data, line graphs of the data for two sites were generated so as to ascertain and display the range of roadway and vehicle operation characteristics present in the database. There are 3 dependent variables and eight independent variables. The two sites used for the sample plots were Route 193 and 460. Route 193 is a two-lane rural road with severe alignment as contrasted to the Route 460 four-lane divided rural road with mild alignment. The plots are presented as a pair of graphs for the same variable, one for each route, thus providing a contrasting view of the data. The same abscissa axis scale is used. A consistent ordinal scale is employed except when the scales differ too greatly to view the graphic detail on a comparative basis. The abscissa interval is 16.1 m (52.8 ft or 0.01mi).

Variable data shown in the plots are color coordinated with the dependent variable – independent variable correlation 3-D bar charts contained in this report.

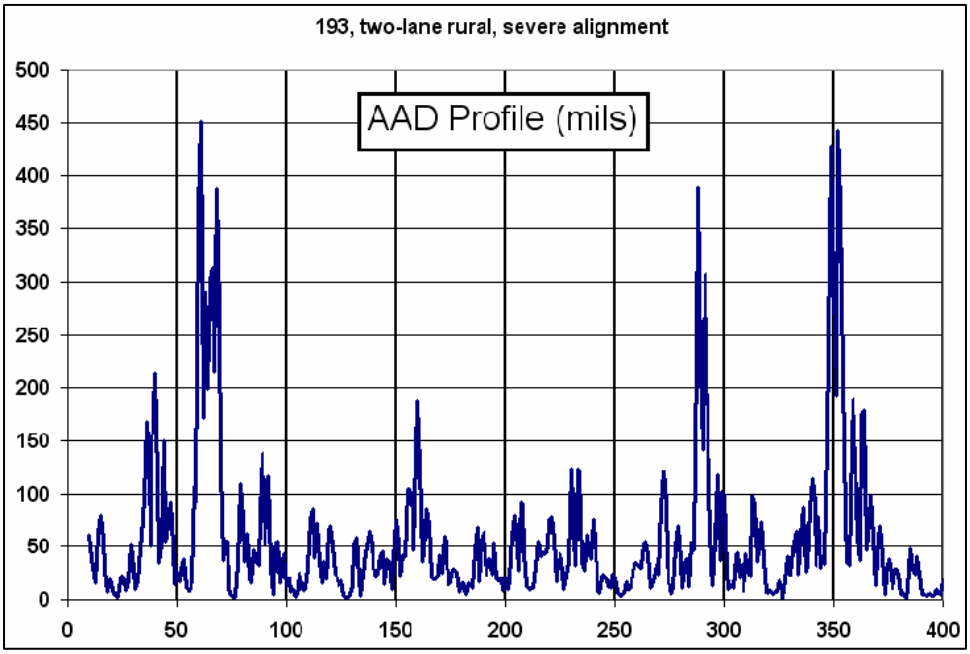

Figure 42. Line graph. Plot of 193 AAD Profile versus 0.01 mi (16.1 m) section number.

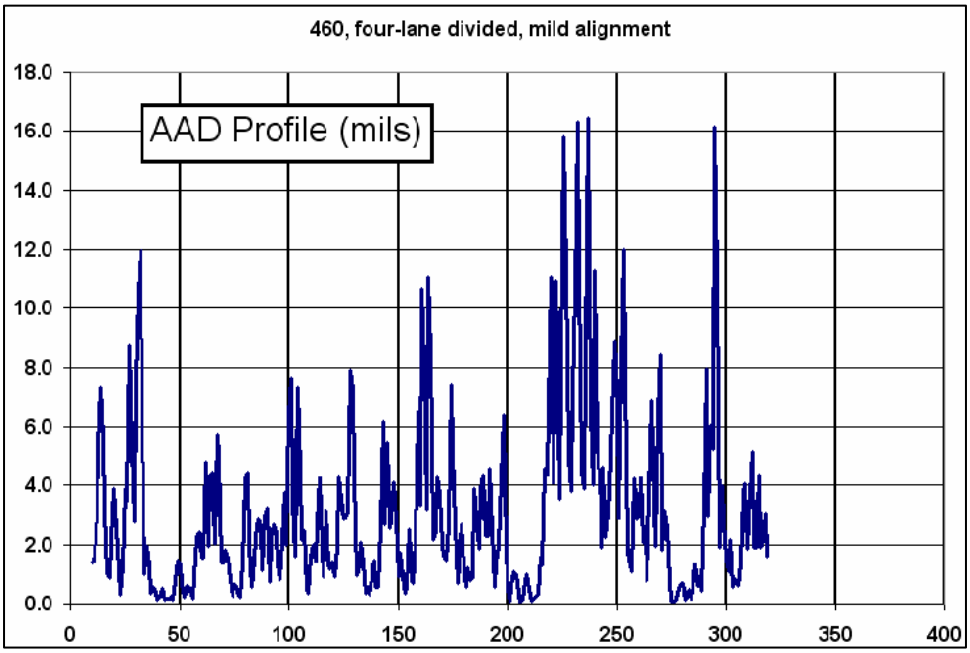

Figure 43. Line graph. Plot of 460 AAD Profile versus 0.01 mi (16.1 m) section number.

The effect of the severe alignment (figure 42) of the two-lane road compared to the four-lane divided highway mild alignment (figure 43) on AAD profile is very evident from the scale of the two graphs.

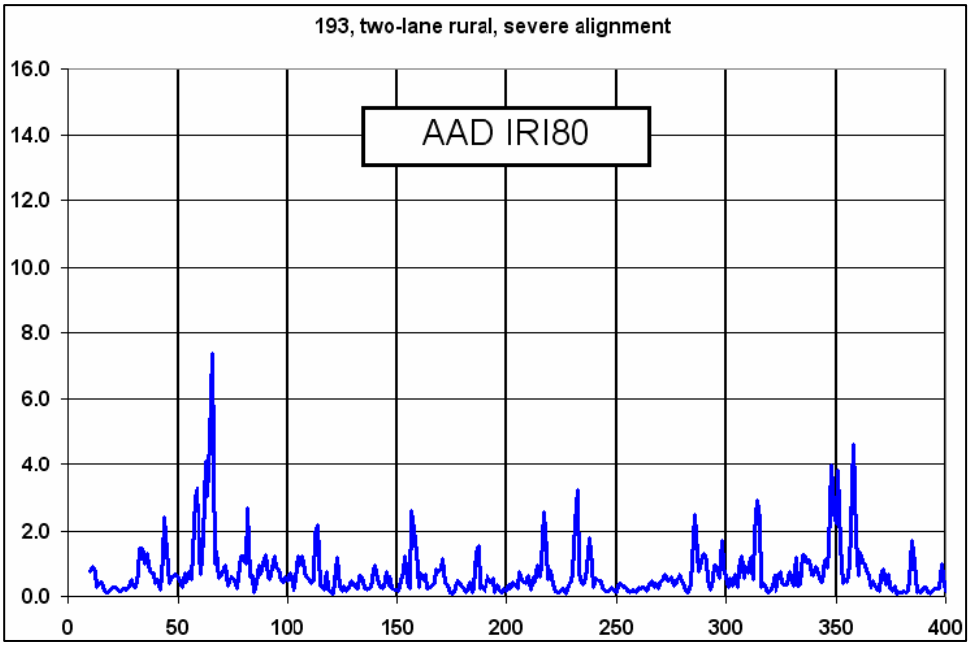

Figure 44. Line graph. Plot of 193 AAD IRI80 versus 0.01 mi (16.1 m) section number.

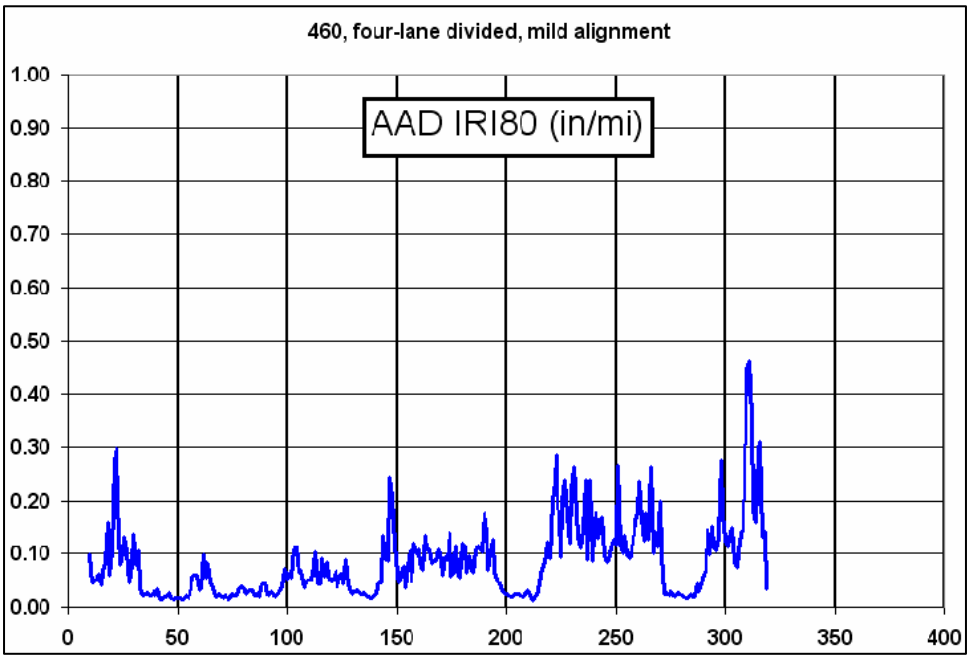

Figure 45. Line graph. Plot of 460 AAD IRI80 versus 0.01 mi (16.1 m) section number.

The effect of the severe alignment (figure 44) of the two-lane road compared to the four-lane divided highway mild alignment (figure 45) on AAD IRI80 is as expected given the differences in AAD profile.

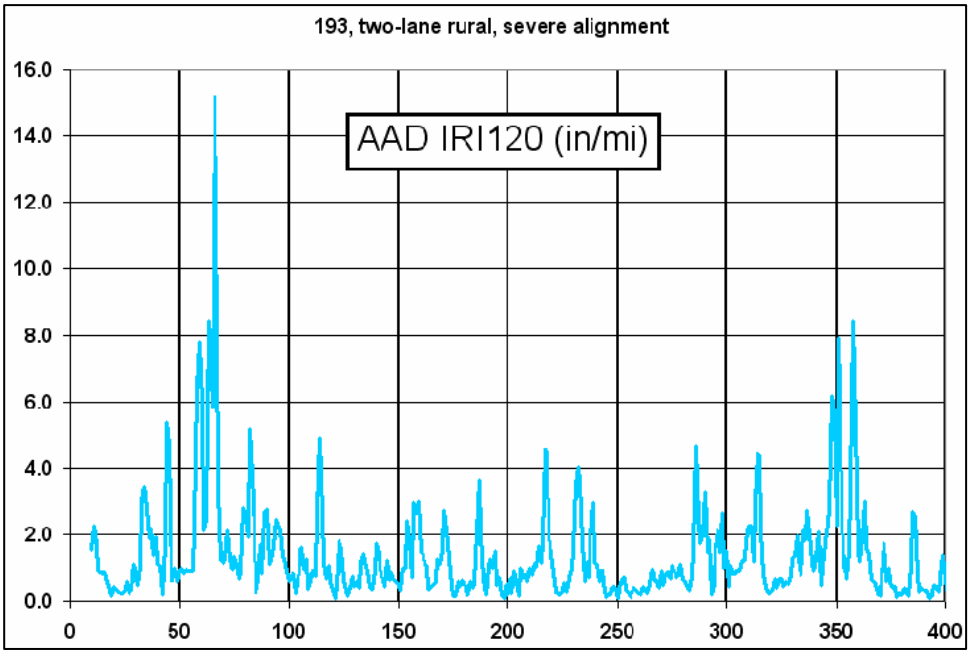

Figure 46. Line graph. Plot of 193 AAD IRI120 versus 0.01 mi (16.1 m) section number.

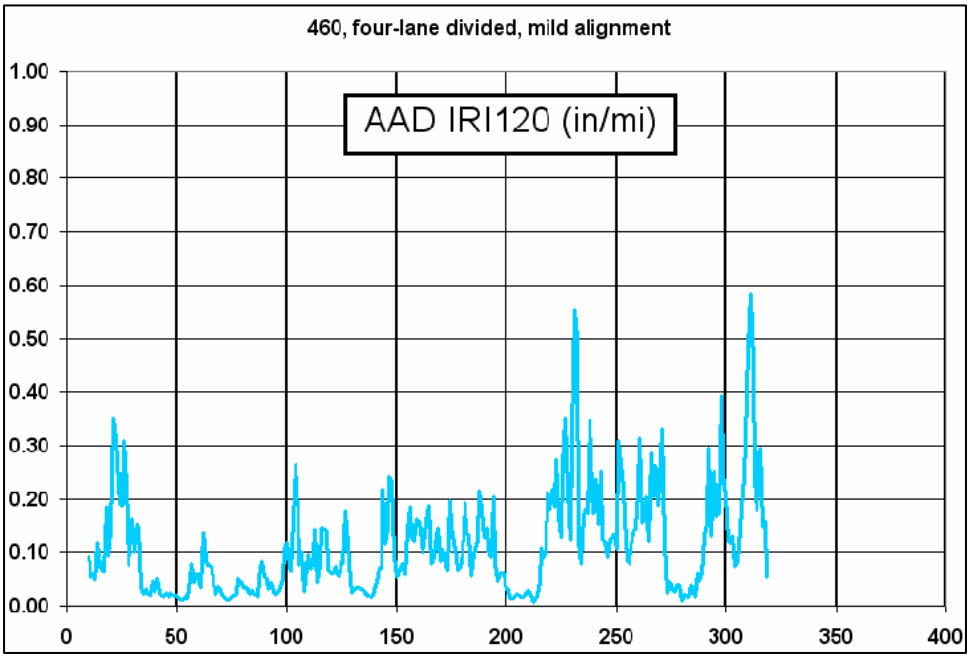

Figure 47. Line graph. Plot of 460 AAD IRI120 versus 0.01 mi (16.1 m) section number.

The effect of the severe alignment (figure 46) of the two-lane road compared to the four-lane divided highway mild alignment (figure 47) on AAD IRI120 is similar to that of AAD IRI80. AAD IRI120 values are generally greater than the corresponding AAD IRI80 values.

Figure 48. Line graph. Plot of 193 speed versus 0.01 mi (16.1 m) section number.

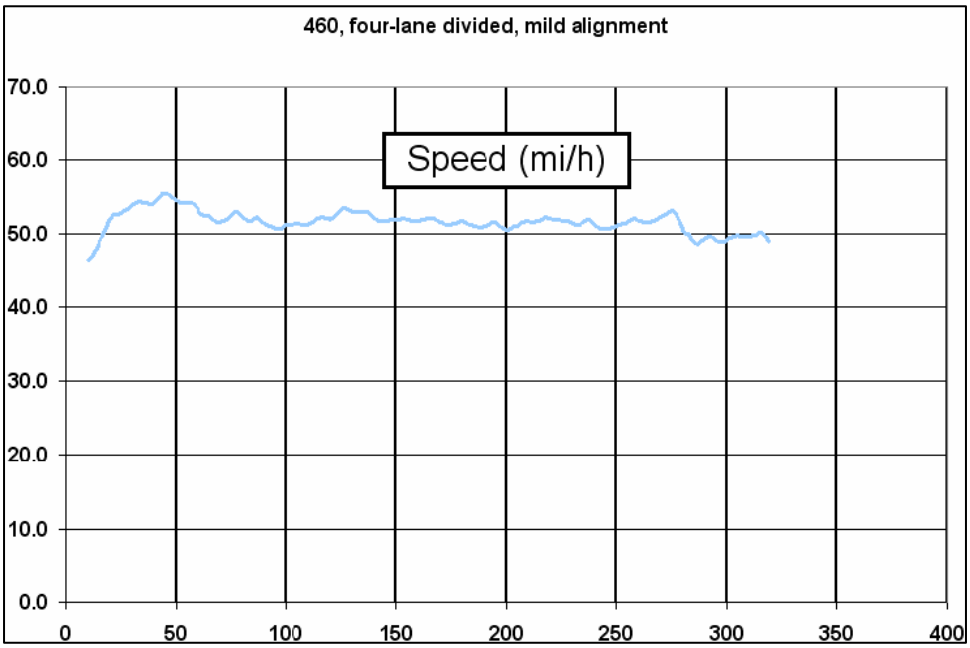

Figure 49. Line graph. Plot of 460 speed versus 0.01 mi (16.1 m) section number.

The severe alignment (figure 48) of 193 is very evident from the range of the speed data resulting from the numerous tight turns while for 460 (figure 49), the speed range is very small with the greatest fluctuation occurring at the beginning and ending of the site.

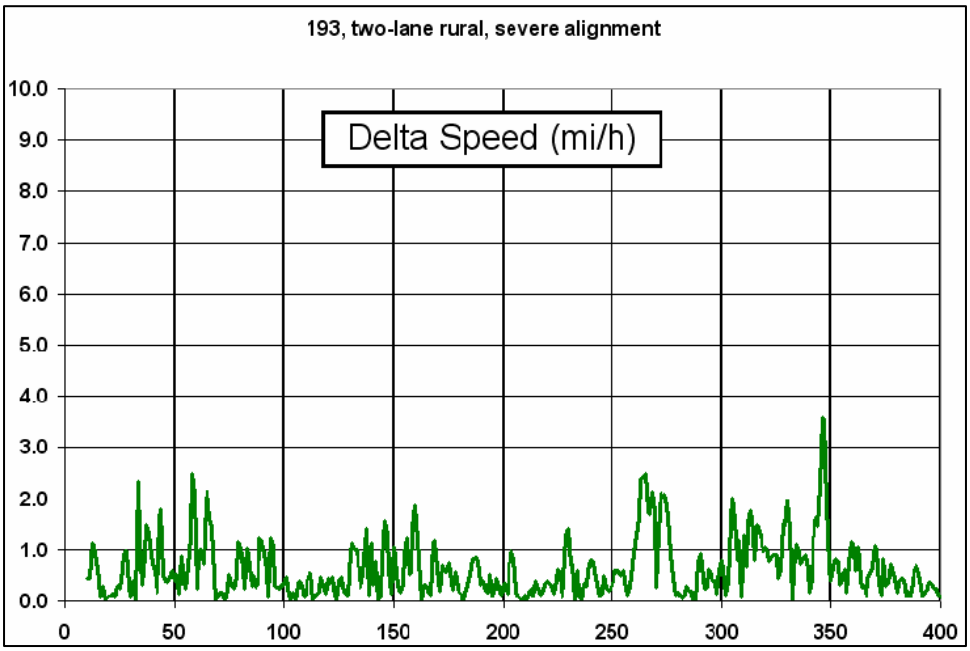

Figure 50. Line graph. Plot of 193 absolute delta speed versus 0.01 mi (16.1 m) section number.

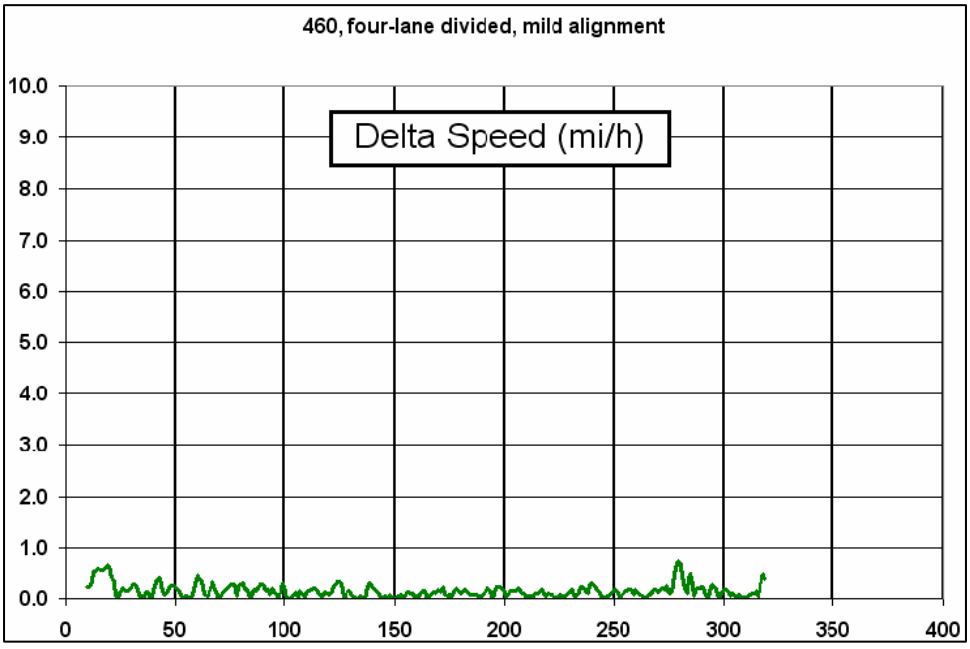

Figure 51. Line graph. Plot of 460 absolute delta speed versus 0.01 mi (16.1 m) section number.

The change in speed within the mild alignment 460 site is far less than the severe alignment 193 site.

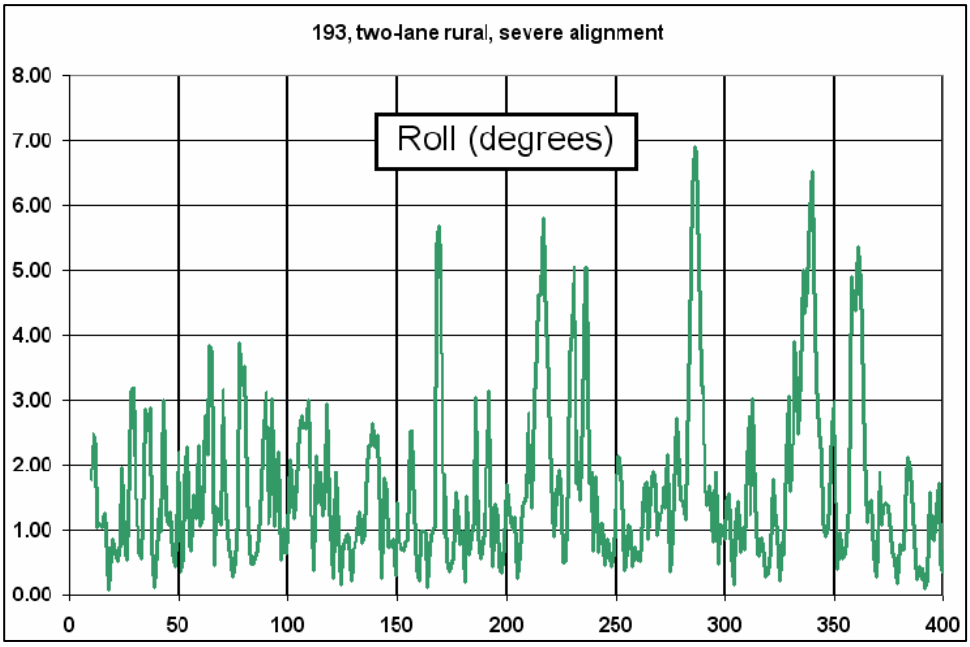

Figure 52. Line graph. Plot of 193 absolute roll versus 0.01 mi (16.1 m) section number.

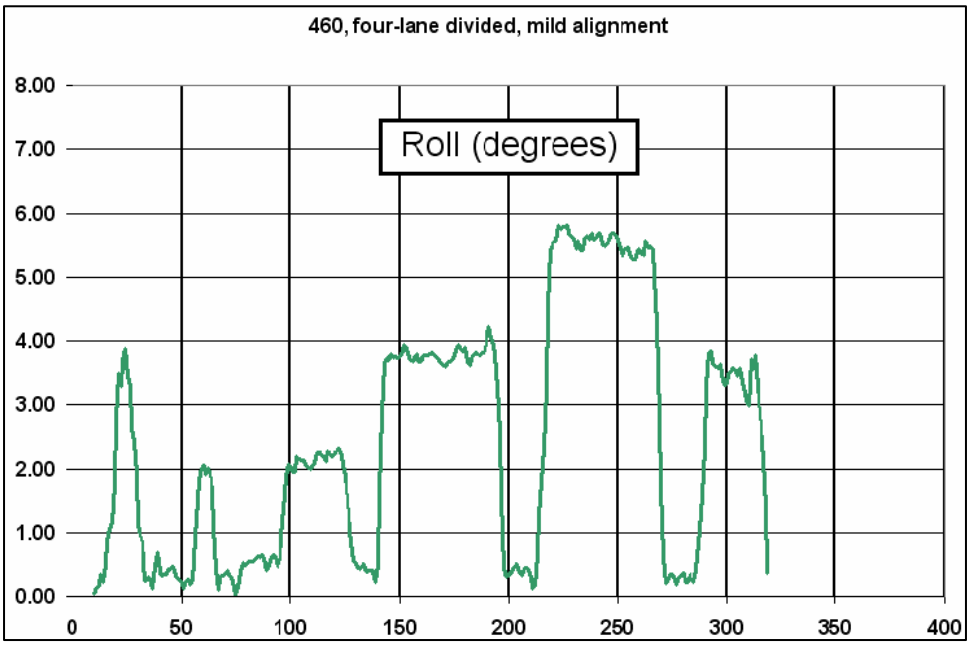

Figure 53. Line graph. Plot of 460 absolute roll versus 0.01 mi (16.1 m) section number.

The range in roll for the two sites is similar but the nature of roll sequences and number of roll changes is very different. For 193, the multiple roll changes seen in figure 52 are indicative of the roadway's poor cross slope in tangent sections and presence of many horizontal curves. The vehicle roll due to long horizontal curves with consistent cross slope is very evident for route 460 in figure 53. The individual horizontal curves are clearly seen.

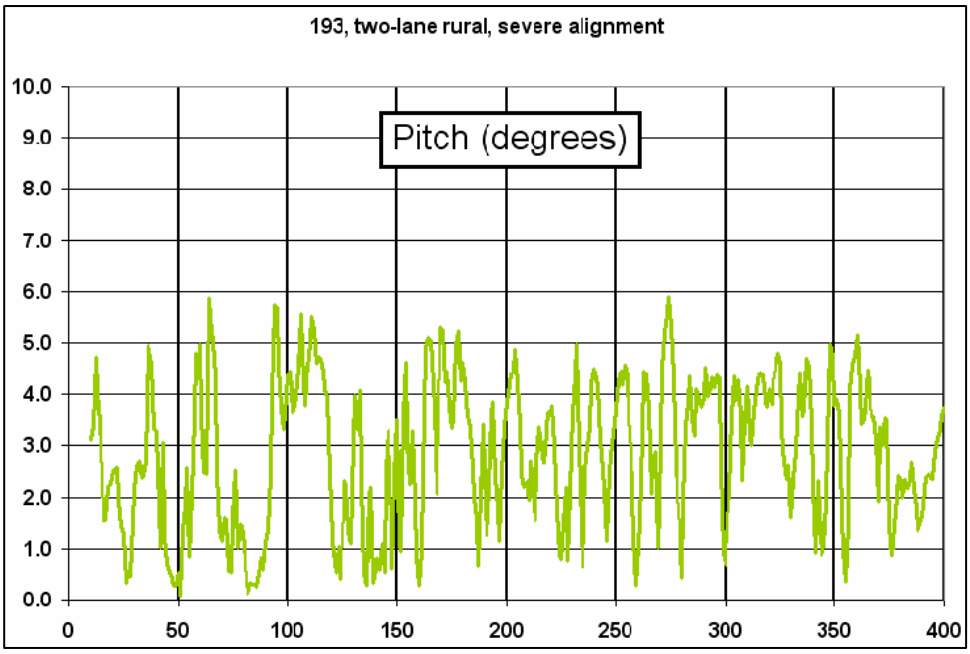

Figure 54. Line graph. Plot of 193 absolute pitch versus 0.01 mi (16.1 m) section number.

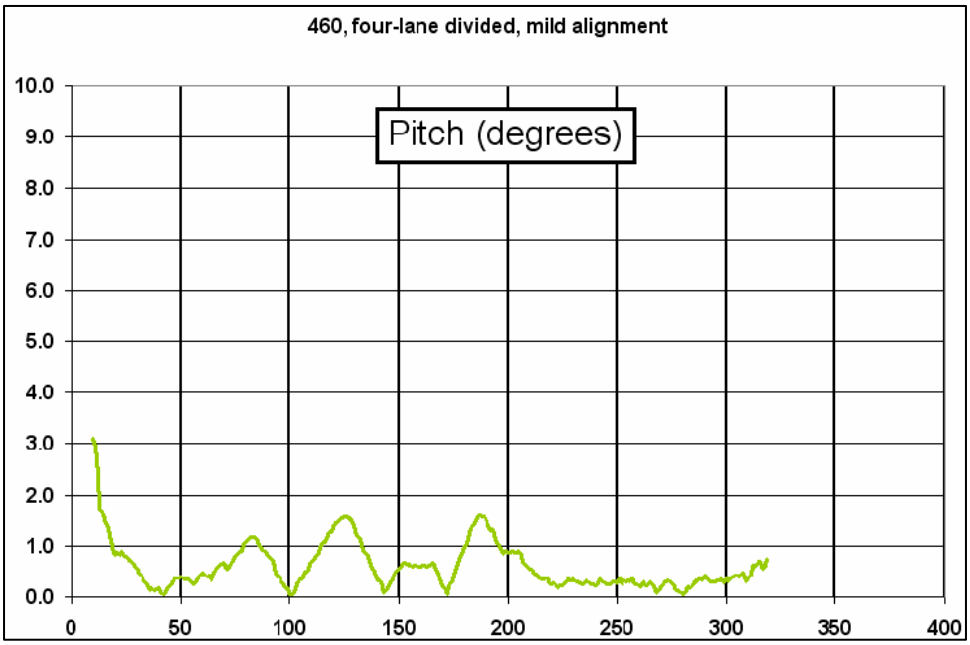

Figure 55. Line graph. Plot of 460 absolute pitch versus 0.01 mi (16.1 m) section number.

Pitch changes rapidly for severe alignment 193 site (figure 54) due to the hilly terrain and rough road. Pitch is as high as 6 percent. Route 460 (figure 55) the mild alignment site, has small and infrequent pitch changes due to a fairly level terrain and a relatively smooth road with pitch generally not exceeding 1.6 percent except at the beginning.

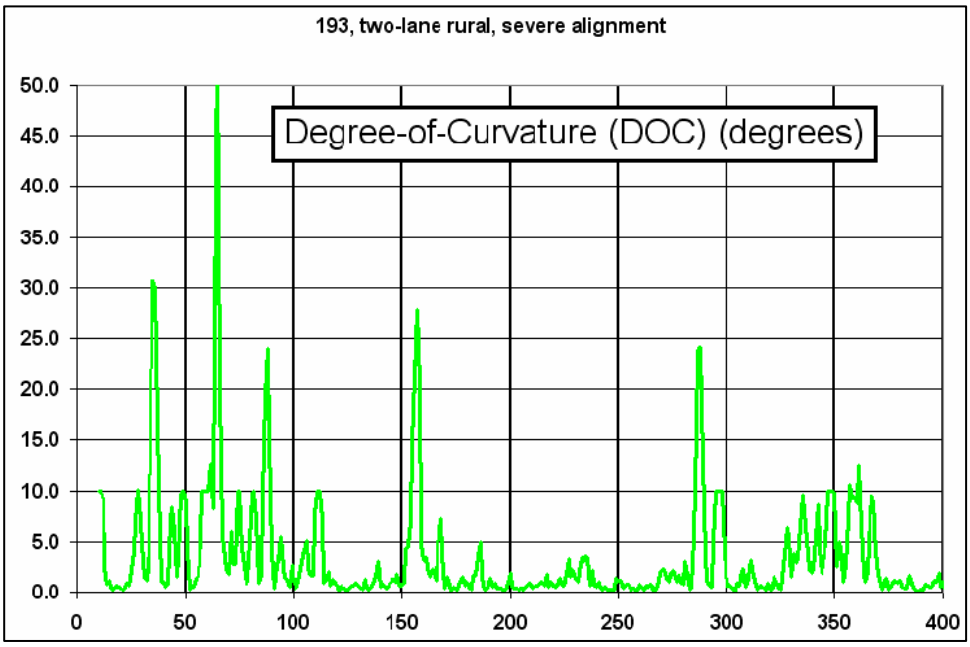

Figure 56. Line graph. Plot of 193 degree-of curvature versus 0.01 mi (16.1 m) section number.

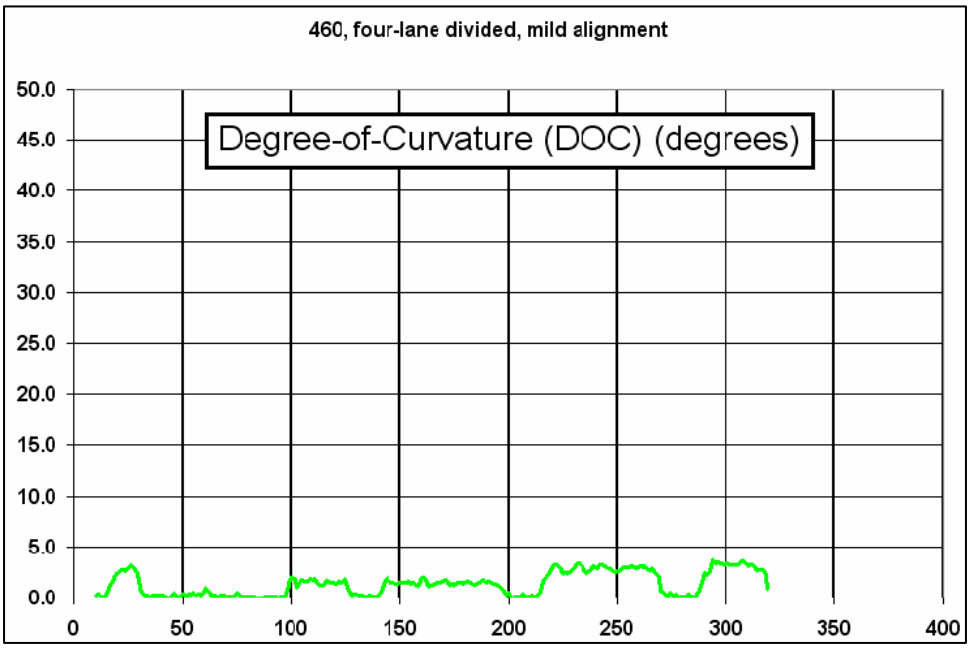

Figure 57. Line graph. Plot of 460 degree-of curvature versus 0.01 mi (16.1 m) section number.

The above figures for degree-of-curvature clearly show the difference in horizontal alignment severity. Route 193 has tight turns while 460 has long gentle turns.

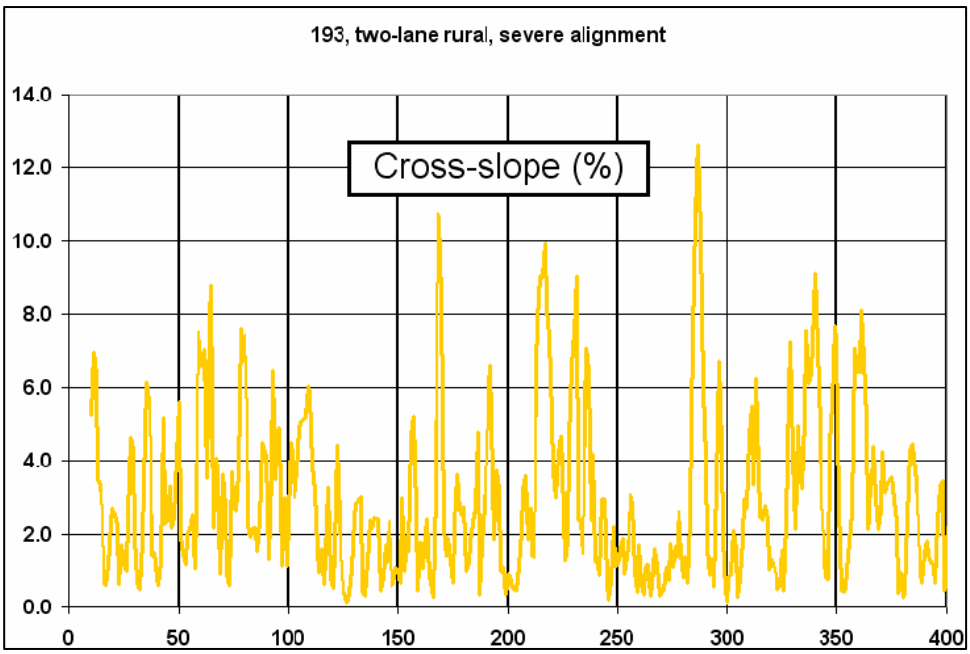

Figure 58. Line graph. Plot of 193 absolute cross slope versus 0.01 mi (16.1 m) section number.

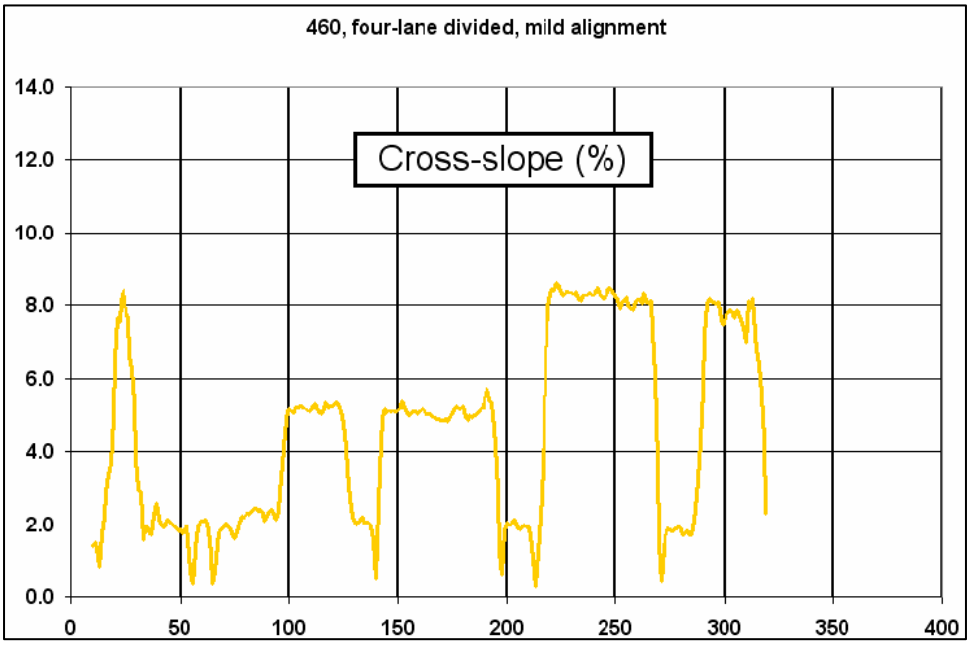

Figure 59. Line graph. Plot of 460 absolute cross slope versus 0.01 mi (16.1 m) section number.

Cross slope and vehicle roll are closely related. Again, the severe alignment of route 193 (figure 58) compared to the mild alignment of 460 (figure 59) is clearly seen in the graphs.

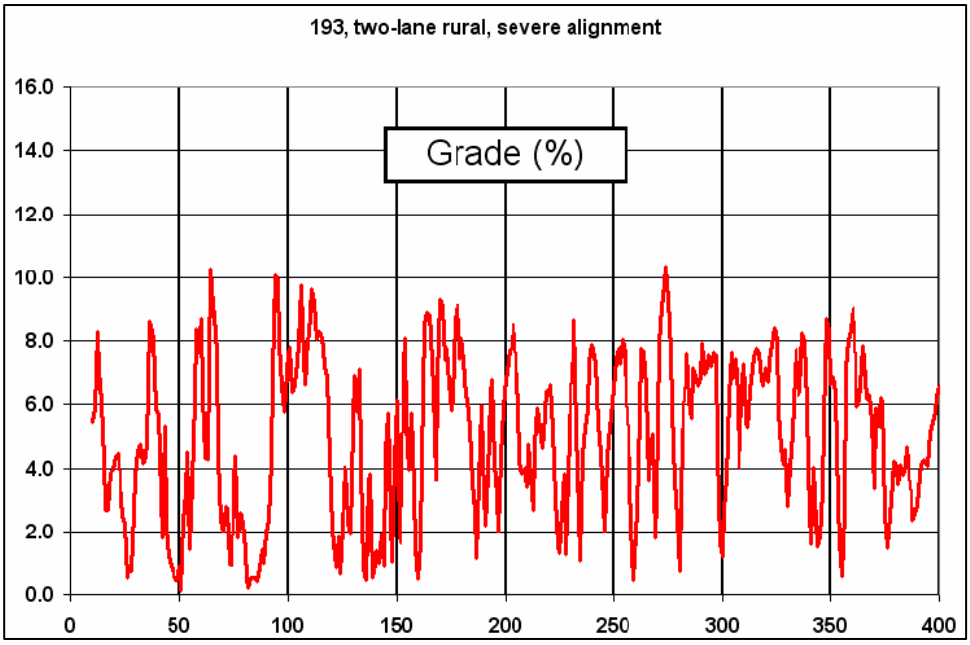

Figure 60. Line graph. Plot of 193 absolute grade versus 0.01 mi (16.1 m) section number.

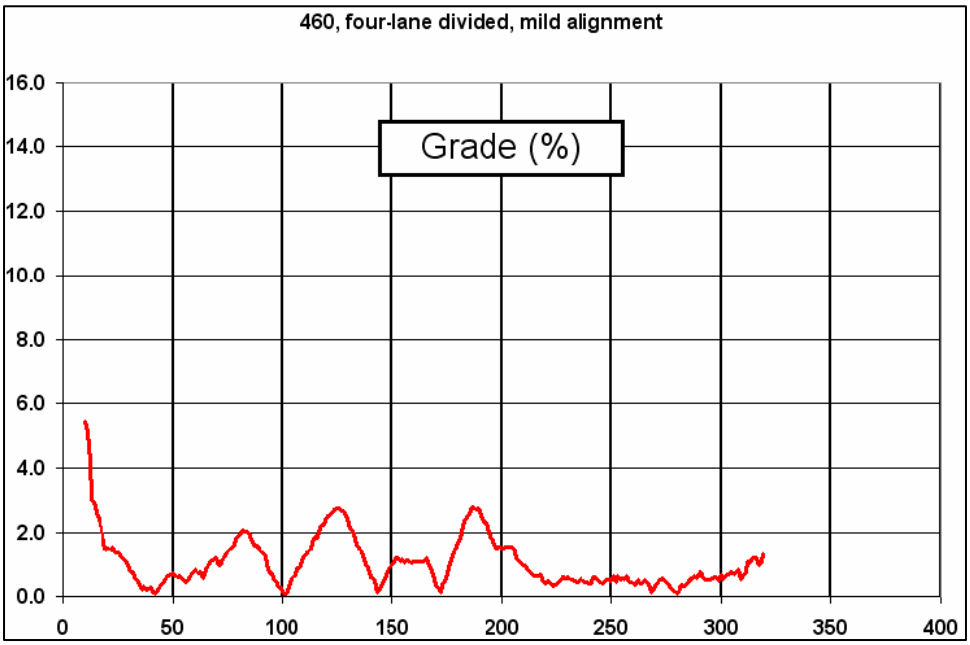

Figure 61. Line graph. Plot of 460 absolute grade versus 0.01 mi (16.1 m) section number.

Again, the severity of vertical alignment (and changes in vertical alignment) in the 193 data (figure 60) is dramatic compared to 460 (figure 61).

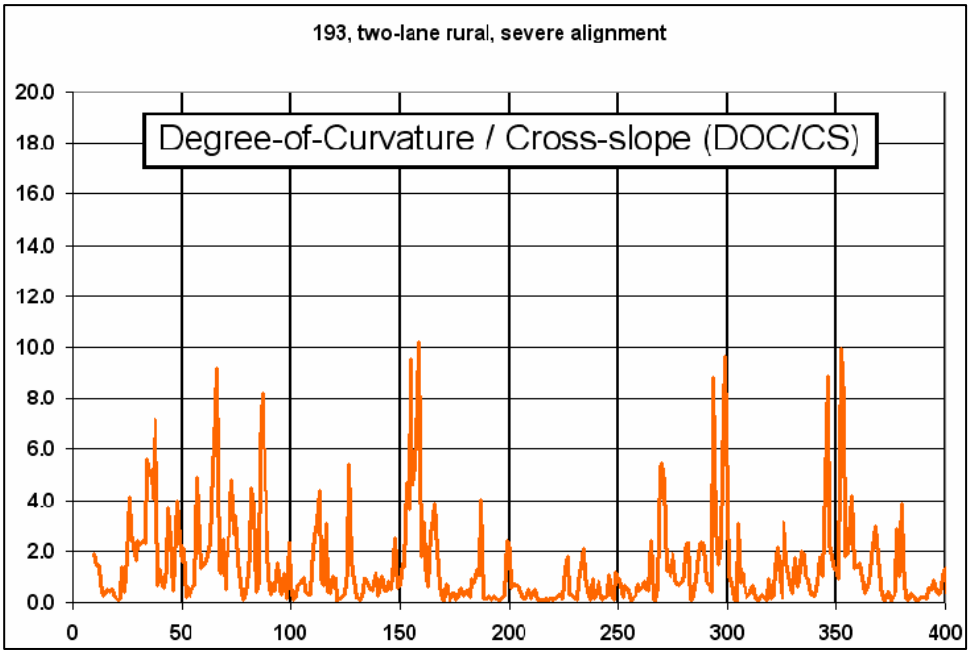

Figure 62. Line graph. Plot of 193 degree-of-curvature / cross slope versus 0.01 mi (16.1 m) section number.

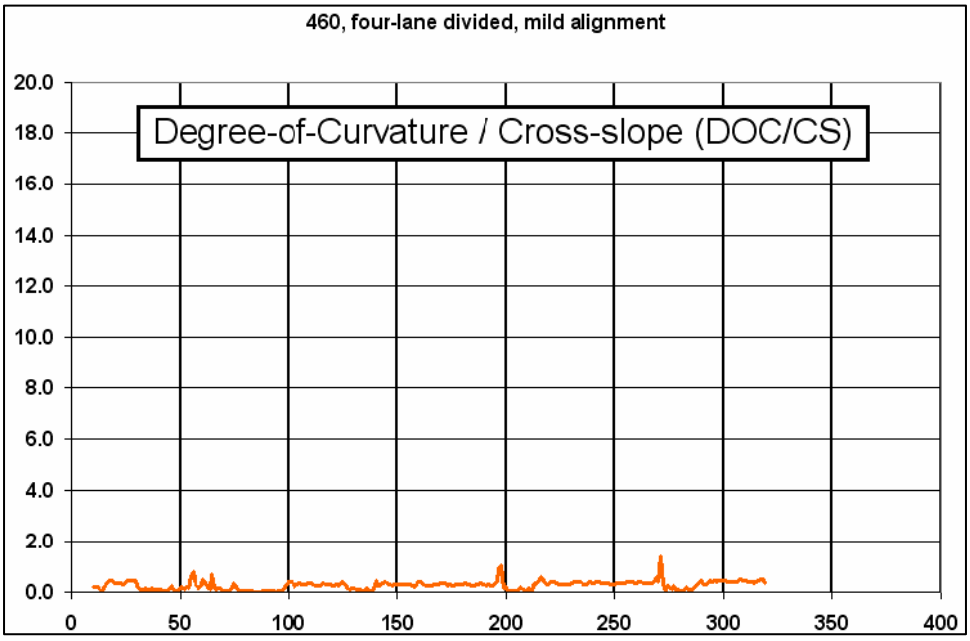

Figure 63. Line graph. Plot of 460 degree-of-curvature / cross slope versus 0.01 mi (16.1 m) section number.

The independent variable degree-of-curvature / cross slope was an attempt to represent how greater cross slope (superelevation) counters, to some extent, higher degrees-of-curvature. For route 193, this variable combination still shows a great difference between the 193 and 460 sites.

ANALYSIS OF DATA MATRIX

There are six data collection run datasets for each of the four sites. Table 7 documents the source of the data from the DHMS database, average speed for each run, and run number reference used within the following analysis.

Table 7. Data matrix run numbers and average speed for each run.

Site Description	Run Number*	Average Speed (km/h (mi/h))	Dataset Number
193 **two-lane rural** **severe alignment**	1	49.6 (30.8)	1
	2	51.8 (32.2)	2
	22	52.5 (32.6)	3
	42	55.5 (34.5)	4
	41	57.3 (35.6)	5
	43	64.2 (39.9)	6
851 **two-lane rural** **severe alignment**	10	41.8 (26.0)	7
	12	67.3 (41.8)	8
	20	61.5 (38.2)	9
	23	58.7 (36.5)	10
	26	64.1 (39.8)	11
	31	62.4 (38.8)	12
9 **two-lane rural** **moderate alignment**	1	79.8 (49.6)	13
	2	84.7 (52.6)	14
	3	84.7 (52.6)	15
	4	84.0 (52.2)	16
	5	76.3 (47.4)	17
	6	85.9 (53.4)	18
460 **four-lane divided highway** **mild alignment**	2	84.2 (52.3)	19
	3	82.6 (51.3)	20
	4	77.9 (48.4)	21
	5	66.9 (41.6)	22
	7	82.2 (51.1)	23
	10	82.6 (51.3)	24

* Run number from DHMS database

** Run number reference for data matrix analysis

As can be seen in the table, some variation in average speed amongst the data collection runs is present and therefore provides a greater sample space for analysis.

Principle Component Analysis of Each Data Set

A Principal Component Analysis (PCA) was conducted on each of the 24 data sets. The analysis consisted of the four steps, 1) normalize data, 2) calculate covariance matrix, 3) find eigenvalues and eigenvectors, and 4) compute percent contribution of each principal component based on their eigenvalues.

Normalizing data is performed using the three equations show in equations 43 through 45.

$$mn_j := \frac{1}{N} \cdot \sum_i Set1_{i,j} \tag{43}$$

$$variance_j := \frac{1}{N-1} \cdot \sum_i \left(Set1_{i,j} - mn_j\right)^2 \tag{44}$$

$$X_{i,j} := \frac{Set1_{i,j} - mn_j}{\sqrt{variance_j}} \tag{45}$$

Compute covariance matrices using equations 46 and 47.

$$mn_j := \frac{1}{N} \cdot \sum_i X_{i,j} \tag{46}$$

$$V_{j,k} := \frac{1}{N-1} \cdot \sum_i \left(X_{i,j} - mn_j\right) \cdot \left(X_{i,k} - mn_k\right) \tag{47}$$

The variances of the principal components are the eigenvalues of the covariance matrix (step 3). We are merely changing coordinate systems. Let Eignevalues = eigenvals(V) and Eigenvector = eigenvecs(V). Compute percent contribution of each principal component based on their eigenvalues as shown in equation 48.

$$Percent_j := Eigenvalue_j \cdot \frac{100}{\sum_j Eigenvalue_j} \tag{48}$$

Paired figures 64 and 65 show Principal Component Analysis percentages for the 24 datasets.

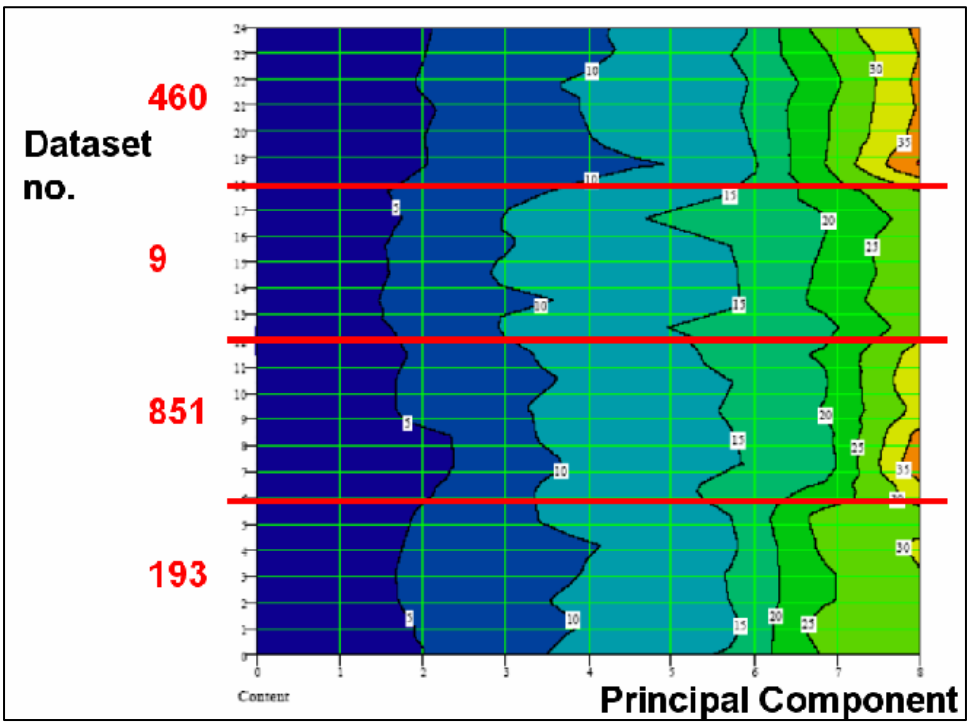

Figure 64. Isochart. Graphical display of Principle Component Analysis for six runs for each of four sites.

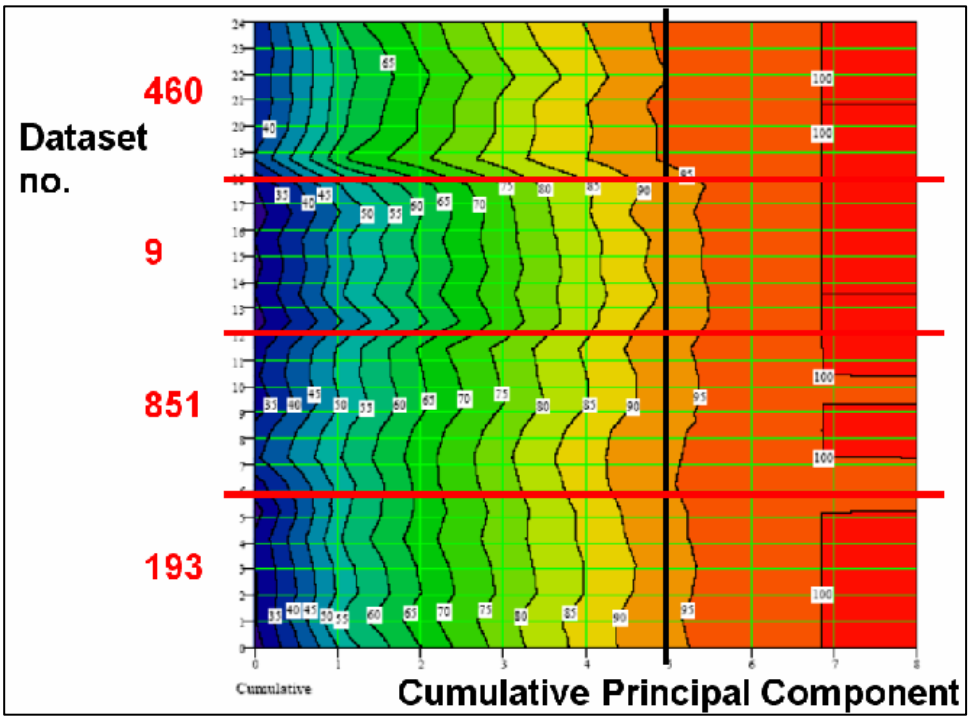

Figure 65. Isochart . Graphical display of Principle Component Analysis for six runs for each of four sites (continued).

In figure 66 the variables found to be similar in the principal component analysis are shown. Speed and change in speed; pitch and grade; and degree-of-curvature (DOC), cross slope (CS); and degree-of-curvature / cross slope (DOC/CS) are similar. The principal component analysis determined that 90% of the variability in the data matrix of the six runs for each of four sites is captured by 5 components (variables).

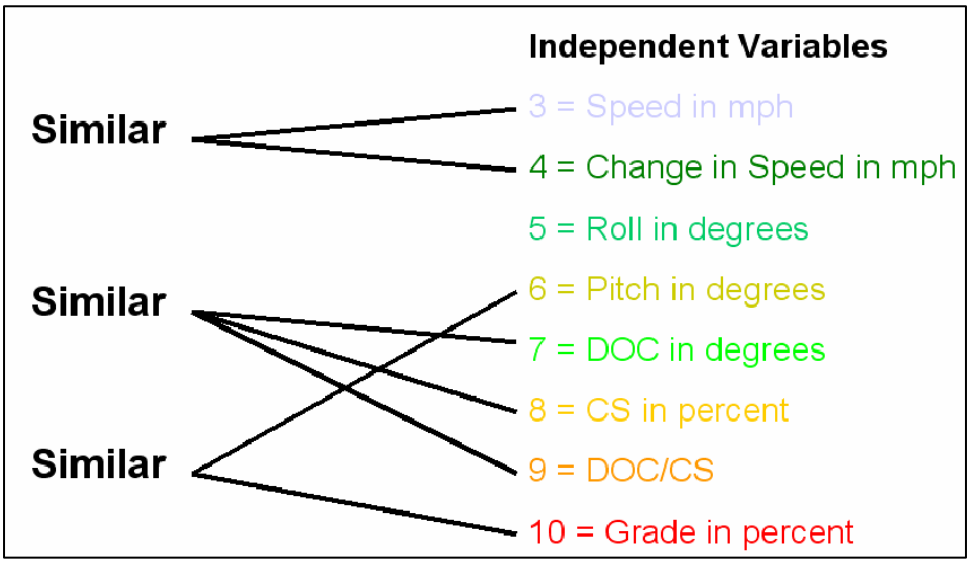

Figure 66. Variable list. Independent variable list with variables being similar shown.

The results of the principal component analysis supported the selection of the cross-variables shown in figure 67

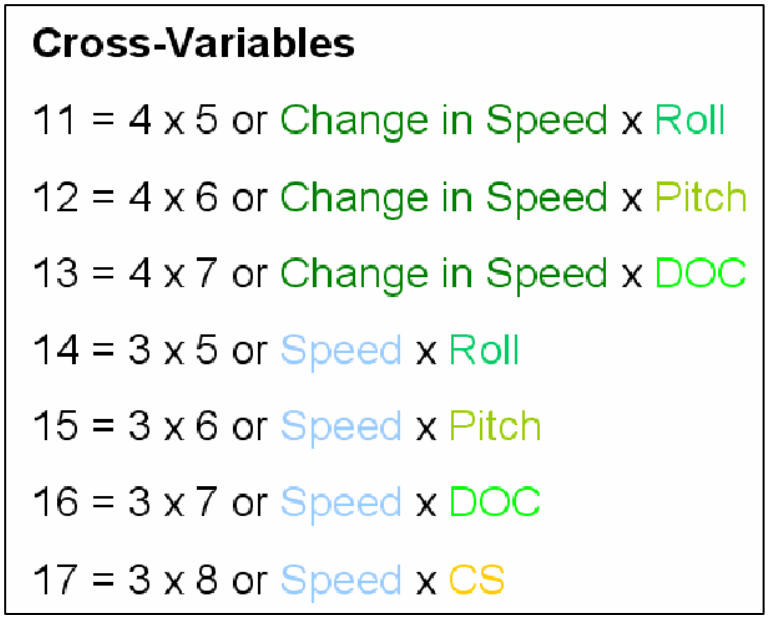

Figure 67. Variable list. Cross-variables for analysis.

Multivariate Analysis of Variance Between Data Sets

For the same set of independent variables and 24 datasets (six runs at the four sites), a multivariate analysis of variance between data sets was conducted. The purpose of the analysis was to determine similarities and differences between the data sets. Each dataset is compared to the other 23 datasets.

Three computational steps are performed in computing a Hotellings T-Squared statistic to determine differences between the data sets, 1) compute covariance matrices, 2) compute pooled sample covariance matrix, and 3) compute Hotellings T-Squared statistics.

Covariance matrices are computed using equations 49 through 52 on each paring (1 and 2 in equations) of the datasets.

$$mean1 := \frac{1}{Nr1} \cdot \sum_{j=0}^{Nr1-1} \left(Set1^{T}\right)^{\langle j \rangle} \tag{49}$$

$$Covariance1 := \frac{1}{Nr1-1} \left[\sum_{j=0}^{Nr1-1} \left[\left[\left(Set1^{T}\right)^{\langle j \rangle} - mean1 \right] \cdot \left[\left(Set1^{T}\right)^{\langle j \rangle} - mean1 \right]^{T} \right] \right] \tag{50}$$

$$\text{mean2} := \frac{1}{Nr2} \cdot \sum_{j=0}^{Nr2-1} \left(Set2^{T}\right)^{\langle j \rangle} \tag{51}$$

$$\text{Covariance2} := \frac{1}{Nr2-1} \left[\sum_{j=0}^{Nr2-1} \left[\left[\left(Set2^{T}\right)^{\langle j \rangle} - \text{mean2} \right] \cdot \left[\left(Set2^{T}\right)^{\langle j \rangle} - \text{mean2} \right]^{T} \right] \right] \tag{52}$$

The pooled sample variance is then computed as shown in equation 53.

$$S := \frac{\text{Covariance1} \cdot (Nr1 - 1) + \text{Covariance2} \cdot (Nr2 - 1)}{Nr1 + Nr2 - 2} \tag{53}$$

Hotellings T-Squared statistic between two samples of combined size Nr1+Nr2-2 and Nc1 variables (degrees-of-freedom) is computed as shown in equation 54.

$$t2 := \frac{Nr1 \cdot Nr2}{Nr1 + Nr2} \cdot (\text{mean1} - \text{mean2})^{T} \cdot S^{-1} \cdot (\text{mean1} - \text{mean2}) \tag{54}$$

Hotelling's T-Squared is related to the F distribution shown in equation 55 and is compared to the F statistic F(Nc1, NR1+Nr2-1-Nc1).

$$\text{fequivalent} := \frac{Nr1 + Nr2 - 1 - Nc1}{(Nr1 + Nr2 - 2) \cdot Nc1} \cdot t2 \tag{55}$$

The results of this dataset pairing comparison are shown in Figure 68.

??? Need figure explanation.

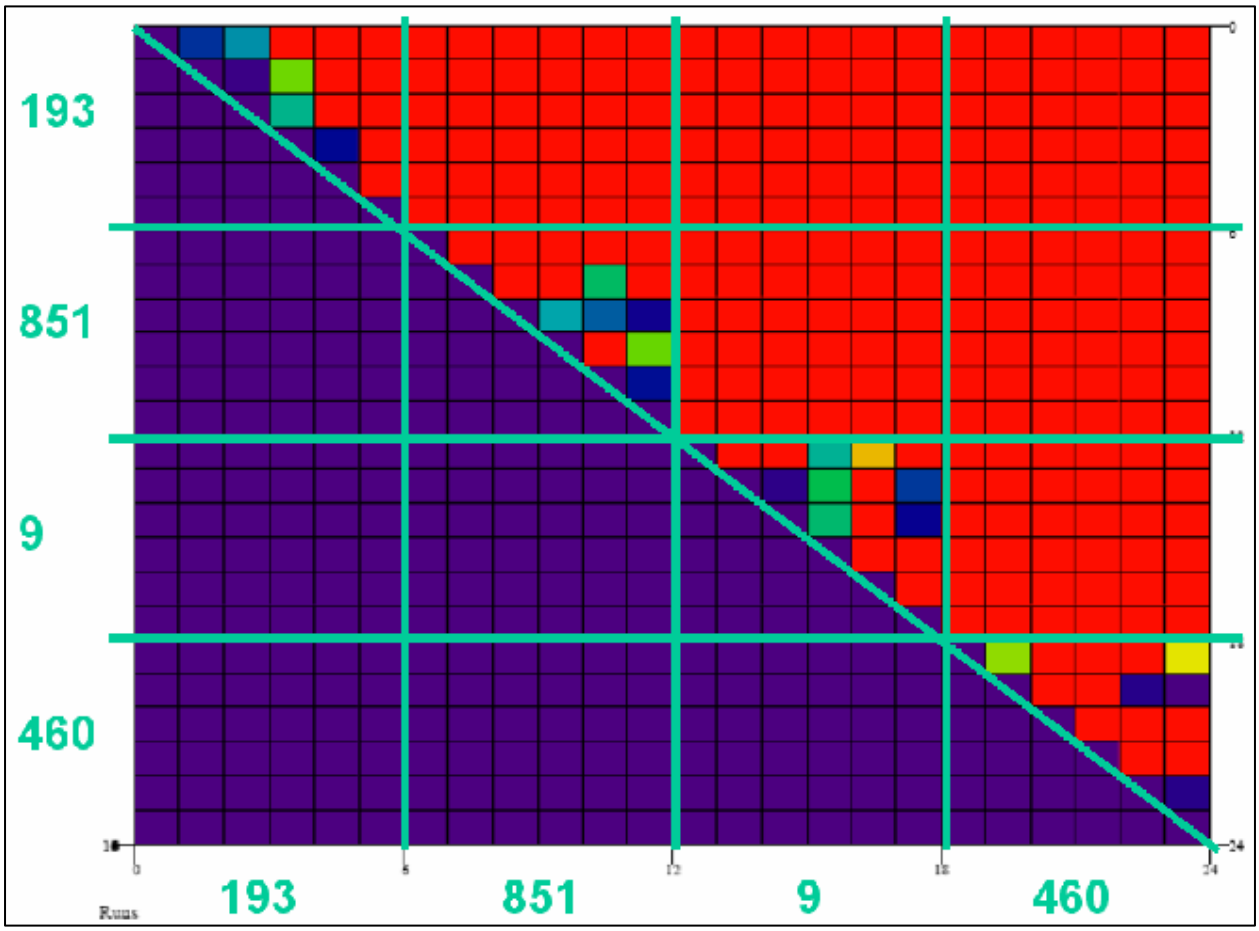

Figure 68. Grid of 24 x 24 cells. Multivariate analysis of variance between datasets.

Considering the eight independent variables and using a 99% confidence interval with Hotelling's T2 analysis, all four sites were found to be very different from each other. Among the six runs within each site, there is significant variance. Note that the DHMS operator ran the sites at different speeds for some of the runs. Only datasets 2 and 3 (site 193) and datasets 20 and 24 (site 460) are most similar.

CORRELATIONS

A correlation analysis was performed between the dependent and independent variables so as to show the strongest correlations and to reveal the patterns between the dependent versus independent variables. From this analysis, a choice of which dependent variable option was to be used in the subsequent analysis was made. Also, the effect of section length was conducted to determine what section length would best represent the data and its variability for subsequent analysis.

Correlations Between Variables

The four figures 69 through 72 present the results of the correlation analysis in a graphical format with one graph for each site. The correlation analysis was based on using a section length of 16.1 m (52.8 ft). In addition to the 3-D bar chart of the correlations, two line charts are provided of the dependent and independent variable pair with the highest correlation. A scatter plot of the highlighted dependent and independent variable is also provided. These four graph groupings are shown on the next four pages. The depth axis is of the dependent variables. From back to front, they are AAD Profile (0), AAD IRI80 (1), and AAD IRI120(2). The independent variables are represented along the width of the 3-D bar chart. A legend key for the independent variables is provided within the figure.

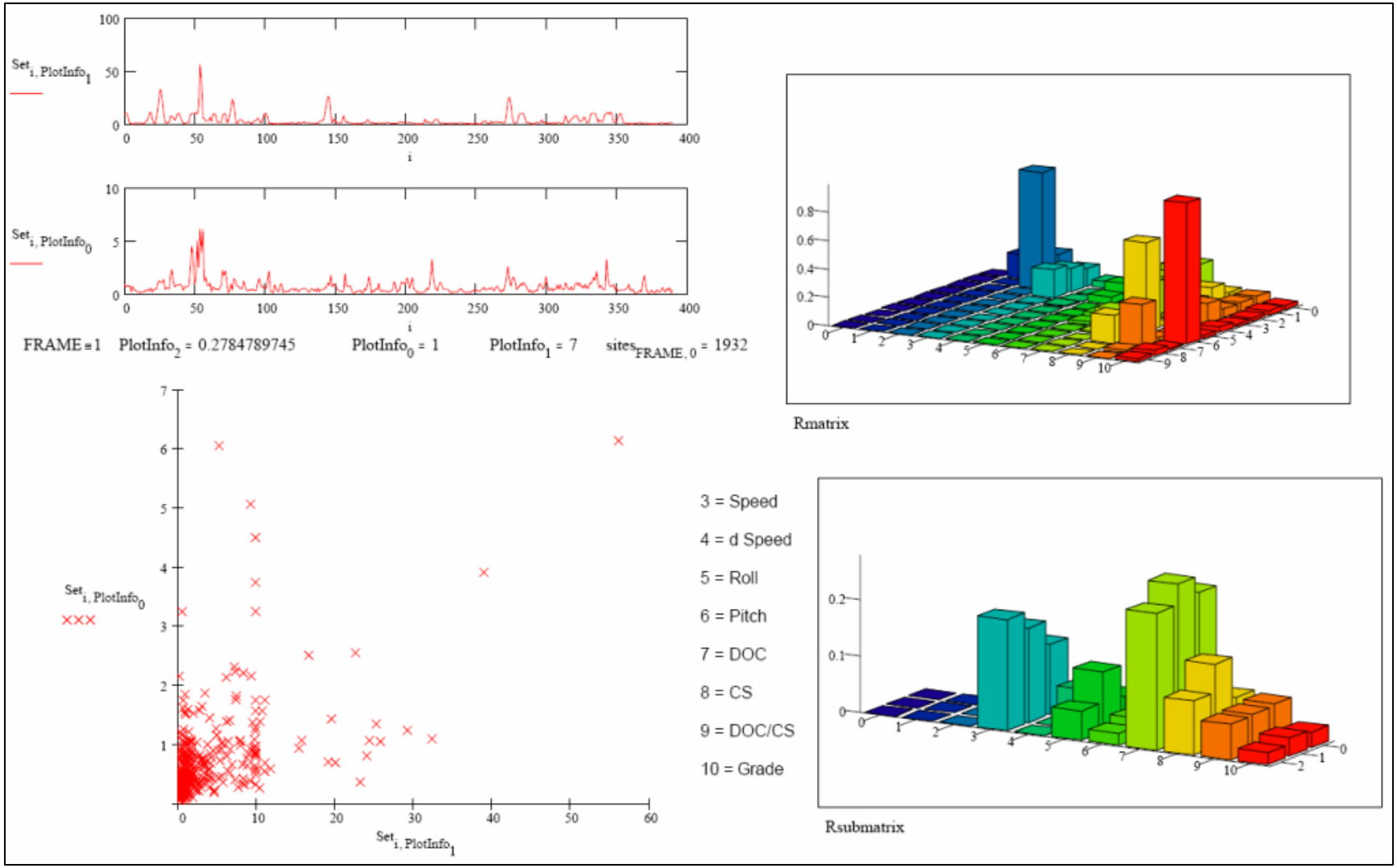

Figure 69. Graph. Correlations for route 193 (typical).

Speed, degree-of-curvature and cross slope have the highest correlations with AAD Profile, AAD IRI80 and AAD IRI120.

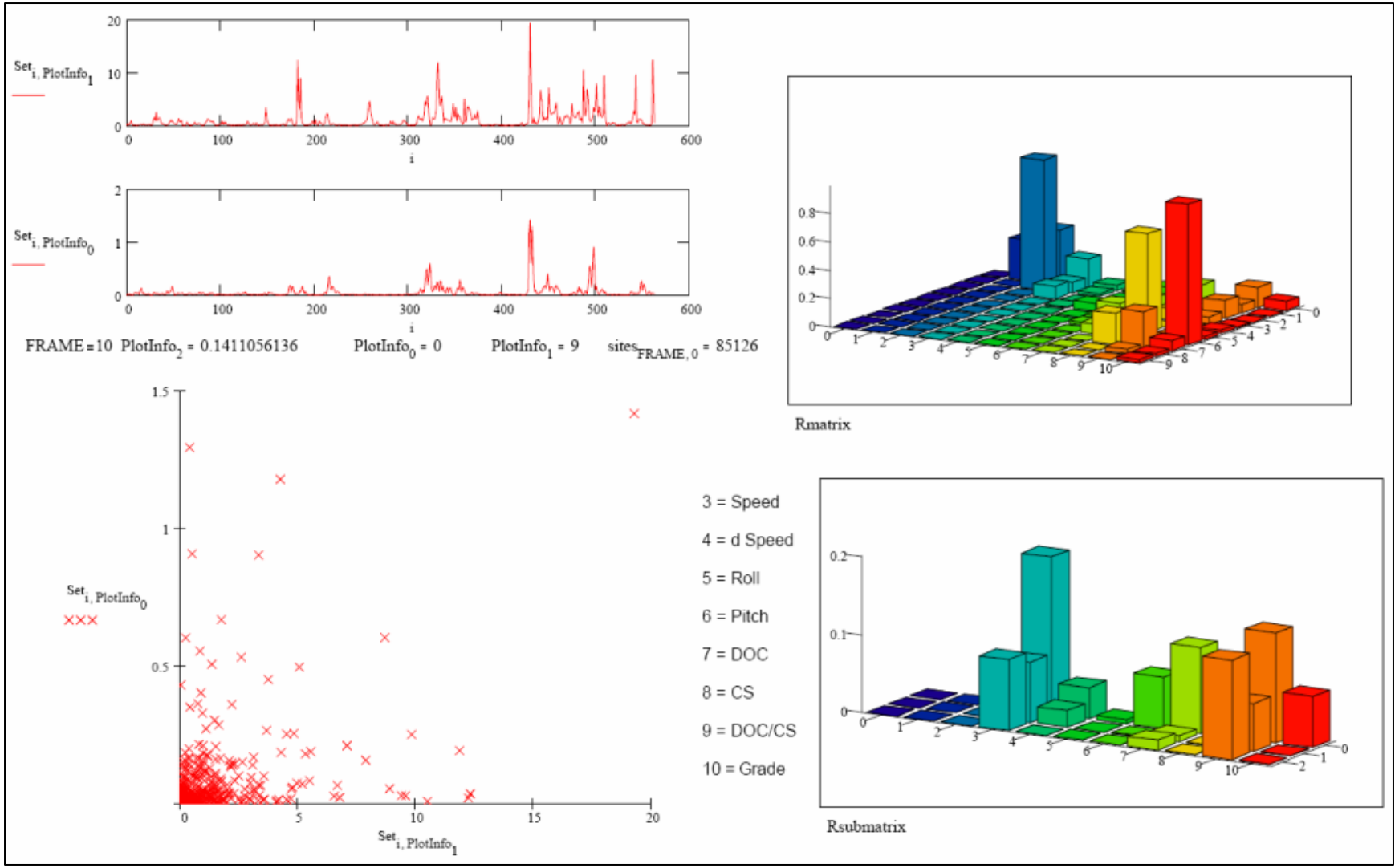

Figure 70. Graph. Correlations for route 851 (typical).

Speed, degree-of-curvature, and degree-of-curvature/cross slope have the highest correlations with AAD Profile.

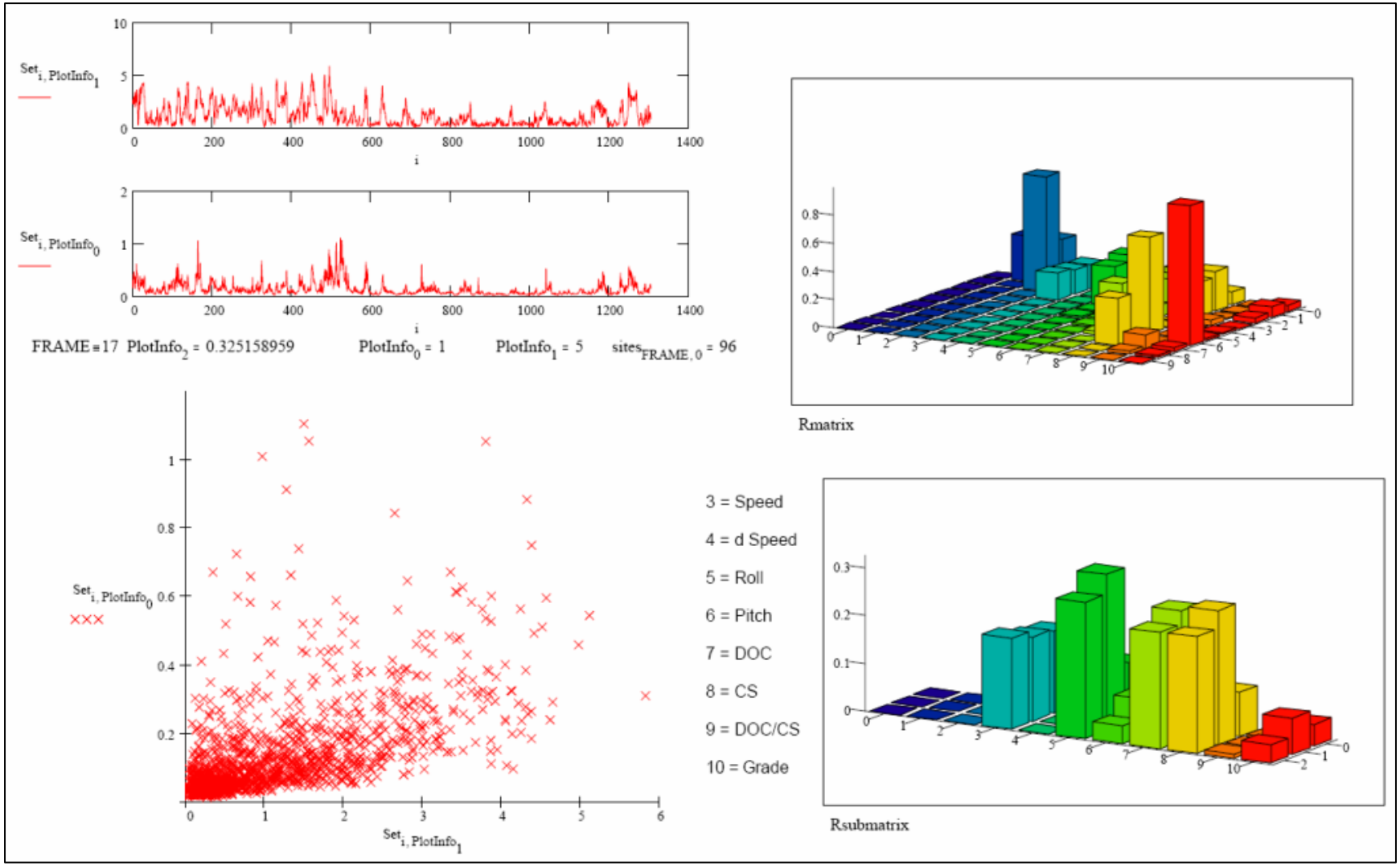

Figure 71. Graph. Correlations for route 9 (typical).

Speed, roll, degree-of-curvature, and cross slope have the highest correlation with AAD IRIs.

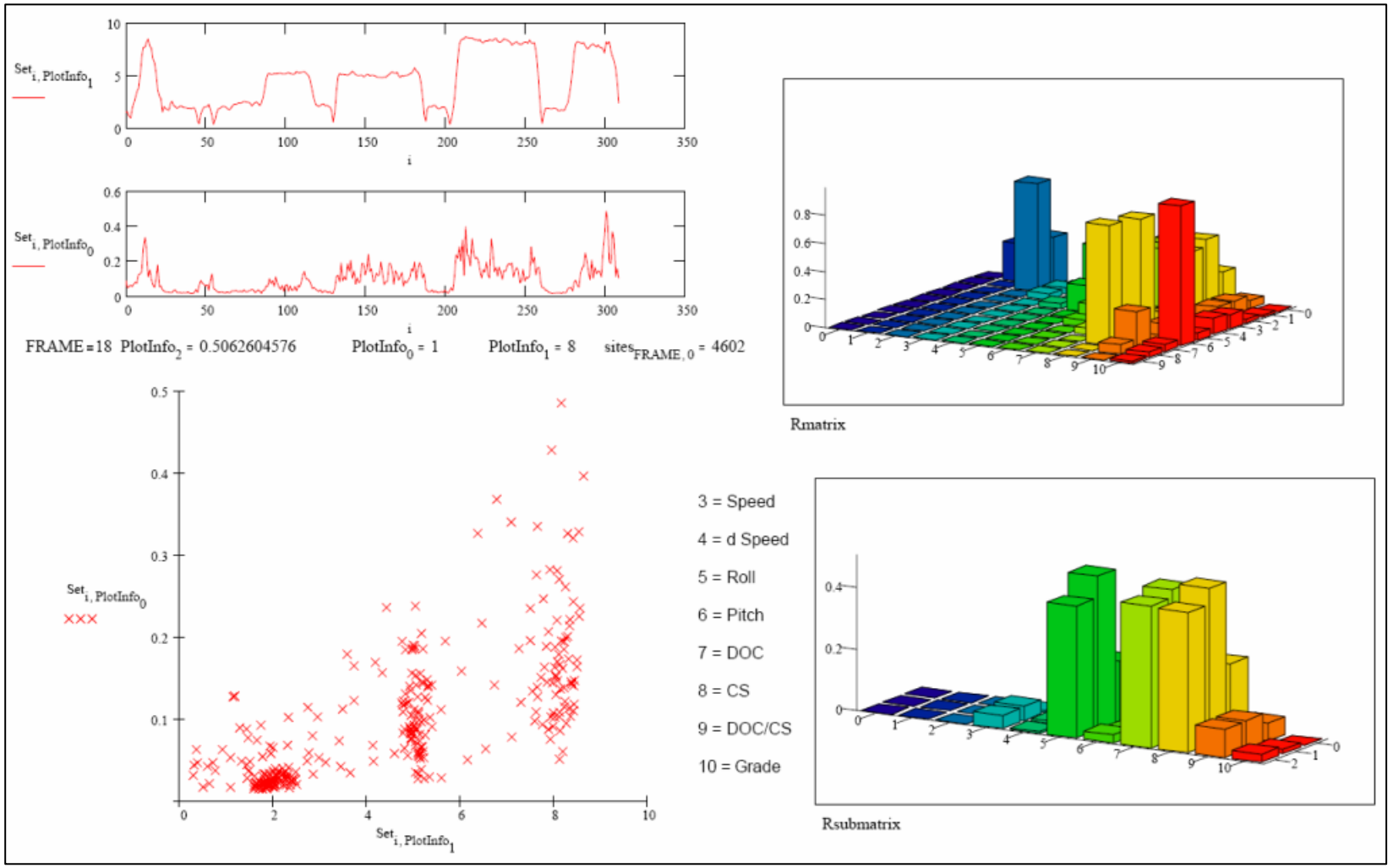

Figure 72. Graph. Correlations for route 460 (typical).

Roll, degree-of-curvature, and cross slope have the highest correlations with AAD IRIs. Route 460 has highest overall correlations. Speed is not highly correlated as for the other three sites.

Selection of Dependent Variables

Figure 73 shows a comparison of AAD and Correlation dependent variables values versus roadway sections for profile, IRI80, and IRI120. Range and variation in the AAD is more apparent than that present for Correlation.

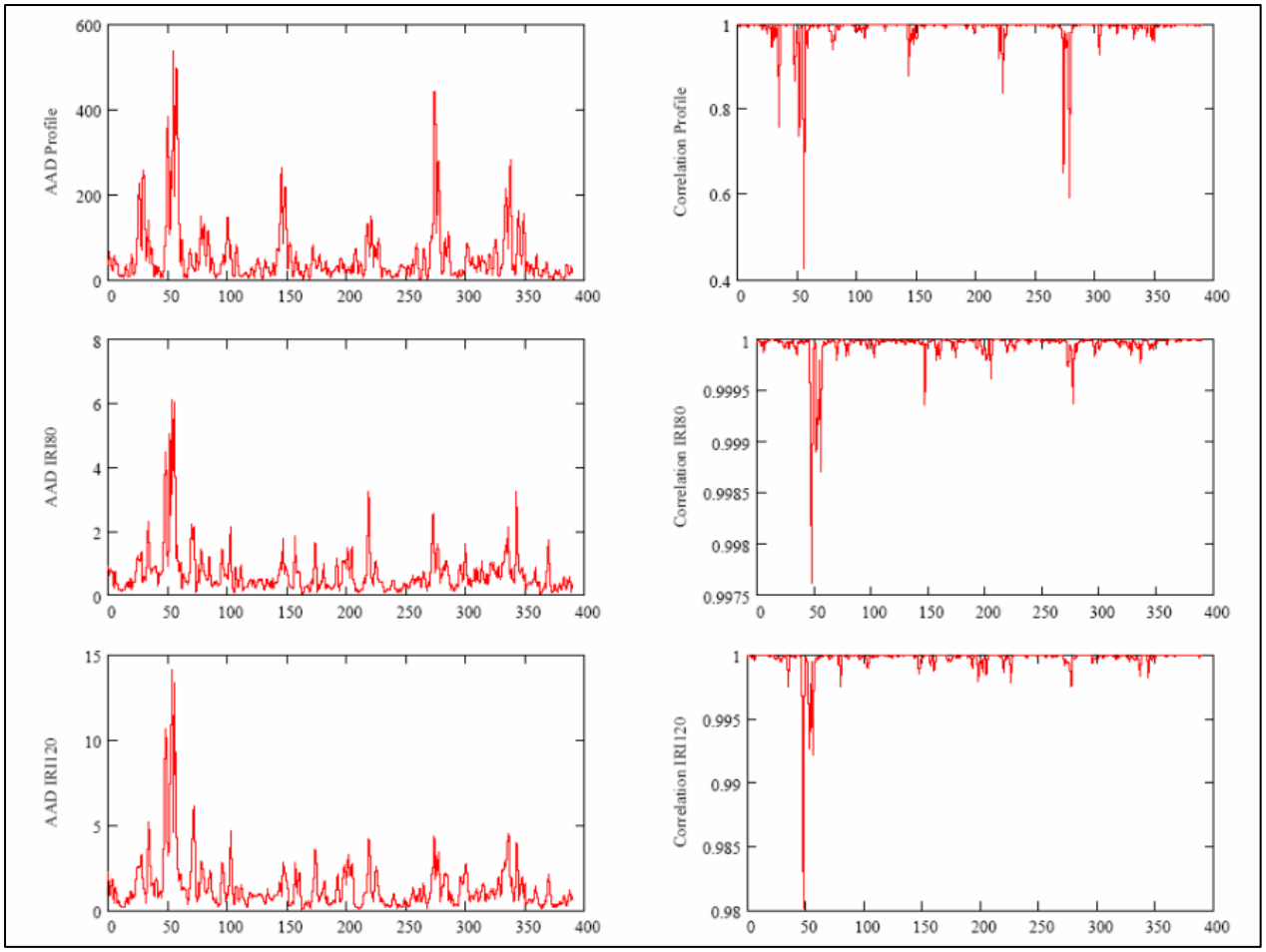

Figure 73. Graph. AAD (left) and Correlation (right) dependent variable comparison.

In figure 74 is a set of 3-D bar charts showing the relative correlations of the road section dependent variables AADs and Correlations (depth axis) versus the independent variables (width axis). The AAD dependent variables option 1 was selected for subsequent analysis as it captures more of the variability and reality of the data.

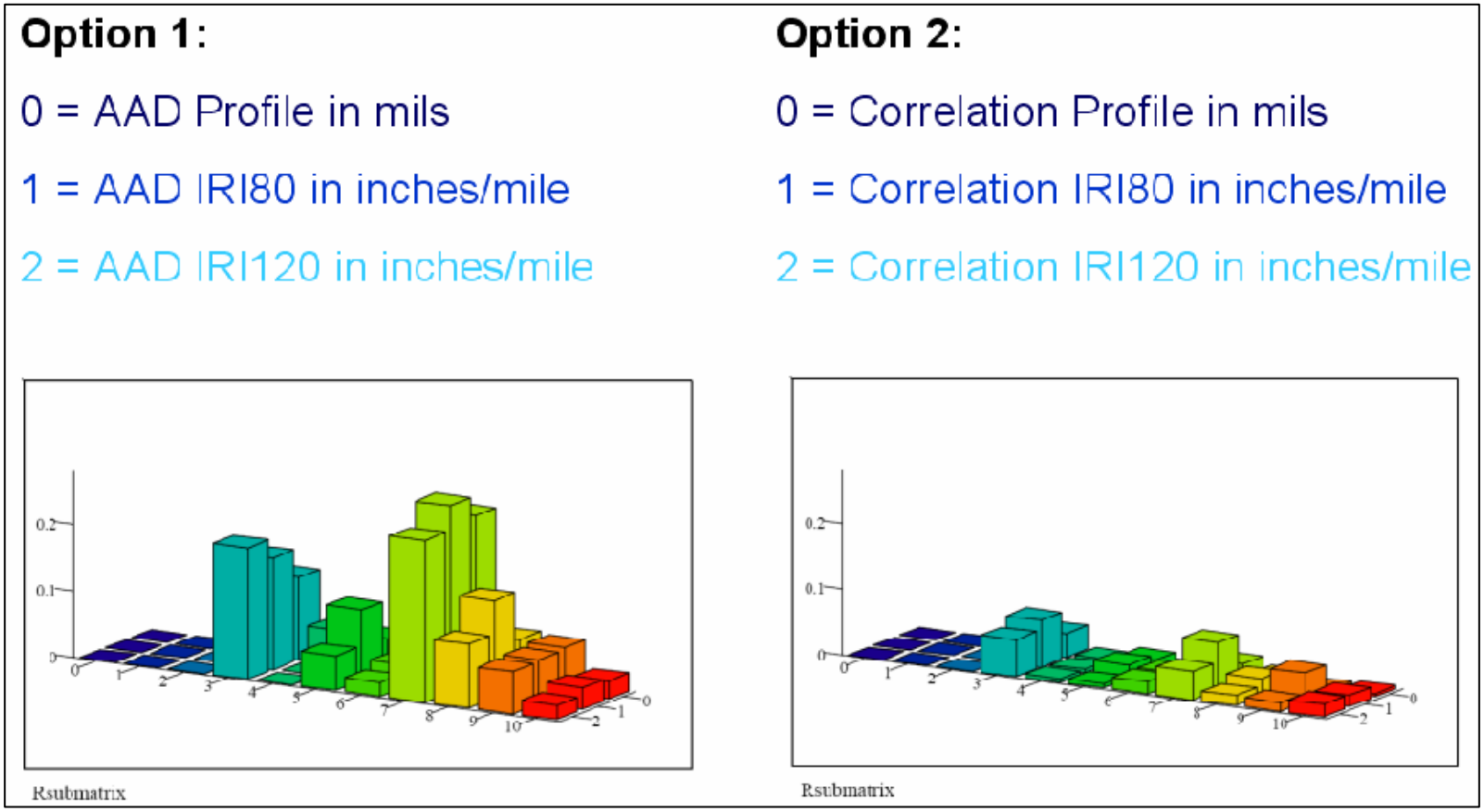

Figure 74. 3-D bar chart . AAD and correlation dependent variable correlation with independent variables

Effect of Section Length

Figures 75 through 78 compare the correlations between the dependent AAD variables (depth axis) and the independent variables (width axis) for road section lengths of 16.1 m and 160.9 m (52.8 ft and 528 ft) for the four sites. Road section length of 16.1 m (52.8 ft), Option 1, was selected for subsequent analysis work. Road section length of 160.9 m (528 ft) was also acceptable for site 9 and 460. Sites 9 and 460 have better alignments then sites 193 and 851 in terms of severity.

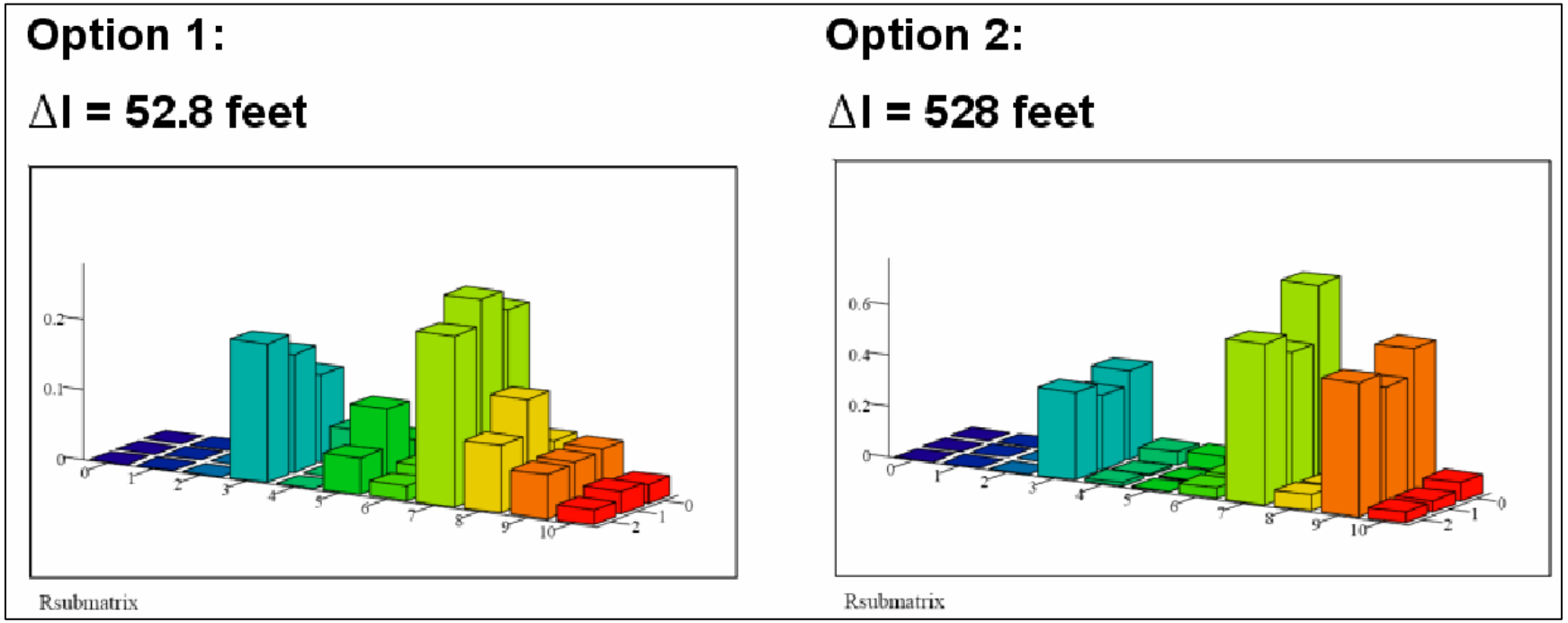

Figure 75. 3-D bar chart. AAD dependent variable correlation with independent variables for two roadway section lengths for site 193 (typical).

In Figure 75, Option 1, 16.1 m (52.8 ft) road section length, captures more of the variability.

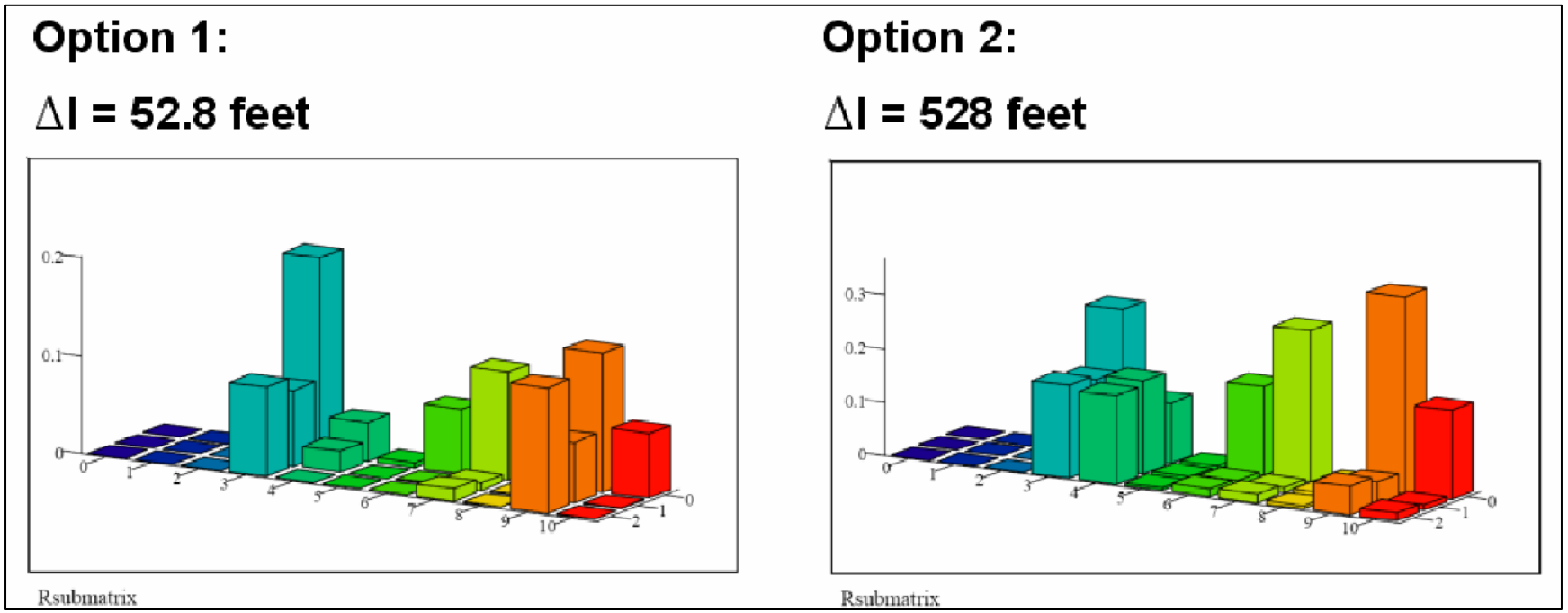

Figure 76. 3-D bar chart. AAD dependent variable correlation with independent variables for two roadway section lengths for site 851 (typical).

In figure 76, Option 1, 16.1 m (52.8 ft) road section length, captures more of the variability.

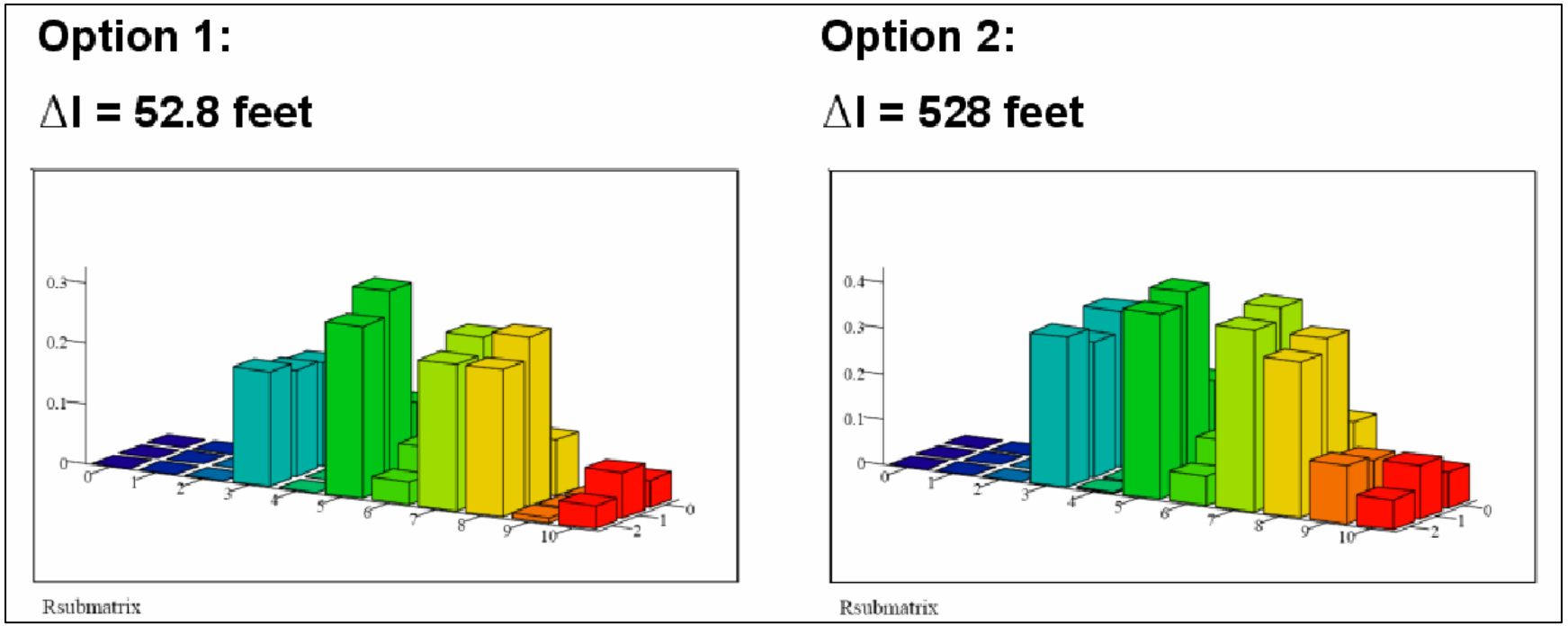

Figure 77. 3-D bar chart. AAD dependent variable correlation with independent variables for two roadway section lengths for site 9 (typical).

In figure 77, Option 1, 16.1 m (52.8 ft) road section length was selected as it captures more of the variability, but Option 2 is acceptable in the case of site 9.

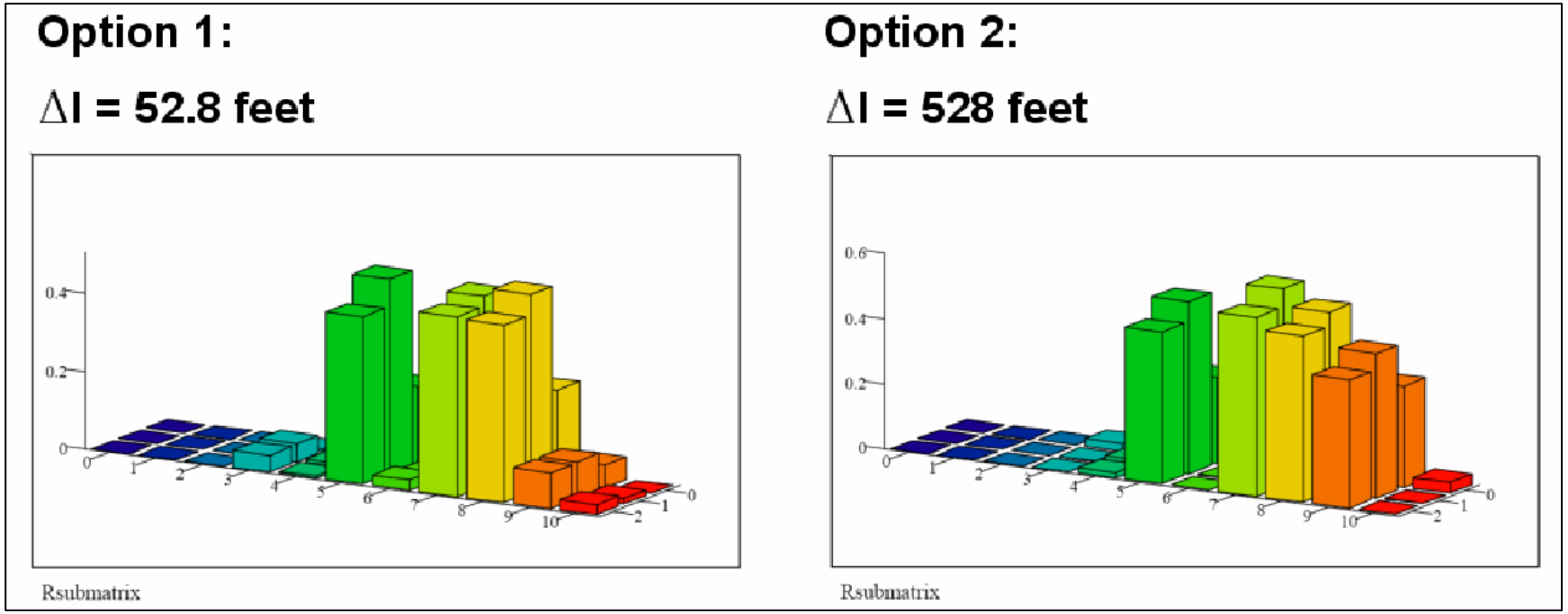

Figure 78. 3-D bar chart. AAD dependent variable correlation with independent variables for two roadway section lengths for site 460 (typical).

In figure 78, Option 1, 16.1 m (52.8 ft) road section length was selected as it captures more of the variability, but Option 2 is acceptable in the case of site 460.

Observations

The correlation pattern for all three dependent AAD variables is similar for all sites other than site 460. Site 460 is quite different than sites 193, 851, and 9. The mild alignment for site 460 resulted in a consistent speed profile compared to the other sites and therefore was not well correlated to AAD Profile, AAD IRI80 or AAD IRI120. Roll (and cross slope) were significant for sites 9 and 460 where cross slope was a consistent design element of the respective roads.

HYPOTHESIS

Experience with conventional 1-D high-speed, light-weight, and ultra-light inertial profilers have indicated that vehicle pitch and roll along with speed changes may introduce an error source into accelerometer sensor readings. An understanding of the sources of error and their statistical significance to the estimation of the road profile and subsequent IRI computation is needed.

The primary hypothesis is:

> Pitch, roll, and change in speed of an inertial profiler vehicle as a result of roadway alignment and driver operations are correlated to errors in inertial profile estimates and subsequent IRI calculations.

The significance of an independent variable relative to the other variables will vary between sites as the sites possess these independent variables to varying degrees dependent on the type of site in terms of the severity of the horizontal and vertical alignments, road roughness, and driver operation of the vehicle.

The next section focuses on determining the truth of this primary hypothesis.

REGRESSION ANALYSIS

Linear regression was chosen as one of the statistical techniques for determining which independent variables and cross-terms are statistically significant in explaining variances within the dependent variables AAD profile, AAD IRI80, and AAD IRI120.

In linear regression, the “t” statistic and corresponding significance level associated with an independent variable permits the identification of variables that help explain the AAD associated with a site Profile, IRI80, and IRI120 computations. No attempt was made at this time to develop a mathematical model of the AAD Profile, AAD IRI80, and AAD IRI120 as a function of the independent variables

When there are a lot of potential independent variables and cross-terms to consider, a graph showing relative importance of the independent variables relative to AAD Profile, AAD IRI80, and AAD IRI120 is a useful method to present the information.

Independent Variables

Following is the list of independent variables (with acronyms and units) and cross-terms used in the linear regression analysis:

- Roll (degrees).
- Pitch (degrees).
- Degree-of-Curvature (DOC) (degrees) computed as change in heading (degrees) over an arc distance of 100 ft (30.48 m).
- Cross Slope (CS) (%).
- DOC/CS as Degree-of-Curvature divided by Cross Slope.
- Speed (Spd) (mi/h), (1 mi/h = 1.609 km/h).
- Delta Speed (DS) (mi/h) as the difference in speed between to successive sections of a given length.
- DS x Roll
- DS x Pitch
- DS x DOC
- Spd x Roll
- Spd x Pitch
- Spd x DOC
- Spd x CS

The "t" Statistic and Significance Levels

The "t" statistic is computed as shown in equation 56.

$$t = \text{coefficient} / \text{Standard Error} \quad (56)$$

where,

coefficient determined from linear regression procedure,
Standard Error = square root of variance explained by regression variable.

Significance level α is based on the two-tail test for the "t" statistic with degrees of freedom (df) computed as shown in equation 57.

$$df = n-p \quad (57)$$

where,

n = sample size,
p = number of coefficients(independent variables plus one) in the regression model.

Table 8 provides the "t" statistic for various significance levels of alpha and sample size.

Table 8. "t" statistic given significance level and degrees of freedom.

t(1-alpha/2,n-p)		significance level alpha		
		0.01	0.05	0.10
n-p	93	2.63	1.986	1.661
	100	2.626	1.984	1.660
	500	2.586	1.965	1.648
	1000	2.581	1.962	1.646

Linear Regression Results to Identify Significant Variables

Figures and tables presenting the linear regression results for AAD Profile, AAD IRI80 and AAD IRI120 are presented on the next three pages. The regression analysis on the dependent variables included the independent variable and some two-way cross-terms.

Figure 79 and table 9 provide the results of the linear regression of AAD Profile with the independent variables. Of significant note is the importance of Delta Speed for route 9, 851, and 193; Delta Speed x Roll for routes 9 and 851; and Delta Speed x Degree-of-Curvature for route 9. For route 460, Roll and Degree-of-Curvature are the key independent variables.

Figure 80 and table 10 provide the results of the linear regression of AAD IRI80 with the independent variables. Highlights of this regression is the importance of Delta Speed for route 851, 9, and 193; Delta Speed x Roll for route 9 and 851; Delta Speed x Pitch for route 9 and 851; and Delta Speed x Degree-of-Curvature for route 9 and 851.

Figure 81 and table 11 provide the results of the linear regression of AAD IRI120 with the independent variables. Highlights of this regression is the importance of Delta Speed for route 851, 9, and 193; Delta Speed x Roll for route 9 and 851; Delta Speed x Pitch for route 9 and 851; and Delta Speed x Degree-of-Curvature for route 9 and 851. This result is similar to that for AAD IRI80 but in general with higher "t" statistic values (higher significance).

For route 460, the independent variables of interest are Roll and Cross Slope. Speed x Roll and Speed x Cross Slope have a similar pattern to Roll and Cross Slope. Since speed on 460 was very consistent, Speed x Roll and Speed x Cross Slope are basically echoes of the Roll and Cross Slope results.

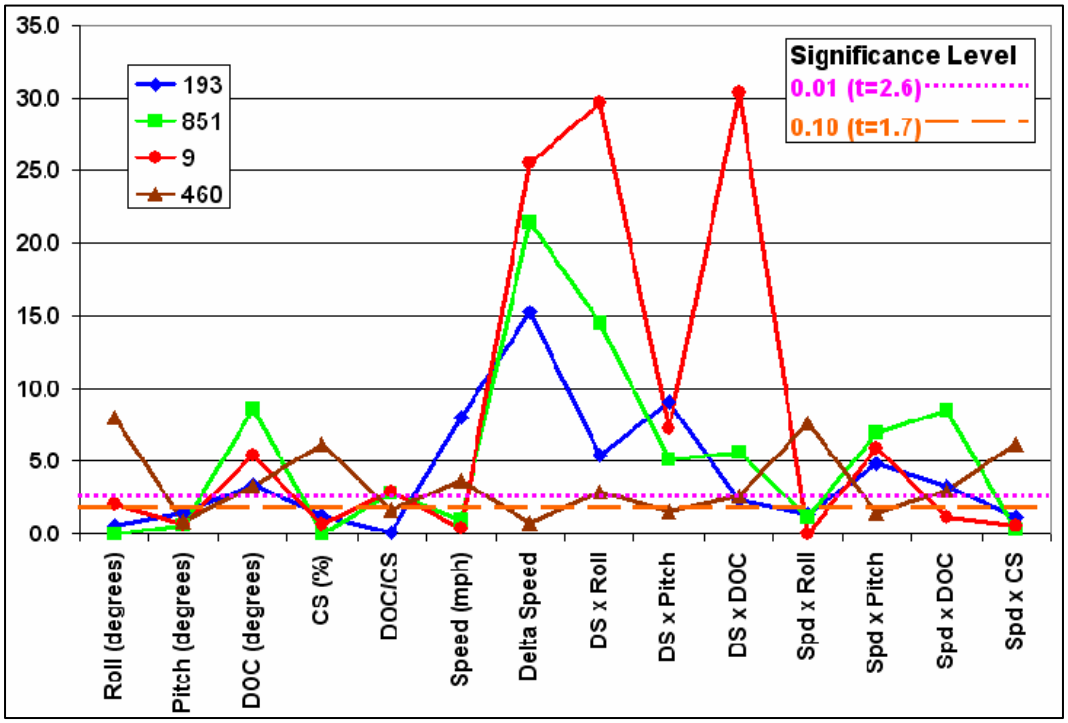

Figure 79. Line chart. AAD Profile linear regression variable "t" statistic for DHM database selected four sites.

Table 9. AAD Profile linear regression variable "t" statistic for DHM selected four sites.

Variables	193	851	9	460
Roll (degrees)	0.63	0.02	2.08	8.00
Pitch (degrees)	1.44	0.61	0.69	0.85
DOC (degrees)	3.42	8.62	5.39	3.33
CS (%)	1.27	0.02	0.64	6.20
DOC/CS	0.10	2.76	2.88	1.68
Speed (mi/h)	8.06	1.01	0.34	3.72
Delta Speed (mi/h)	15.28	21.51	25.50	0.77
DS x Roll	5.46	14.47	29.69	2.88
DS x Pitch	9.07	5.14	7.26	1.52
DS x DOC	2.28	5.64	30.41	2.59
Spd x Roll	1.38	1.17	0.03	7.68
Spd x Pitch	4.88	6.97	5.92	1.41
Spd x DOC	3.24	8.50	1.13	3.04
Spd x CS	1.15	0.30	0.57	6.16

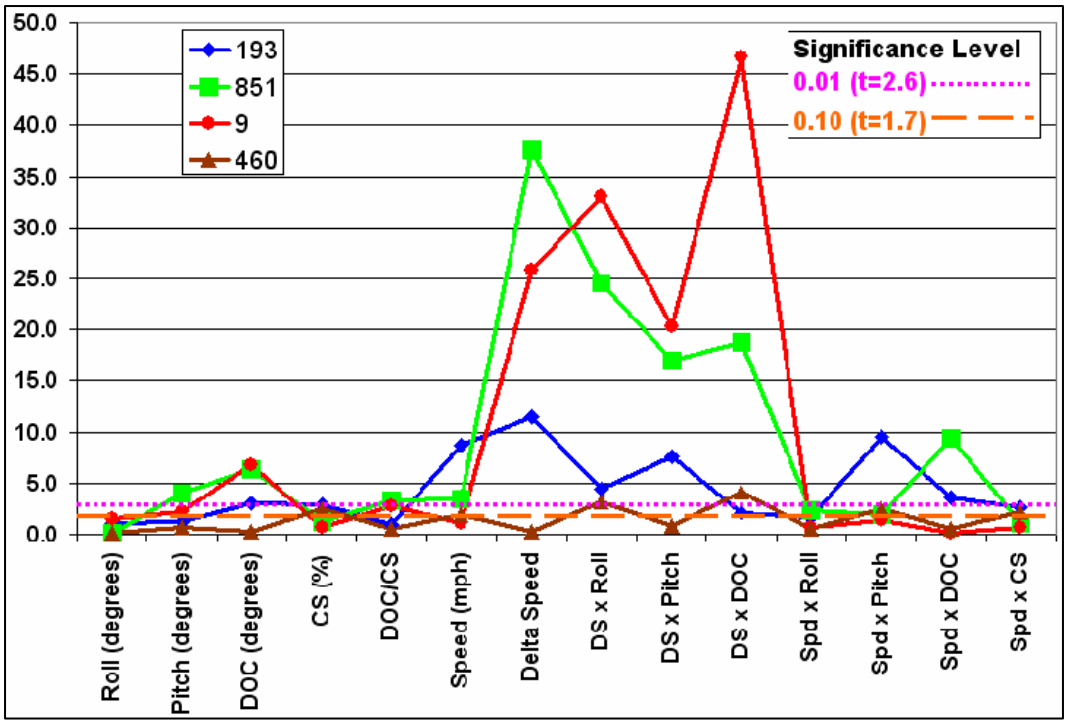

Figure 80. Line chart. AAD IRI80 linear regression variable "t" statistic for DHM database selected four sites.

Table 10. AAD IRI80 linear regression variable "t" statistic for DHM selected four sites.

Variables	193	851	9	460
Roll (degrees)	1.07	0.15	1.52	0.13
Pitch (degrees)	1.30	4.02	2.22	0.63
DOC (degrees)	3.00	6.41	6.82	0.25
CS (%)	2.90	1.21	0.69	2.47
DOC/CS	1.01	3.35	2.75	0.56
Speed (mi/h)	8.75	3.48	1.08	1.91
Delta Speed (mi/h)	11.41	37.55	25.88	0.32
DS x Roll	4.38	24.58	32.96	3.15
DS x Pitch	7.57	17.00	20.24	0.78
DS x DOC	2.04	18.82	46.64	4.21
Spd x Roll	1.69	2.34	0.69	0.53
Spd x Pitch	9.48	1.96	1.32	2.45
Spd x DOC	3.64	9.37	0.10	0.58
Spd x CS	2.64	1.06	0.63	2.22

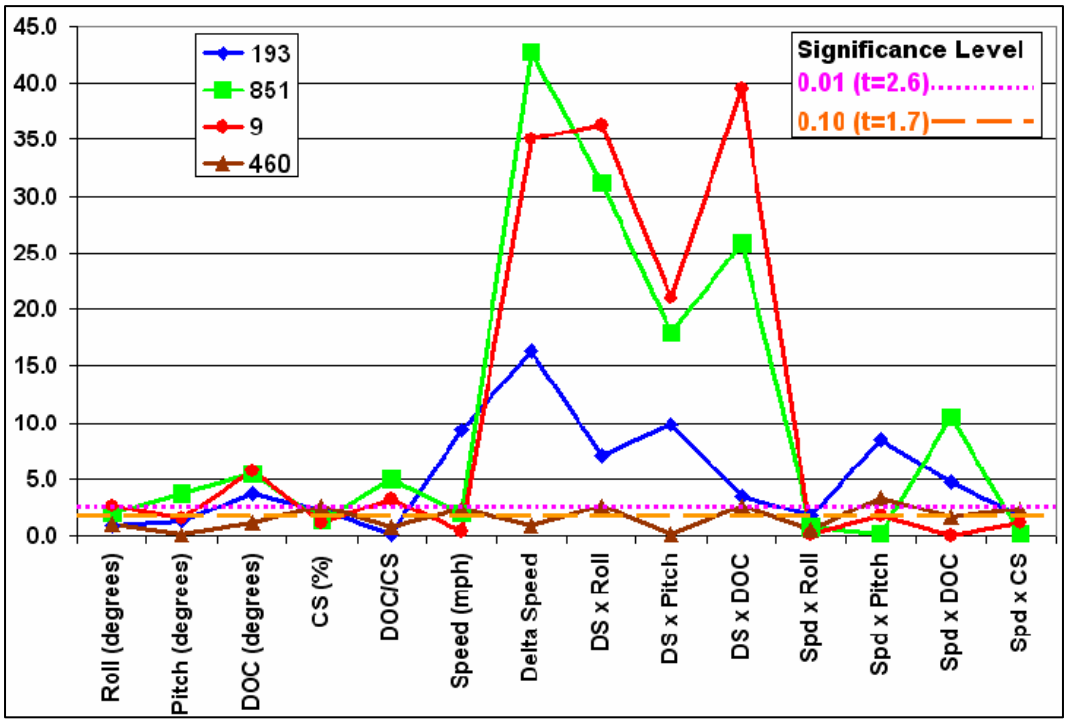

Figure 81. Line chart. AAD IRI120 linear regression variable "t" statistic for DHM database selected four sites.

Table 11. AAD IRI120 linear regression variable "t" statistic for DHM selected four sites.

Variables	193	851	9	460
Roll (degrees)	0.92	1.97	2.55	0.97
Pitch (degrees)	1.25	3.69	1.51	0.16
DOC (degrees)	3.68	5.42	5.71	1.15
CS (%)	2.21	1.32	1.16	2.60
DOC/CS	0.14	5.00	3.18	0.69
Speed (mi/h)	9.34	1.97	0.39	2.37
Delta Speed (mi/h)	16.26	42.80	35.01	0.89
DS x Roll	7.11	31.20	36.24	2.57
DS x Pitch	9.85	17.88	20.96	0.13
DS x DOC	3.51	25.84	39.56	2.67
Spd x Roll	1.77	0.73	0.12	0.49
Spd x Pitch	8.49	0.10	1.71	3.40
Spd x DOC	4.69	10.43	0.06	1.63
Spd x CS	1.80	0.18	1.07	2.41

Another way to visualize the relative significance of the independent variables for the four DHM database sites with their differing level of alignment severity is to normalize the ”t” statistic relative to the maximum values and then arrange the data for the three dependent variables AAD Profile, AAD IRI80, and AAD IRI120 by decreasing order of independent variable significance to AAD Profile for each site. The resulting graphs are shown in figures 82 through 85 for sites 193, 460, 851 and 9 respectively on the next two pages. The order of the figures was chosen to show how the sites differ from each other relative to the independent variables and cross-terms given the varying level of alignment severity.

As seen in figure 82 for route 193, the trends in “t” statistic for AAD Profile, AAD IRI180 and AAD IRI120 relative to the independent variables was similar, that is the roadway features (independent variables) impacted the three dependent variables similarly in terms of order of importance.

As seen in figure 83 for route 460, the AAD IRI80 and AAD IRI120 did not follow the AAD Profile “t” statistic trend in terms of order of importance. That is, the road features that affected AAD Profile were different than those that affected the AAD IRI values.

As seen in figure 84 for route 851, the order of importance was similar for the highest and lowest ordered independent variables and mixed in the mid-portion.

For route 9, as seen in figure 85, the order of importance of the independent variables was very similar for AAD Profile, AAD IRI80 and AAD IRI120.

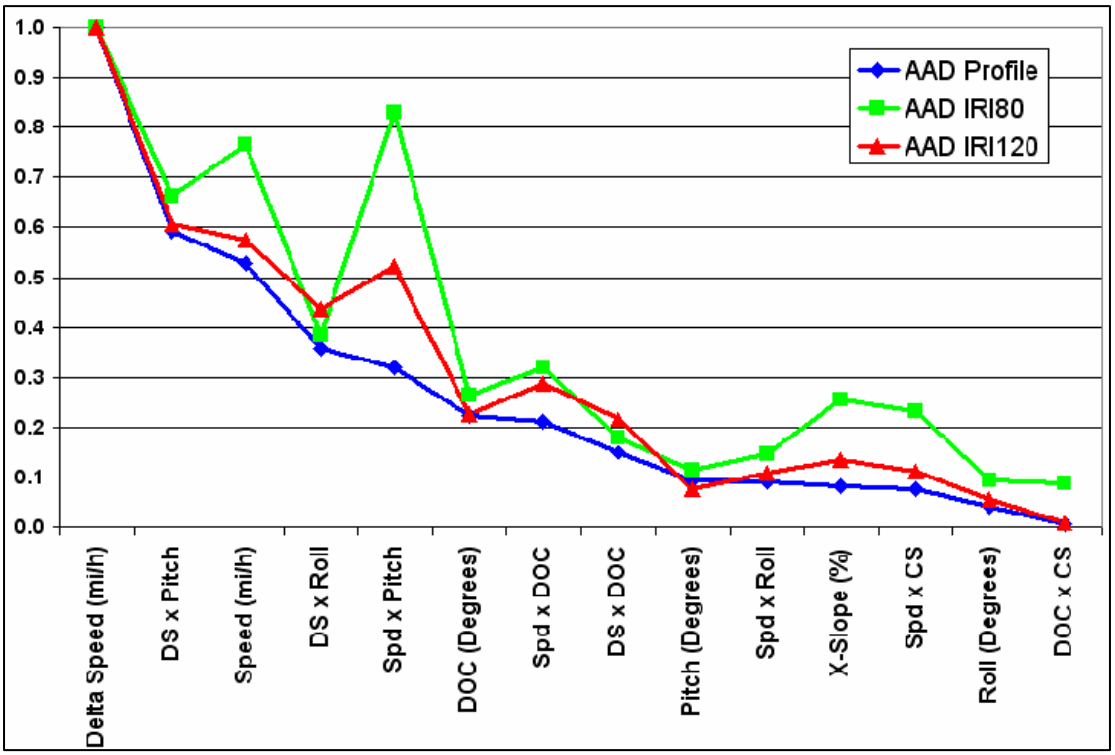

Figure 82. Line chart. Trend in "t" statistic among dependent variables for site 193.

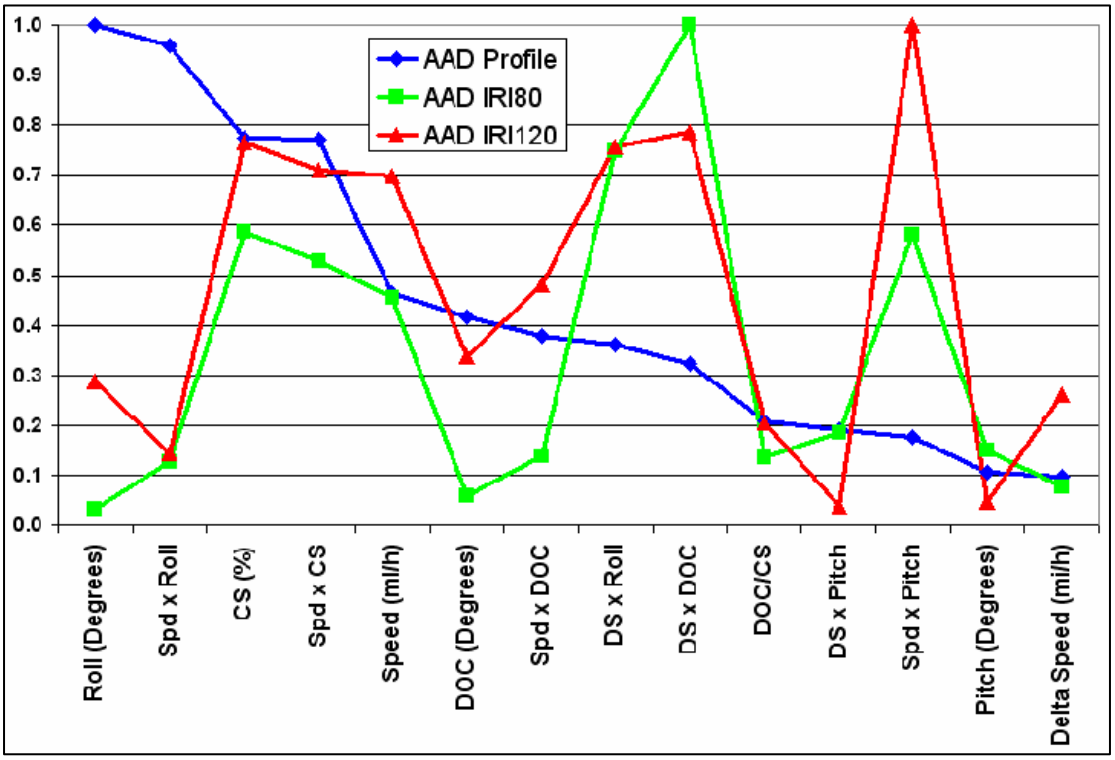

Figure 83. Line chart. Trend in "t" statistic among dependent variables for site 460.

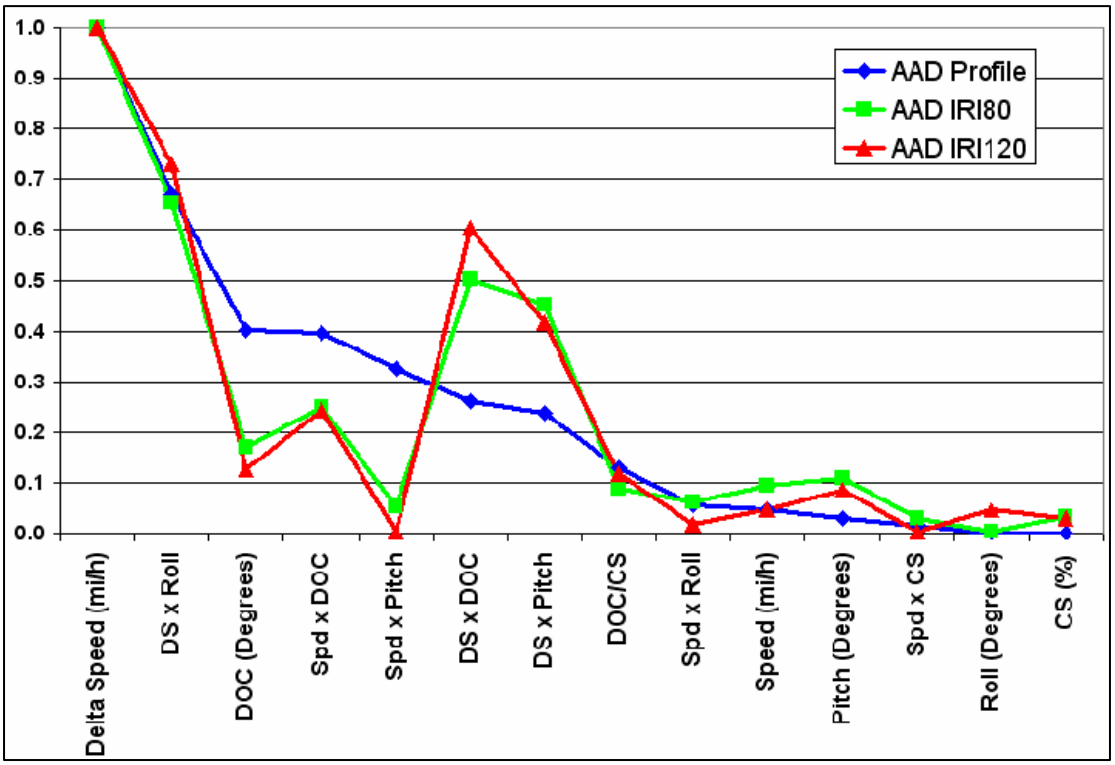

Figure 84. Line chart. Trend in "t" statistic among dependent variables for site 851.

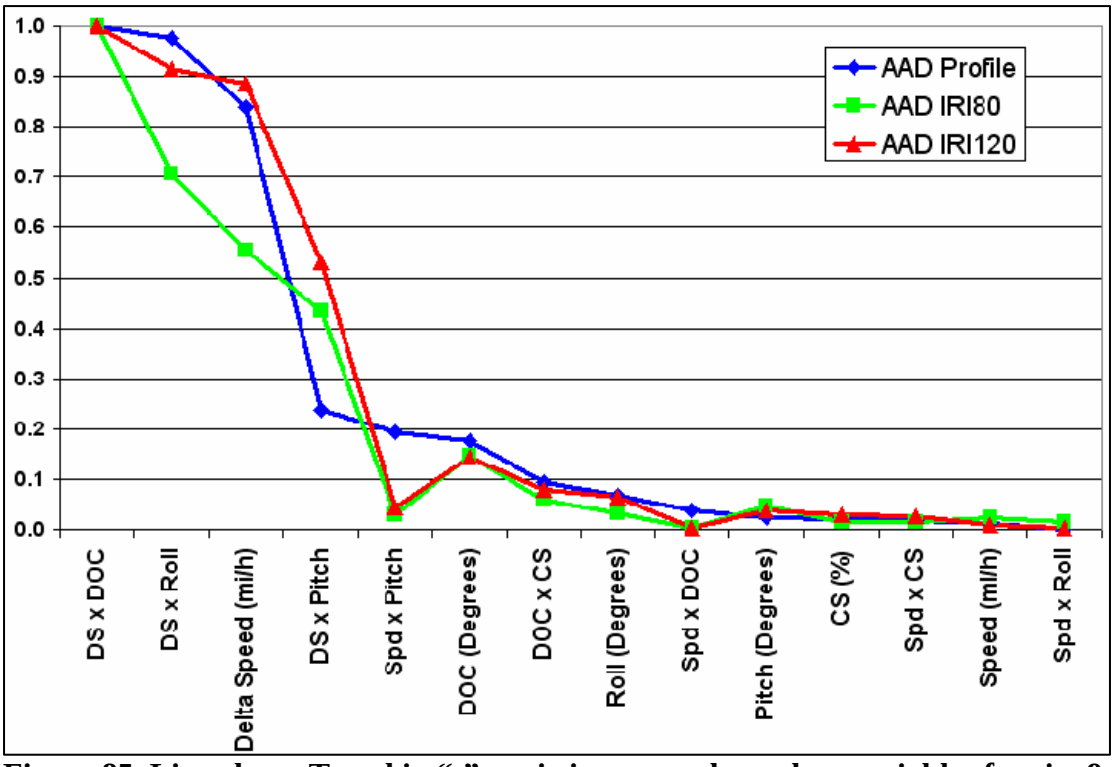

Figure 85. Line chart. Trend in "t" statistic among dependent variables for site 9.

FOCUS ON SECTIONS WITH LARGEST ERRORS

A subset analysis was conducted on the sections with the largest AAD Profile errors. The analysis database of sections of 16.1 m (52.8 ft) length was used in this analysis. The subset consisted of those sections with an AAD Profile of 60 mils or greater based on the accuracy limit specified in AASHTO Provisional Specification PP51-02. Based on the above definitions, the subset consisted of 1500 sections distributed as follows:

- Route 193 610 sections
- Route 851 775 sections
- Route 9 115 sections
- Route 460 0 sections

The lack of sections for route 460 does not impact the data mining of the subset.

The correlation and regression analysis was performed on these sections with largest AAD Profile error subset.

The three figures 86 through 88 present the results of the correlation analysis in a graphical format with one graph for each site. These three graphs are shown on the next three pages. For route 193, primary difference is that Degree-of-Curvature/Cross Slope variable is not as significant for the reduce set of data. For route 851, the primary difference is the significant reduction in the number of variables correlated with AAD Profile. And, for route 9, the primary difference is the large change in correlation value for many of the independent variables across all dependent variables.

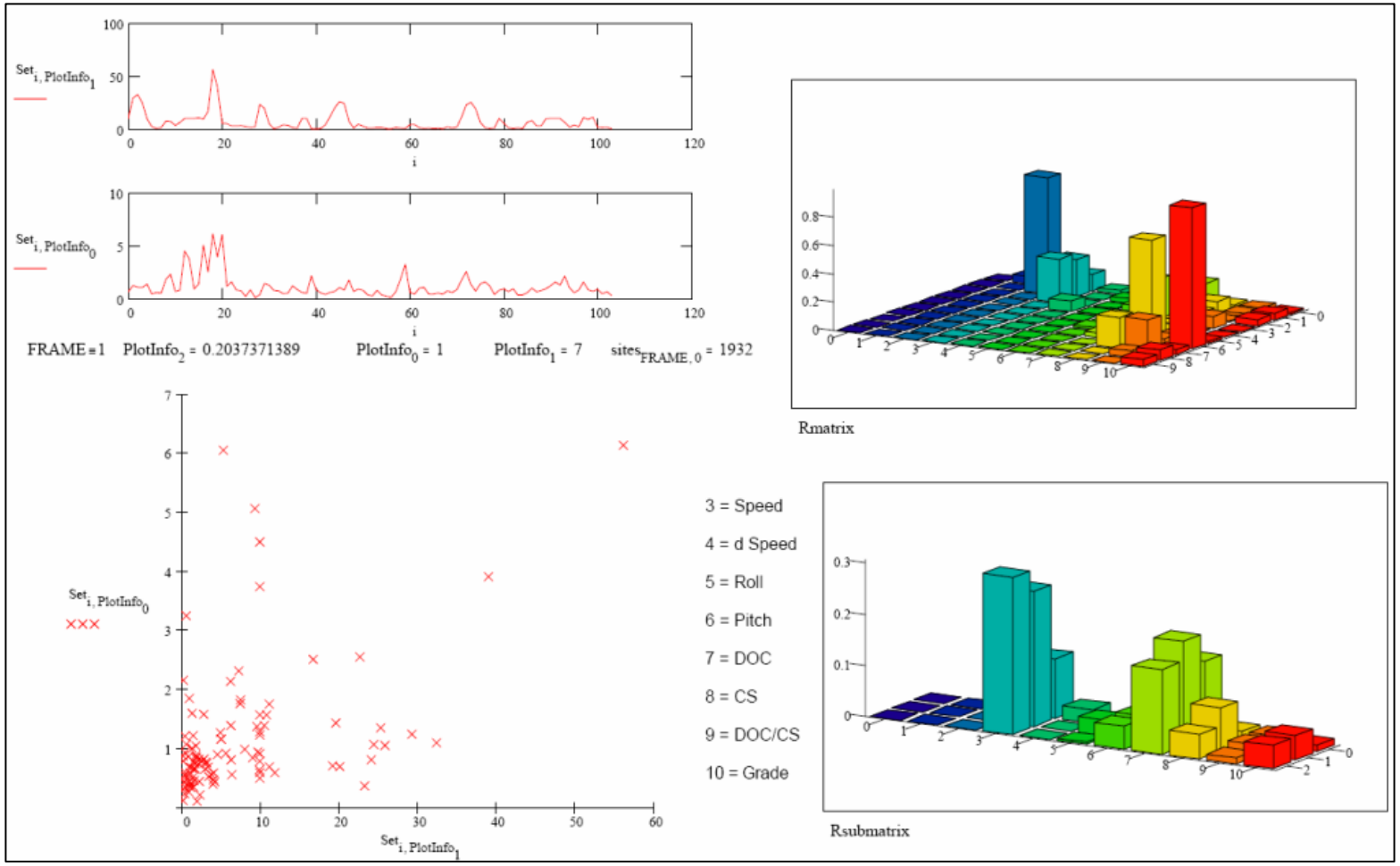

Figure 86. Graph. Largest AAD Profile section error correlation analysis for route 193.

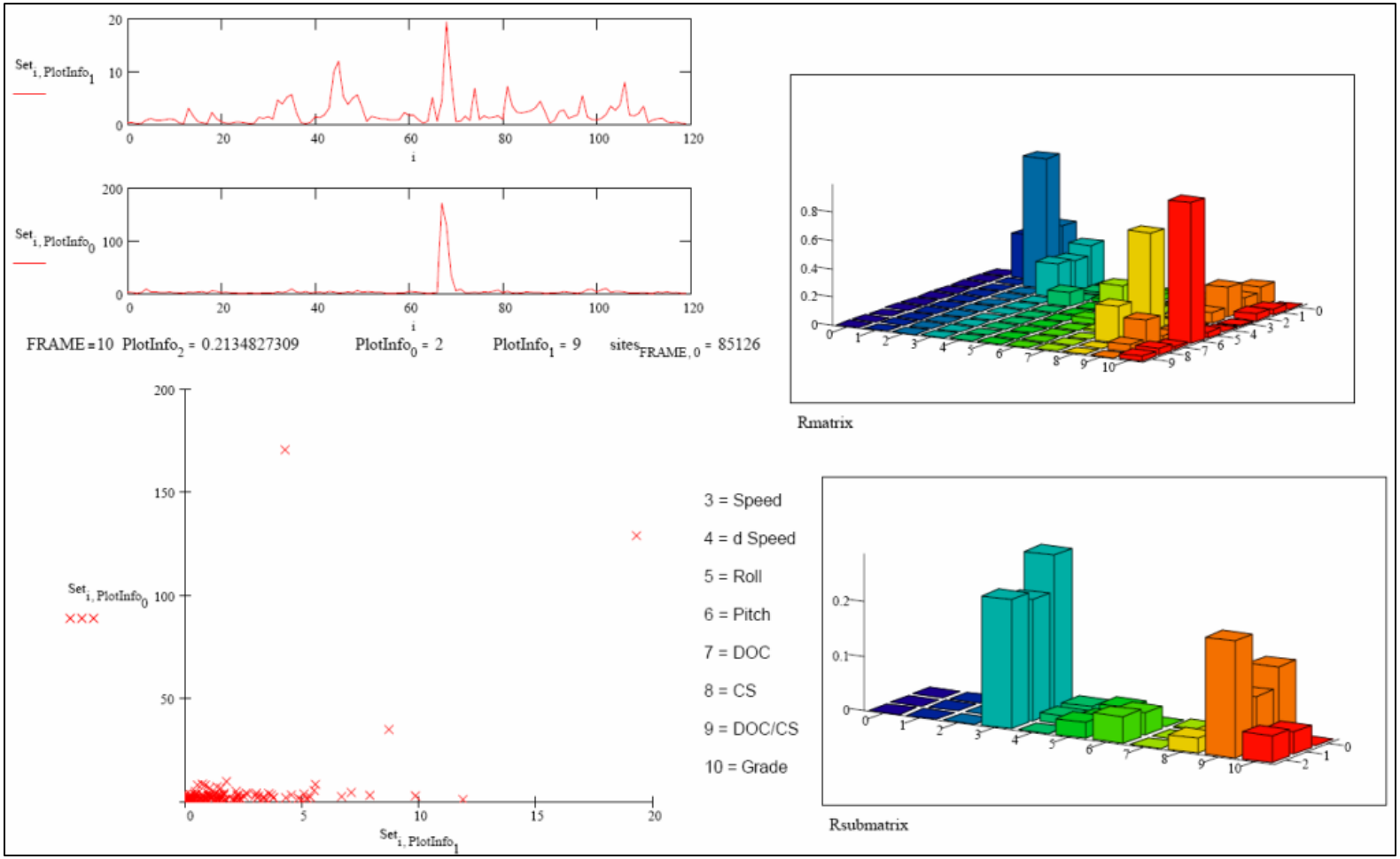

Figure 87. Graph. Largest AAD Profile section error correlation analysis for route 851.

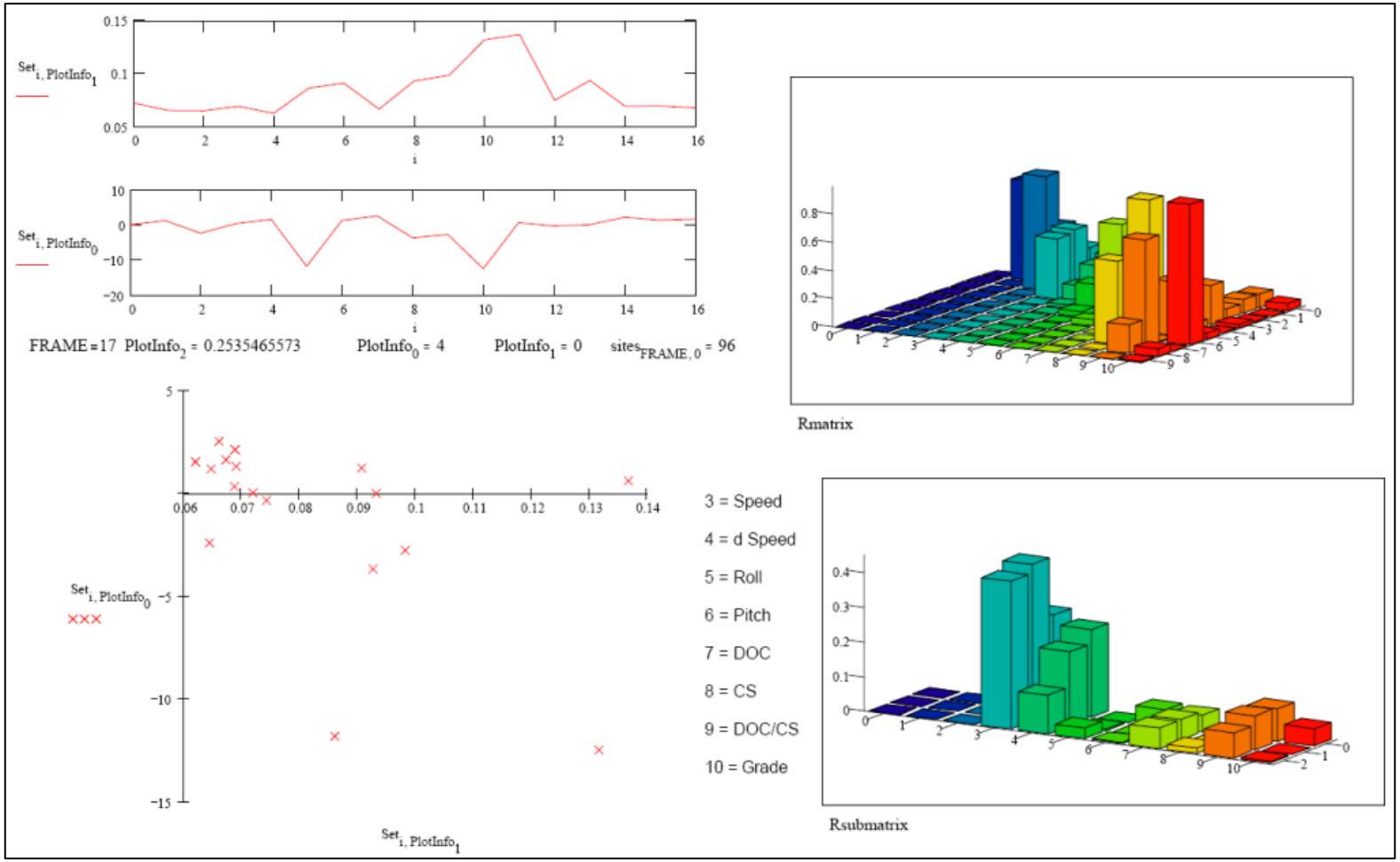

Figure 88. Graph. Largest AAD Profile section error correlation analysis for route 9.

Figures and tables of the linear regression results for largest AAD Profile error sections data sets are presented for AAD Profile, AAD IRI80 and AAD IRI120 on the following three pages.

Figure 89 and table 12 provide the results of the linear regression of the largest error section AAD Profile dependent variable with the independent variables. Figure 90 and table 13 provide the results of the linear regression of the largest error section subset data AAD IRI80 dependent variable with the independent variables. Figure 91 and table 14 provide the results of the linear regression of the largest error section subset data AAD IRI120 dependent variable with the independent variables.

The plot (figure 89) of the “t” statistic for the sections with the largest AAD Profile error show that routes 193 and 9 are similar for the AAD Profile dependent variable but that route 851 is very different in terms of the significance of the independent variables on this reduced dataset. Delta Speed and the Delta Speed x Roll for 851 have a more prominent “t” statistic value compared to route 193 and 9 for AAD Profile.

The plot (figure 90) of the “t” statistic for the sections with the largest AAD Profile error show that routes 193 and 9 are similar for AAD IRI80 dependent variable but that route 851 is again very different in terms of the significance of the independent variables on this reduced dataset. Speed, Delta Speed, Delta Speed cross-terms, and Speed cross-terms Roll, Pitch and DOC for 851 have a more prominent “t” statistic value compared to route 193 and 9.

The plot (figure 91) of the “t” statistic for the sections with the largest AAD Profile error show that routes 193 and 9 are similar for AAD IRI120 in a manner similar to the AAD IRI80 dependent variable. Route 851 is again very different in terms of the significance of the independent variables on this reduced dataset. Like AAD IRI80, Speed, Delta Speed, Delta Speed cross-terms, and Speed cross-terms Roll and DOC for 851 have a more prominent “t” statistics value compared to route 193 and 9.

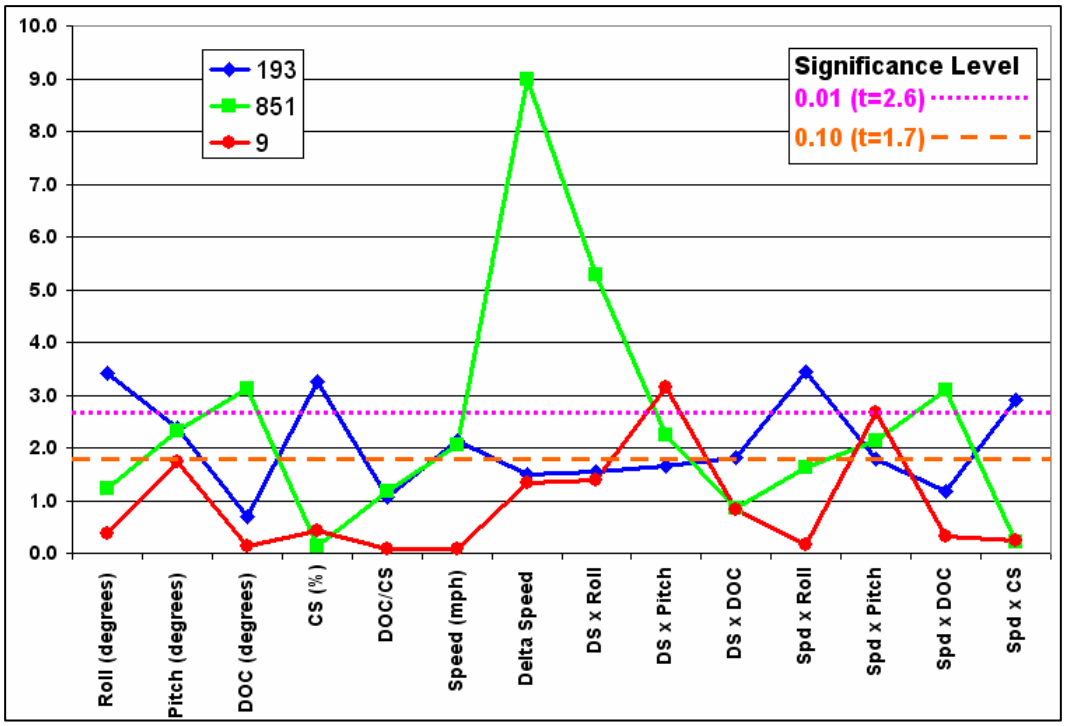

Figure 89. Line chart. AAD Profile linear regression variable "t" statistic for three DHM database sites, largest error section subset.

Table 12. AAD Profile linear regression variable "t" statistic for three DHM selected sites, largest error section subset.

Variables	193	851	9
Roll (degrees)	3.41	1.22	0.36
Pitch (degrees)	2.37	2.33	1.74
DOC (degrees)	0.69	3.13	0.14
CS (%)	3.24	0.14	0.41
DOC/CS	1.06	1.19	0.08
Speed (mi/h)	2.14	2.05	0.09
Delta Speed (mi/h)	1.49	8.97	1.32
DS x Roll	1.55	5.29	1.38
DS x Pitch	1.64	2.25	3.14
DS x DOC	1.82	0.85	0.84
Spd x Roll	3.43	1.62	0.16
Spd x Pitch	1.78	2.13	2.66
Spd x DOC	1.16	3.08	0.32
Spd x CS	2.91	0.22	0.25

"t" statistic for given significance level: t(0.10)=1.7, t(0.01)=2.6.

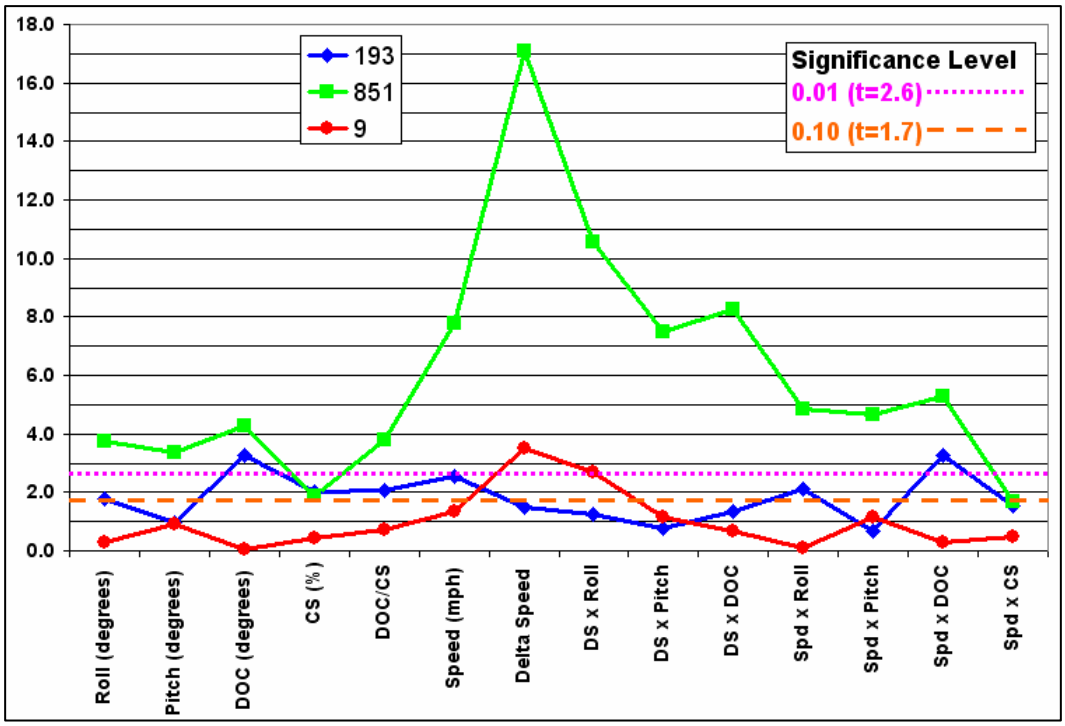

Figure 90. Line chart. AAD IRI80 linear regression variable "t" statistic for three DHM database selected sites, largest error section subset.

Table 13. AAD IRI80 linear regression variable "t" statistic for three DHM selected sites, largest error section subset.

Variables	193	851	9
Roll (degrees)	1.80	3.76	0.28
Pitch (degrees)	0.97	3.36	0.94
DOC (degrees)	3.28	4.29	0.06
CS (%)	2.04	1.88	0.44
DOC/CS	2.06	3.80	0.73
Speed (mi/h)	2.53	7.75	1.36
Delta Speed (mi/h)	1.48	17.10	3.52
DS x Roll	1.25	10.56	2.67
DS x Pitch	0.79	7.47	1.14
DS x DOC	1.33	8.26	0.67
Spd x Roll	2.09	4.87	0.09
Spd x Pitch	0.66	4.66	1.14
Spd x DOC	3.27	5.28	0.30
Spd x CS	1.54	1.68	0.50

"t" statistic for given significance level: t(0.10)=1.7, t(0.01)=2.6.

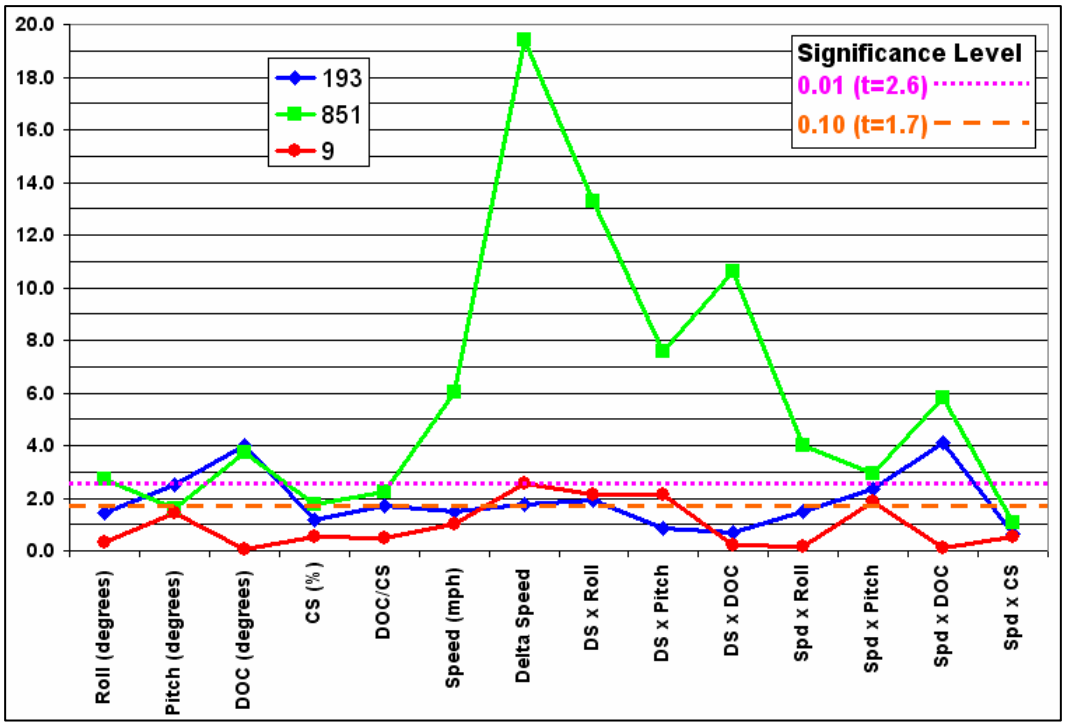

Figure 91. Line chart. AAD IRI120 linear regression variable "t" statistic for three DHM database selected sites, largest error section subset.

Table 14. AAD IRI120 linear regression variable "t" statistic for three DHM selected sites, largest error section subset.

Variables	193	851	9
Roll (degrees)	1.44	2.72	0.33
Pitch (degrees)	2.52	1.58	1.45
DOC (degrees)	4.00	3.74	0.03
CS (%)	1.19	1.75	0.53
DOC/CS	1.70	2.25	0.45
Speed (mi/h)	1.48	6.05	1.02
Delta Speed (mi/h)	1.73	19.44	2.58
DS x Roll	1.92	13.28	2.13
DS x Pitch	0.88	7.59	2.13
DS x DOC	0.69	10.63	0.22
Spd x Roll	1.49	4.02	0.17
Spd x Pitch	2.37	2.92	1.88
Spd x DOC	4.13	5.81	0.08
Spd x CS	0.65	1.05	0.52

"t" statistic for given significance level: t(0.10)=1.7, t(0.01)=2.6.

Another way to visualize the relative significance of the independent variables for the three DHM database sites subset for largest error sections with their differing level of alignment severity is to normalize the ”t” statistic relative to the maximum values and then arrange the data for the three dependent variables AAD Profile, AAD IRI80, and AAD IRI120 by decreasing order relative to AAD Profile for each site. The resulting graphs are shown in figures 92, 93 and 94 for sites 193, 851 and 9 respectively on the next two pages.

Whereas the “t” statistic trends for route 193 were similar for AAD IRI80 and AAD IRI120 relative to AAD Profile for the full dataset, the largest error subset AAD IRI trends are very different from the AAD Profile trend in terms of the order of importance for the independent variables. For route 851, the “t” statistic trends are similar across the three dependent variables except for Delta Speed x DOC cross-term. For route 9, the “t” statistic trends relative to AAD Profile are mixed for the first five variables.

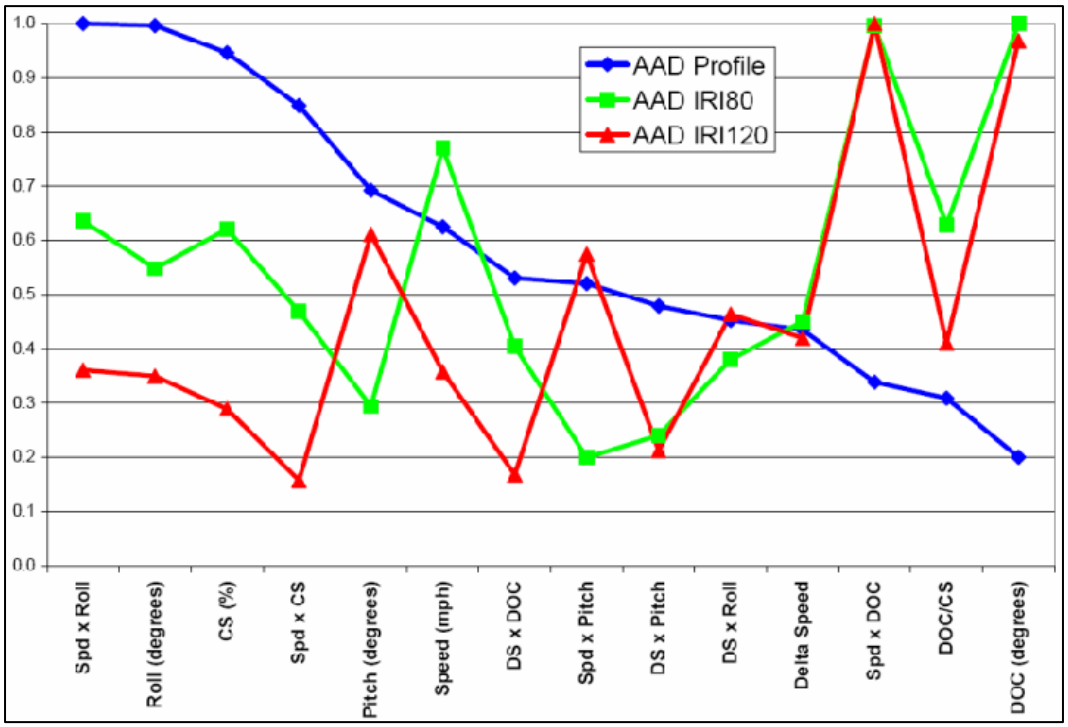

Figure 92. Line chart. Trend in "t" statistic among dependent variables for site 193, largest error section subset.

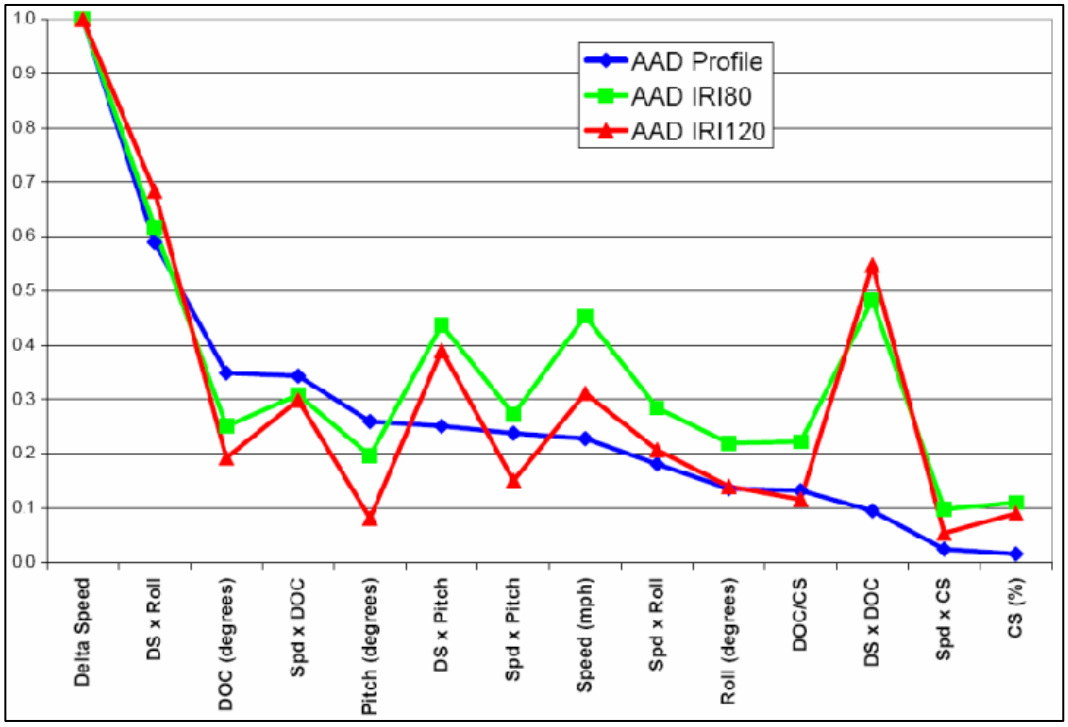

Figure 93. Line chart. Trend in "t" statistic among dependent variables for site 851, largest error section subset.

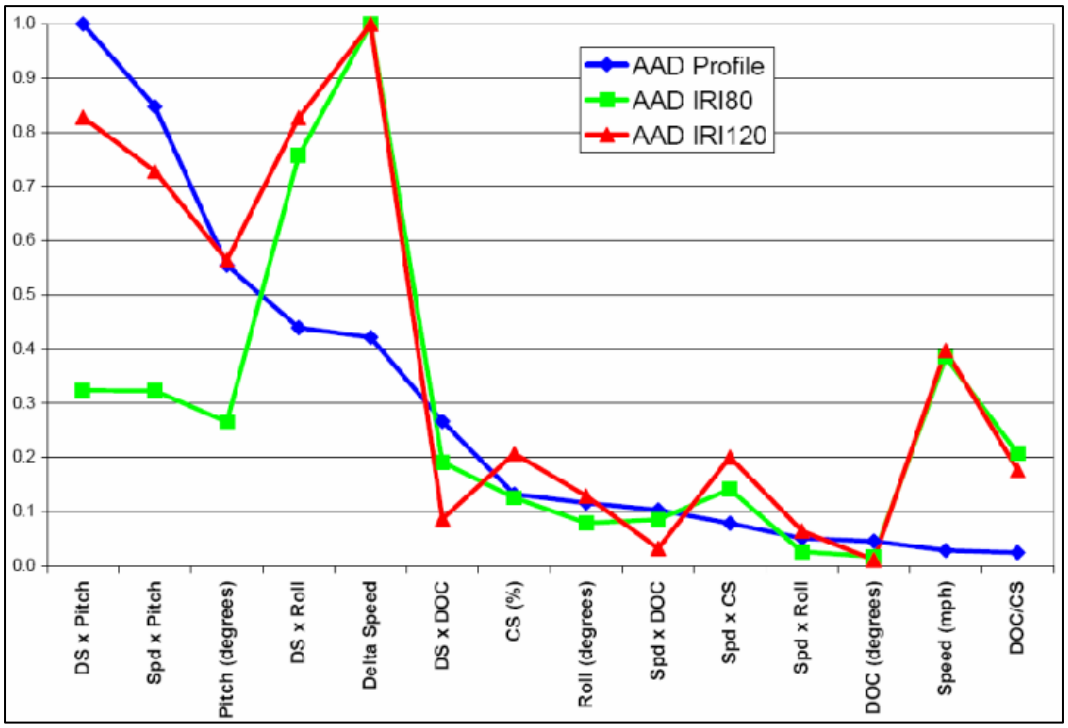

Figure 94. Line chart. Trend in "t" statistic among dependent variables for site 9, largest error section subset.

The under-sampling based on largest error sections AAD profile changed the relative significance of parameters. Speed and Roll are still the primary factors on the roughest sections. As shown in figure 95 as a reminder, there is some inherent interrelationship of the independent variables used in the analysis.

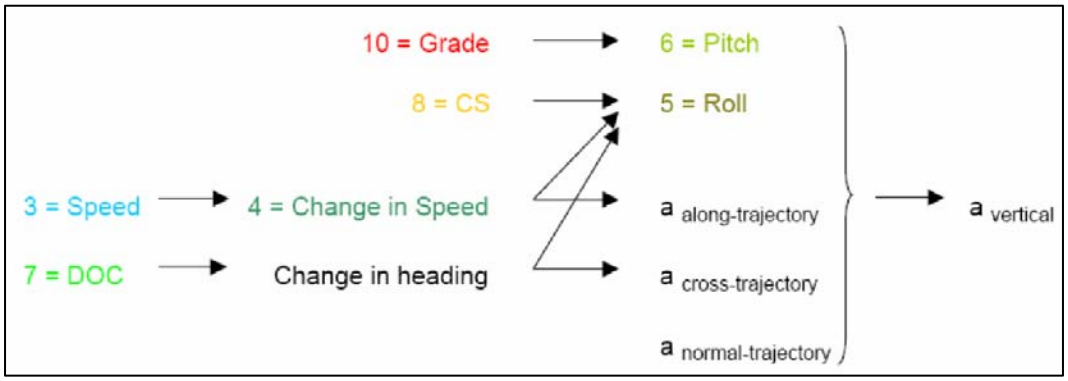

Figure 95. Illustration. Interrelationship of a subset of the variables used in analysis.

7. ANALYSIS SUMMARY

The analysis summary covers four major areas of interest, 1) data matrix description, 2) correlation analysis, 3) road section length for analysis, and 4) regression analysis.

DATA MATRIX

The four sites selected for analysis and the six data collection runs within each site varied significantly in terms of their roadway alignment features and operating speeds as shown using the Principal Component Analysis, Multivariate Analysis, and sample data plots. Some sites had very clean, design quality, roadway alignment features (460 and 9) while two sites (851 and 193) had what could be described as evolved alignment features based on the historical origin of the roads over time (100, 200 plus years).

CORRELATION ANALYSIS

Correlation analysis indicated that speed, change in speed, roll, and curvature were significant variables with respect to AAD Profile, AAD IRI80, and AAD IRI 120. Variation in significance amongst the independent variables and cross-variable terms was found between the four sites with route 460 being significantly different because speed was consistent (minimal operator variance), and horizontal and vertical alignment variables were also consistent with the design of the four-lane divided highway with gentle terrain and long, low degree-of-curvature horizontal curves.

Plots of dependent variables versus independent variables were generally not informative due to significant compounding of alignment and vehicle operations variable effects. Route 460 had the plot with the highest single variable correlation with AAD Profile where roll (cross slope) was the dominant characteristic and consistent relative to proper design throughout the length of the road. Correlation analysis for an independent variable versus a dependent variable does not consider explanation of variance contribution by other variables.

Correlation numbers based on 161 m (528 ft) long sections does not reveal the local impact of multiple cross slope, grade, curvature and other variable changes on older two-lane roads. Analysis results based on AAD values determined from road section length of 16.1 m (52.8 feet) captured more of the localized variability of the data.

REGRESSION ANALYSIS

Regression analysis was used to identify significant relationships between the dependent variables and the independent and cross-variable terms. No effort was made at this time to develop an AAD error model. Cross-variable terms were found be important contributors to explaining the variance in the AAD dependent variables.

The relative importance of the independent variables varied between sites and also within sites were AAD Profile and the AADs for IRI did not always coincide in terms of importance ranking. Different road features result in different profile effects in terms of wavelengths present.

Largest AAD Profile Error section analysis (cluster subset of full sample space) resulted in variables having a different order of importance. Route 851 was notably different from route 193 and 9 in terms of the higher “t” statistics of the independent variables. The selection of a cluster small subset of the full sample space may impact the quality of the analysis as a large portion of the overall sample space is not present in the analysis.

8. RESULTS

The Hypothesis was shown to be true:

> Pitch, roll, and change in speed of an inertial profiler vehicle as a result of changing roadway alignment and driver operations contribute to errors in inertial profile estimates and subsequent IRI calculations.

A variety of factors cause changes in pitch, roll, and speed of the data collection vehicle. The factors are often occurring simultaneously and thus lead to a compounding of effects that can be difficult to isolate. Route 460 was one case in which one factor, roll (cross slope), was dominant but consistent relative to good design practice while poor alignment and cross section factors were not present. It was very easy to visually observe the correspondence of vehicle roll to accelerometer error, as other compounding factors were not present.

The vehicle pitch, roll and change in speed impact on inertial profiles and subsequent IRI computations is less on well-designed high-type roads with consistent design elements and where a consistent speed can be maintained. The errors introduced on these high-type design roads by the typical pitch and roll are of longer wavelengths that get removed by the high pass filter and also have little output impact from the Quarter-Car model and subsequent IRI calculation.

9. DISCUSSION

Resulting vehicle pitch, roll, and speed changes do affect inertial profiles and IRI computations. Compounding of independent variables and their cross-terms make clearly defining relationships difficult when using real-world data, especially if the road has poor horizontal, vertical, and cross section alignment characteristics.

Analysis of the four sites indicated that road features are often unique to a site and may therefore influence inertial profile computations and IRI estimates differently. The influence may be where:

- Road features impact inertial profile more significantly than IRI.
- Road features impact IRI more significantly than inertial profile.
- Road features impact both inertial profile and IRI significantly.

Different features and their characteristics result in different accelerometer/laser inputs to inertial profile estimates and subsequent wavelengths input to the IRI filter. The geometry elements of a road and vehicle operations combine to produce both short-wave and long-wave effects on the inertial profile and IRI measurements. Roadway elements and vehicle operations may cause a change in profile but do not necessarily mean a significant change in IRI. For a particular road, some factors only affect profile while for other roads the factors may affect IRI significantly.

The question is how to define levels of cross slope, grade, and curvature that produces a pre-defined level of error, is difficult to achieve based on the findings. A 1-D model is not robust enough to withstand most combinations of sequence of cross slope, grade, and curvature and their impact on change in speed, and other acquisition factors.
The analysis also confirmed the general knowledge that higher data collection speeds result in more repeatable profiles and IRI measurements as evidenced by the negative coefficient for speed relative to the AAD variables. Assuming that the accelerometer range is not exceeded, there is less accelerometer error influence when data is collected at higher speeds. Error “noise” is still present, but is low in magnitude compared to the accelerometer signal strength.

A simulation model where profile factors and vehicle speed are controlled would permit defining effects due to individual variables and cross-terms. This would permit coverage of a larger simulated sample space under controlled conditions.

10. CONCLUSIONS

Pitch, roll, and change in speed of an inertial profiler vehicle as a result of roadway alignment and driver operations contribute to errors in inertial profile estimates and subsequent IRI calculations.

The sequence of conditions for curvature, grade and cross slope that generate levels of pitch, roll, cross-trajectory and along trajectory accelerations capable of significant profile and IRI errors may be further quantified and classified using a road-vehicle simulation model. A simulation model may be the only reasonable method to fully explore the impact of roll, pitch, and change in speed on inertial profile estimates as it relates to a road's alignment and cross section elements.

Change in Speed may be a good, overall Quality Control Parameter in a 1-D profile measurement system. When associated with curvature, cross slope, and grade, the combined effects on vehicle attitude are significant in terms of accelerometer error.

All Objectives but the last were achieved in this project: Defining guidelines based on the sole input of 1-D data is difficult since it depends on the knowledge of 3-D parameters for a given dataset. A simulation model may be the best tool to measure the affects of pitch, roll, and change in speed on inertial profile error and IRI analysis.

11. RECOMMENDATIONS

The four data sites provided a wealth of information in regards to relationships between roadway alignment features and vehicle operations impact on profiles and IRI computations. The sequence of conditions for curvature, grade and cross slope that generate levels of pitch, roll, cross-trajectory and along trajectory accelerations capable of significant profile and IRI errors may be further quantified and classified using a road-vehicle simulation model. Simulation would permit a very controlled experiment to be conducted where all combinations of input factors could be modeled and results analyzed with clarity. Amplitude and frequency of features would be precisely controlled and resulting profile and ride quality measurements observed. A full range of situations can be analyzed that could not be easily found and assembled using real world data.

12. ACKNOWLEDGEMENTS

The following states are participants in the pooled fund study–TPF-5(063) Profile Quality, under which this project was sponsored:

- California DOT
- Colorado DOT
- Connecticut DOT
- Florida DOT
- Georgia DOT
- Illinois DOT
- Kansas DOT
- Kentucky Transportation Cabinet
- Maryland DOT
- Mississippi DOT
- New Jersey DOT
- New York DOT
- North Carolina DOT
- North Dakota DOT
- Ohio DOT
- Oklahoma DOT
- Pennsylvania DOT
- South Dakota DOT
- Texas DOT
- Wisconsin DOT

13. APPENDIX A. INERTIAL PROFILER QUESTIONNAIRE RESULTS

INTRODUCTION

A questionnaire on inertial profilers was sent to the participants of the "TPF-5(063) Profile Quality" study. The purpose of Part 1 of the questionnaire was to ascertain what vehicle types (characteristics) and sensors were being used by the relevant agencies, and to help define the range of values for the vehicle and sensors to be used in inertial profiling simulations to estimate corresponding levels of error in single-axis accelerometer road profilers. This appendix is based on the returned questionnaires.

INERTIAL PROFILER VEHICLE AND SENSOR QUESTIONNAIRE SUMMARY

Tables 15 shows profiler and sensor summaries of the returned questionnaires. Information was received for ten high-speed inertial profilers from eight states.

Five different vendors manufactured the ten profilers as shown in table 15. All of the vehicles except for one 1999 Chevrolet Suburban were Ford E350 vans with the oldest two vans manufactured in 1994 and 1999. The other vans were manufactured in 2003 or later.

In table 16, all ten profilers are shown to have LMI Selcom 2207 (three profilers) or SLS 5000 (seven profilers) displacement lasers, all with similar operating characteristics. Six of the ten profilers as shown in table 17 used Jewell Instruments accelerometers, either the LSBC 2G with 1 G bias (3 profilers) or the LCS 100-5G (3 profilers). One profiler uses the Columbia Research Labs SA 127S accelerometer, one profiler used the PCB 3G accelerometer, one profiler used the Enderco 7265A-HS accelerometer, and another profiler used the Honeywell QA-700 accelerometer.

In table 18, it can be seen that sampling intervals ranged from 19 to 76.2 mm (0.75 to 3 inches) for seven of the profilers for whom this information was provided. Another profiler reported having a 76.2 mm (3 in) "summary" interval and another profiler had a 250 mm (9.84 in) interval. Sensors were all front-mounted on the vehicles.

In summary, the profilers are characterized as being very similar in make and model for both the vehicle and sensors. Sensor with the greatest variability was the accelerometers.

Table 15. Questionnaire profiler vehicle summary results.

Profiler Number	Profiler Vendor	Model	Version	Vehicle Make/Model	Year	Wheel Base (cm (in))	Front Wheel Track (cm (in))	Rear Wheel Track (cm (in))
1	Roadware Group Inc.	ARAN	4300	Ford E350	2003	350.5 (138)	182.9 (72)	182.9 (72)
2	ICC	-	MP90XNJ 4.21	Ford E350	2005	350.5 (138)	176.3 (69.4)	69.4/67
3	Pathway	Pathrunner XP	-	Ford E350	2005	350.5 (138)	175.3 (69)	69/66
4	Pathway	Pathrunner XP	-	Ford E350	2005	350.5 (138)	175.3 (69)	69/66
5	ICC	MDR 4083	MP90XKS 3.5	Ford E350	2003	350.5 (138)	-	-
6	ICC	-	-	Ford E350	2003	350.5 (138)	176.3 (69.4)	69.4/67
7	Pathway	LG-23	-	Ford E350	2006	350.5 (138)	176.3 (69.4)	69.4/67
8	Dynatest	5051 Mark III/IV	-	Ford E350	2006	350.5 (138)	176.3 (69.4)	69.4/67
9	Ames Engineering	High Speed	-	Chev/Suburb	1999	334.0 (131.5)	177.8 (70)	177.8 (70)
10	Roadware Group Inc.	ARAN	4900C	Ford E350	1994	350.5 (138)	174.0 (68.5)	174.0 (68.5)

1.0 inch = 2.54 cm

Table 16. Questionnaire profiler vehicle laser sensor summary results.

Profiler Number	Laser Brand/Model	Measurement Range (mm (in))	Mid-Point Standoff (mm (in))	Resolution (mm (in))	Noise (mm (in))
1	SLS 5200/300-RO	200 (7.874)	300 (11.811)	0.05 (0.002) *	0.005 (0.0002) *
2	Selcom 2207	200 (7.874)	325 (12.795)	0.05 (0.002)	0.25 (0.0098)
3	SLS5000	200 (7.874)	300 (11.811)	0.05 (0.002)	0.005 (0.0002)
4	SLS5000	200 (7.874)	300 (11.811)	0.05 (0.002)	0.005 (0.0002)
5	Selcom 2207	200 (7.874)	325 (12.795)	0.05 (0.002)	0.25 (0.0098)
6	Selcom 5200	200 (7.874)	300 (11.811)	0.05 (0.002) *	0.005 (0.0002) *
7	SLS 5200/300-RO	200 (7.874)	300 (11.811)	0.05 (0.002)	0.005 (0.0002)
8	SLS 5200/300-RO	200 (7.874)	300 (11.811)	0.05 (0.002)	0.005 (0.0002)
9	SLS 5200/300-RO	200 (7.874)	300 (11.811)	0.05 (0.002)	0.005 (0.0002)
10	Selcom 2207	200 (7.874)	325 (12.795)	0.05 (0.002)	0.14 (0.0055)

* copied from information provided by other agency for this sensor

1 inch = 25.4 mm

Table 17. Questionnaire profiler vehicle laser sensor summary results.

Profiler Number	Accelerometer	Measurement Range (G)	1G Bias	Resoluton	Noise
1	PCB 3701-G2-FB-3G/003	+/-3	No	0.0015G *	-
2	Jewell LCS 100-5G	+/-5	No	1v/g	0.005
3	Jewell LSBC 2G	+/-2	Yes	0.001G *	0.0002 v/rms
4	Jewell LSBC 2G	+/-2	Yes	0.001G *	0.0002 v/rms
5	Jewell LCS 100-5G	+/-5	No	1v/g	0.005
6	Jewell LCS 100-5G	+/-5	No	1v/g **	0.005 **
7	Jewell LSBC 2G	+/-2	Yes	0.001G *	0.0002 v/rms
8	Honeywell QA-700	+/-5	No	0.000,001 G	-
9	Columbia Research Labs SA 127S (3)	+/-2	Probably	0.04 G	2mV
10	Enderco 7265A-HS	+/-10	No	0.00305G	-

* computed based on 12bit data acquisition

** copied from information provided by other agency for this sensor

Table 18. Questionnaire profiler vehicle sensor location and sampling summary results.

Profiler Number	Sensor Location	Interval (mm (in))	Distance Measurement Instrument (DMI) *
1	Front Bumper	25.4 (1)	BEI
2	-	-	ICC
3	914.4 mm (3 ft) in front of front axle	19.05 (0.75)	Optical encoder
4	914.4 mm (3 ft) in front of front axle	19.05 (0.75)	Optical encoder
5	Front Bumper	76.2 (3) summary	ICC/Applanix
6	Front Bumper	50.8 (2) or less	-
7	914.4 mm (3 ft) in front of front axle	38.1 (1.5)	ABS Pulse
8	965.2 mm (38 in) in front of front axle	25.4 (1) or longer	BEI
9	1092.2 mm (43 in) in front of front axle	76.2 (3)	Accu-Coder
10	In front of vehicle	250 (9.84)	Optical encoder

* type or manufacturer

1 inch =25.4 mm

1 foot = 304.8 mm

14. APPENDIX B. ROADWAY GEOMETRY QUESTIONNAIRE RESULTS

INTRODUCTION

A questionnaire on inertial profilers was sent to the participants of the "TPF-5(063) Profile Quality" study. The purpose of the questionnaire was to ascertain what are the participating state highway alignment design parameters to help define the range of values for the highway geometry parameters that will be used in the inertial profiling simulations to estimate corresponding levels of error in single-axis accelerometer road profilers. This appendix is based on the returned questionnaires.

ROADWAY GEOMETRY QUESTIONNAIRE SUMMARY

Tables 19 and 20 shows the roadway design parameters summary from the returned questionnaires. Two states provide a copy or Internet link to their design tables. The range of values is indicative of the local terrains. As a state's topography becomes more rolling or mountainous, then higher the maximum grades. Maximum grades and super elevation are the more important values for geometry alignment parameters. The design coefficient of friction (0.06-0.08) normally defines the limit for Degree of Curvature (or Radius) of a horizontal curve.

Table 19. Roadway parameter questionnaire summary results for grade and superelevation.

Agency	Freeway Maximum Grade (%)	Two-Lane Road Maximum Grade (%)	Urban Street Maximum Grade (%)	Design Superelevation Maximum (%)	Existing Superelevation Maximum (%)
1	6	8	11	-	-
2 *	4-6	5-8	8-11	6	-
3	3	3-5	6-9	6	8
4	4	6.5	11	13	10
5 *	6	10	10-12	-	-
6 **	4-5	8	9	6	11

* Representative values taken from provided design table

** Existing Maximum Grade of 18%

Bolded DOC or Radius computed for provided Radius or DOC

Table 20. Roadway parameter questionnaire summary results for degree-of-curvature and design minimum radius.

Agency	Design Maximum Degree-of-Curvature (DOC)	Design Minimum Radius (m (ft))	Existing Maximum Degree-of-Curvature (DOC)
1	**20.25**	86 (282)	-
2 *	**6 to 6.75**	254 (835) - 283.4 (930) @ 80.47 km/h (50 mi/h)	-
3 ***	2.25(RI) to 4.25(U)	**776.2 (2546) (RI), 411.0 (1348) (UI)**	6
4	-	-	6.5
5 *	6.75-7.5 @ 80.47 km/h (50 mi/h)	**272.5 (849) and 232.9 (764)**	-
6 **	**28.6**	60.96 (200)	

* Representative values taken from provided design table

** Existing Maximum Grade of 18%

*** RI = Rural Interstate and UI = Urban Interstate

Bolded DOC or Radius computed from provided Radius or DOC

1 foot = 0.3048 meters

1 mi/h = 1.609344 km/h

15. APPENDIX C: COMPUTATIONAL FLOW FOR DATA PREPARATION

Figure 96 shows the first step in the computational flow process to generate the analysis database. Program 1 time synchronizes the 1) DHM Laser and accelerometer data, 2) INU gyroscope pitch, roll and heading data, 3) INU body and tracking accelerations, and 3) pavement cross slope data into a single synchronized temporal data file.

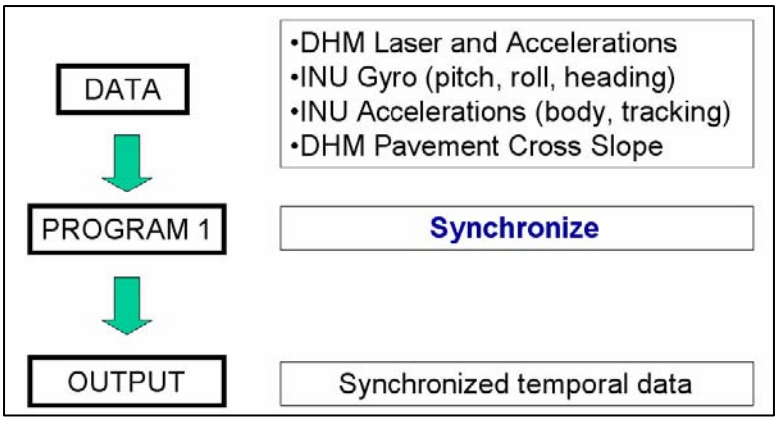

Figure 96. Flow chart. Computational flow--data synchronization step.

In Figure 97, the synchronized temporal data output from program 1 is used as the input to the Program 2 computation and output of corrected DHM vertical axis acceleration.

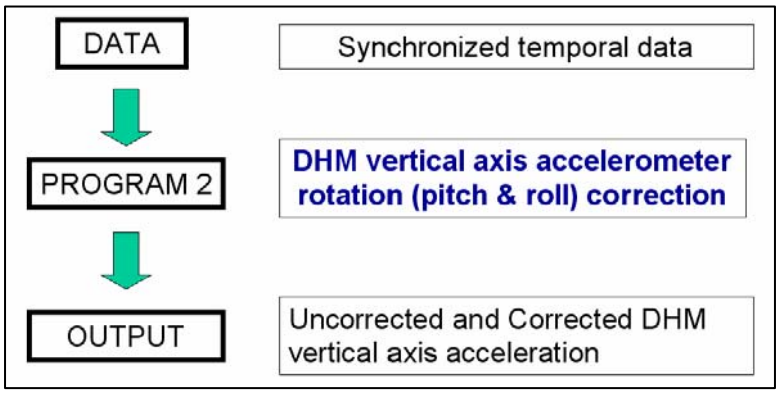

Figure 97. Flow chart. Computational flow--acceleration correction for pitch and roll.

Shown in figure 98 is the input of the uncorrected and corrected DHM vertical axis acceleration as part of the Program 3 inertial profile calculation based on 1-D original and corrected accelerations, cutoff long wavelength of 91.44 m (300 ft) and short wave 250 mm (10 in) profile filtering, and IRI (IRI80 and IRI120) computations with IRI internal speed parameters of 80 and 120 km/h (50 and 75 mi/h).

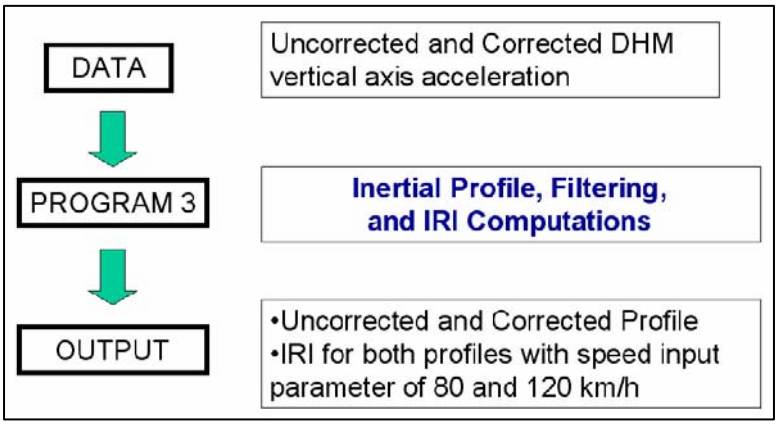

Figure 98. Flow chart. Computational flow--inertial profile, filtering, and IRI calculations.

In figure 99, the parameters for defining the roadway section are computed using a moving average in Program 3B. A window length of 160.93 m (528 ft) was initially used for the moving window size and later recomputed using a 16.09 m (52.8 ft) window size. The reason for using a smaller window size was to capture the greater variability present in the data where interactions of variables were present.

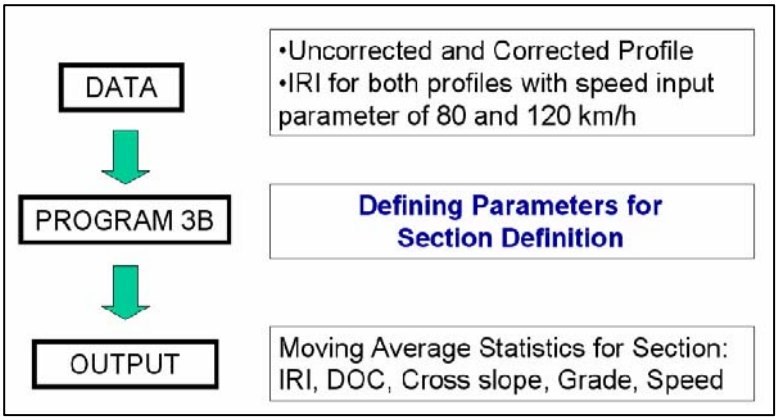

Figure 99. Flow chart. Computational flow—moving average statistics of all variables at a defined window size.

Figure 100 shows that given the computations of the moving average section statistics, Program 4 defines parameters for later section type/categorization level assignment, computes Average Absolute Differences (AAD) for both the uncorrected and correct profiles and AAD for IRI80 and IRI120 roughness measurements, and writes a file used as input to the statistical analysis process. Program 4 also generates a parameter typing summary report.

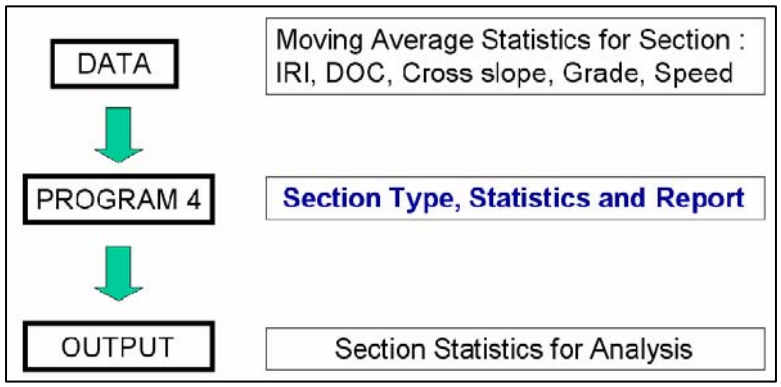

Figure 100. Flow chart. Computational flow—section type/categorization levels given moving average statistics and write reports.

16. APPENDIX D: INITIAL DATA MINING

Following is a series of figures illustrating some basic comparisons of data within the DHMS analysis database.

Figure 101 and 102 show a comparison of corrected versus uncorrected vertical accelerations for the four-lane site with a data collection at a high speed and low speed, respectively. A slightly higher scatter about a 45-degree diagonal is apparent for the low speed case in figure 102.

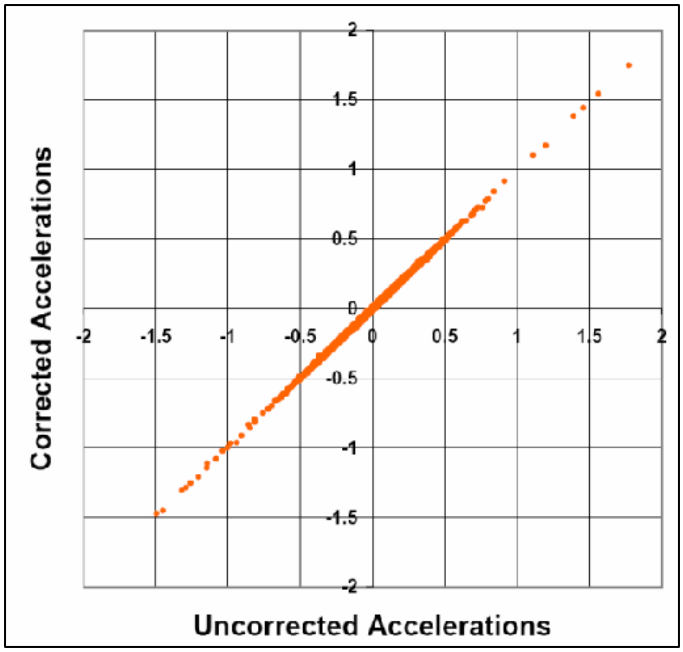

Figure 101. Graph. Comparison plot of corrected versus uncorrected vertical acceleration along a 45-degree diagonal for the four-lane site, high-speed collection.

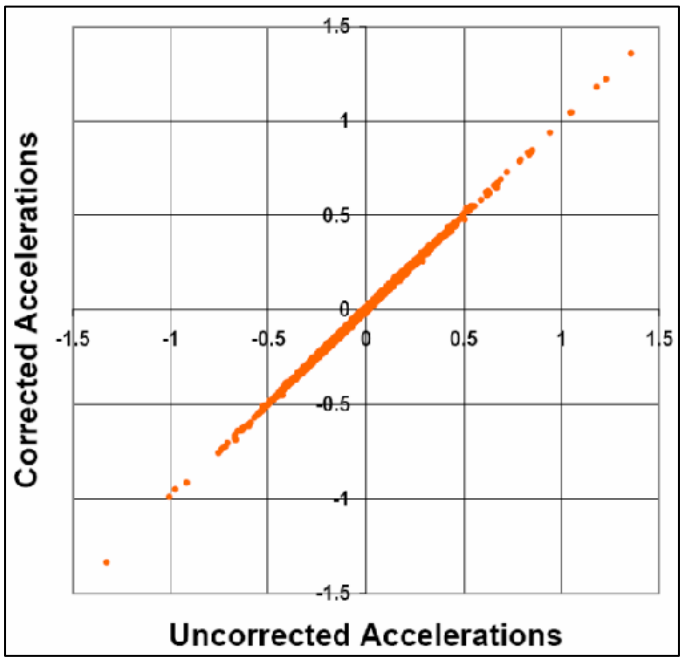

Figure 102. Graph. Comparison plot of corrected versus uncorrected vertical acceleration along a 45-degree diagonal for the four-lane site, low-speed collection.

Figures 103 and 104 show a comparison of corrected versus uncorrected vertical accelerations for one of the two-lane rural road sites with a data collection at a high-speed and low-speed, respectively. Both figures indicate a greater scatter of data about the 45-degree diagonal as compared to the four-lane site, and with the low-speed case having a greater scatter than the high-speed case.

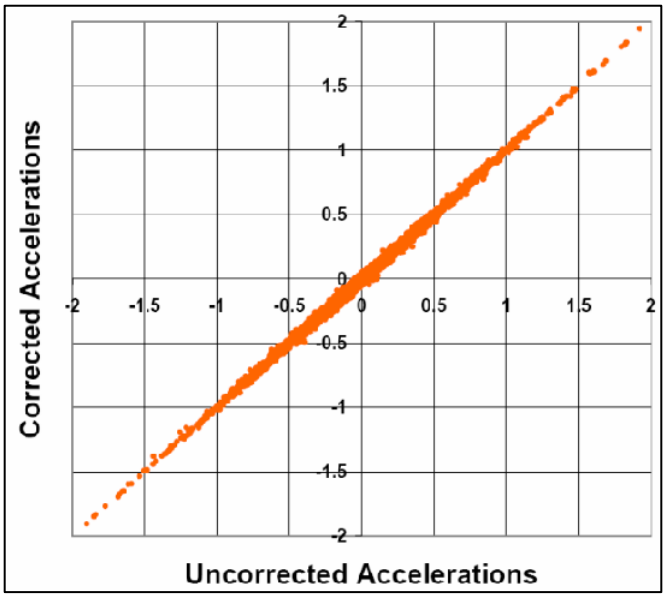

Figure 103. Graph. Comparison plot of corrected versus uncorrected vertical acceleration along a 45-degree diagonal for a two-lane site, high-speed collection.

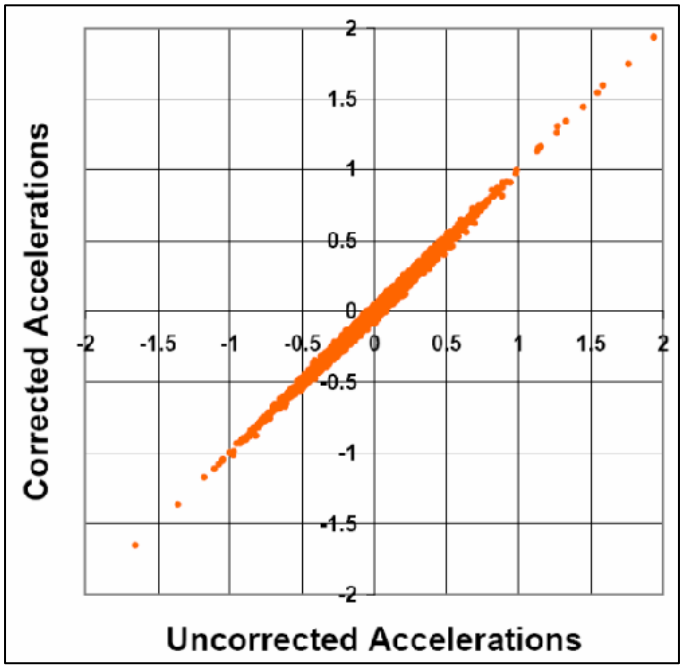

Figure 104. Graph. Comparison plot of corrected versus uncorrected vertical acceleration along a 45-degree diagonal for a two-lane site, high-speed collection.

Initial data mining included looking at the histograms of the profile section Average Absolute Difference (AAD) and IRI section AAD, and the histograms of the profile section and IRI section correlation. The following four figures present this information beginning on the next page. The section length used with these four figures was 16.09 m (52.8 ft).

Figure 105 is a histogram of the corrected and uncorrected inertial profile Average Absolute Difference (AAD) in mils (1 mil = 0.0254 mm). The histogram shows that most of the AAD points fall within 50 mils (1.27mm) and most of the remaining points between 50 (1.27mm) and 100 mils (2.54 mm) with a few points scattered beyond 100 mils (2.54 mm).

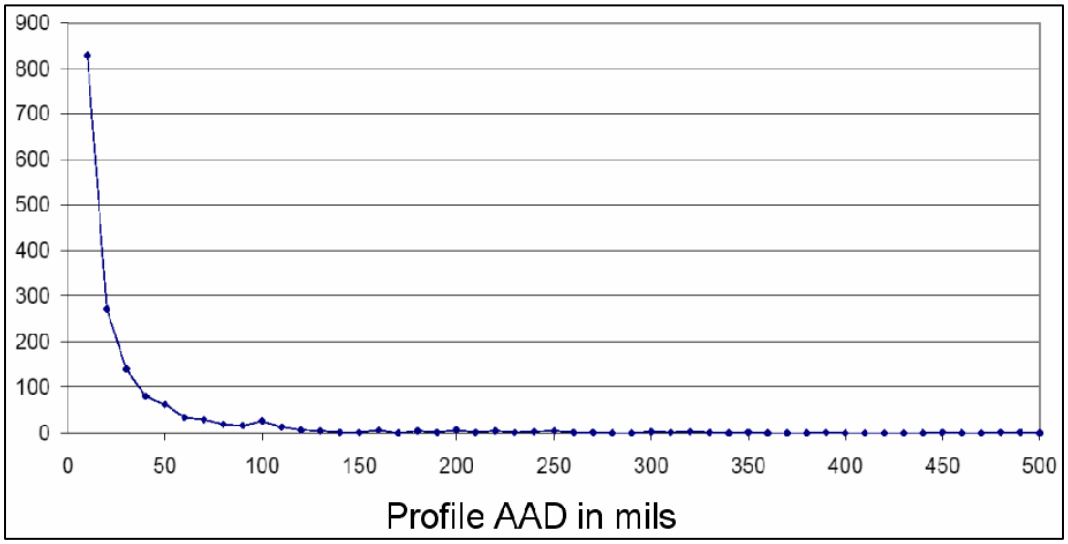

Figure 105. Histogram. AAD histogram of the uncorrected and corrected profile for one of the DHM database sites.

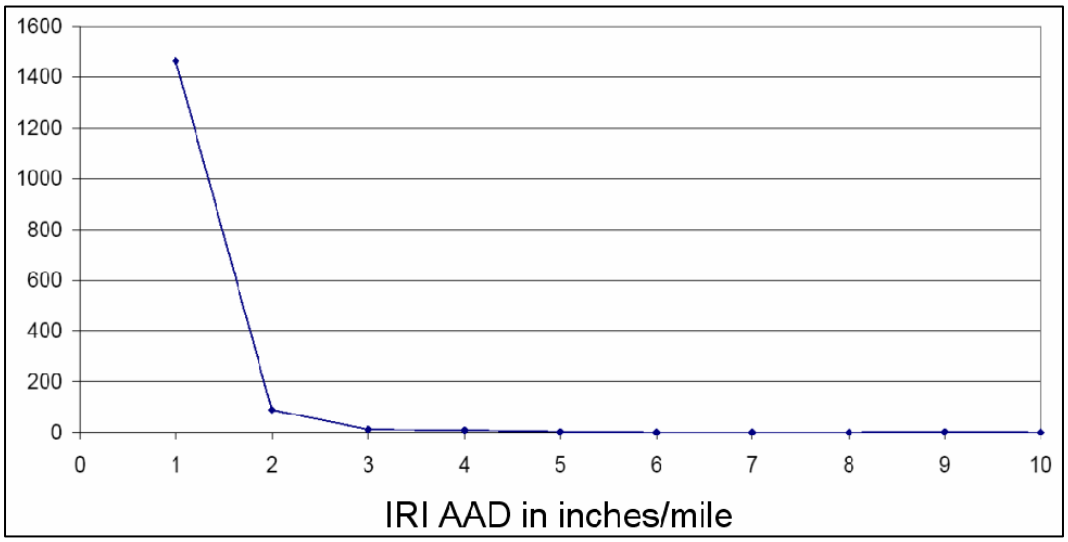

Figure 106. Histogram. AAD histogram of the uncorrected and corrected section IRI80 for one of the DHM database sites.

Figure 106 shows that almost all of the AAD IRI80 comparison points are within 2 in/mi (0.03 m/km) with one a few comparison points higher.

In figure 107, the histogram of the uncorrected and corrected profile section correlation is presented for one of the DHM database sites. Most of the correlation values are at or above 0.80.

Figure 108 shows the histogram plot of IRI section correlations. Most of the correlation values for IRI80 are greater than 0.99.

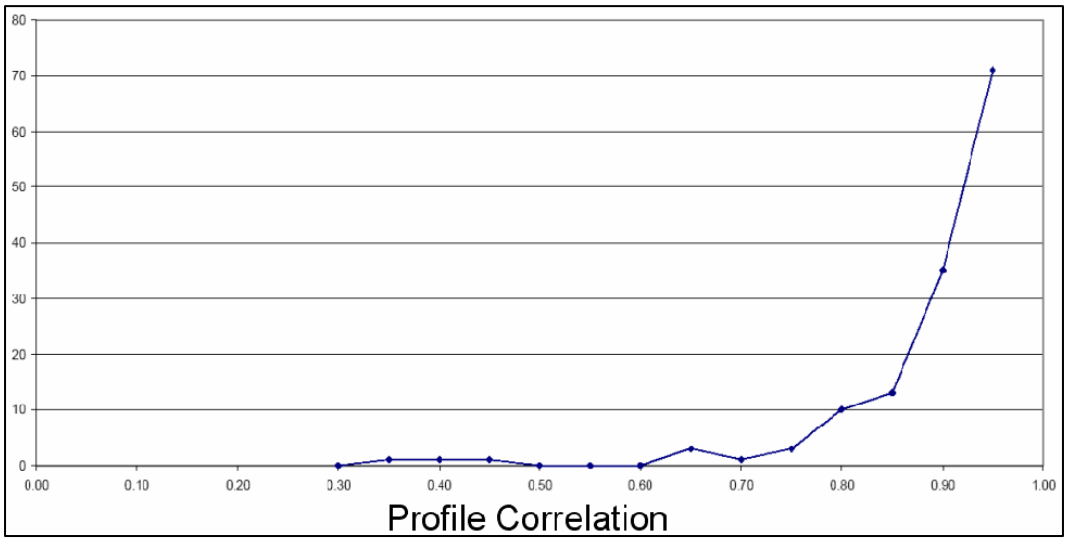

Figure 107. Histogram. Uncorrected and corrected profile histogram of section correlation for one of the DHM database sites.

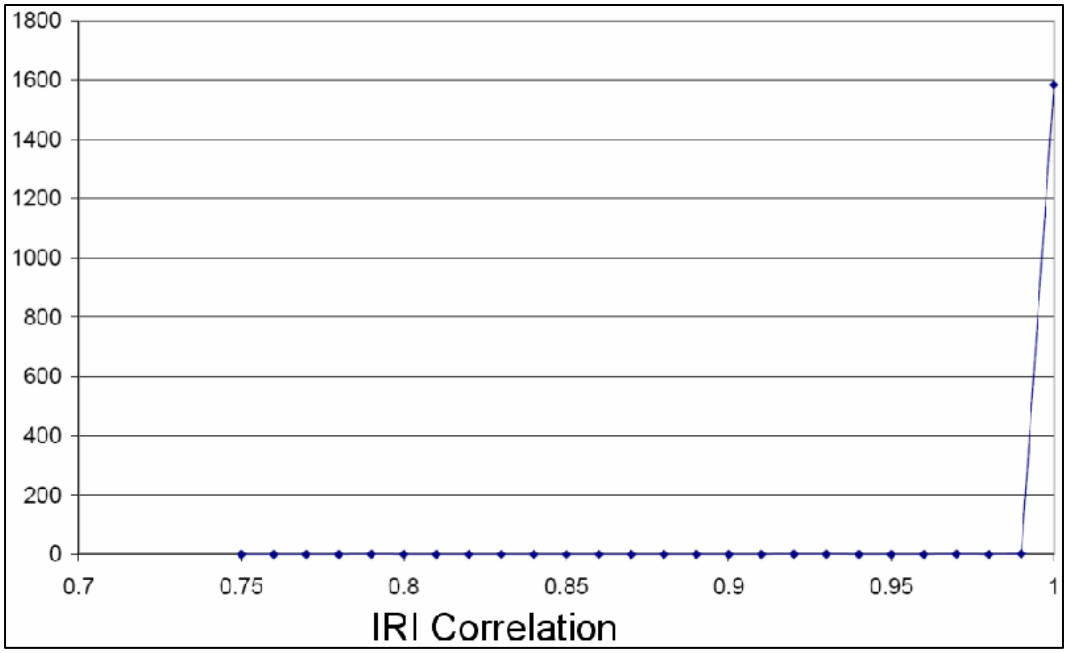

Figure 108. Histogram. Uncorrected and corrected IRI80 section correlation histogram for one of the DHM database sites.

It would appear from the four previous figures that the AAD Profile section information captures a greater variability present in this real world data.

17. REFERENCES

International Standard 2631: Guide for the Evaluation of Human Exposure to Whole-Body Vibration, 1987.

18. BIBLIOGRAPHY

Insert bibliography list here.